

Universität der Bundeswehr München  
Fakultät für Luft- und Raumfahrttechnik  
Institut für Messtechnik

**Object Manipulation and Force Control by  
Using Tactile Sensors**

M. Eng. Somrak Petchartee

Vollständiger Abdruck der bei der  
Fakultät für Luft- und Raumfahrttechnik  
der Universität der Bundeswehr München  
zur Erlangung des akademischen Grades eines

Doktor-Ingenieurs (Dr.-Ing.)

eingereichten Dissertation

Vorsitzender: Univ.-Prof. Dr.-Ing. H.-J. Wünsche

1. Berichterstatter: Univ.-Prof. (i. R.) Dr. rer. nat. V. Graefe
2. Berichterstatter: Univ.-Prof. Dr.-Ing. G. Hirzinger, Deutsches Zentrum für Luft- und Raumfahrt (DLR)

Diese Dissertation wurde am 13.01.2008 bei der Universität der Bundeswehr München, 85577 Neubiberg eingereicht und durch die Fakultät für Luft- und Raumfahrttechnik am 23.04.2008 angenommen.

Tag der Prüfung: 28.07.2008

## ABSTRACT

An important goal in robotics research is to allow the robot to interact with the environment at a much higher level than presently possible, thereby increasing the system's effectiveness. One prerequisite for this is accurate sensors and intelligent use of data. Tactile sensing is an area of research that has much impact potential on a large number of industries and disciplines particularly robotics and automation.

The lack of suitable commercial tactile sensors has limited developments in the robotic handling of fragile objects. This work demonstrates the use of simple tactile sensor arrays based solely on electrically conductive polymer foam. The advantages of this approach include (1) increased robustness because of the polymer substrate material; (2) decreased fabrication cost and complexity; (3) flexibility of integration with robot devices; (4) reliable and stable dc response. Given the accuracy of the position estimation, position feedback is integrated into a grasp controller to make optimal grasping and manipulation of objects possible.

This dissertation describes a new type of tactile sensor and an improved version of the dynamic tactile sensing approach that can provide a regularly updated and accurate estimate of applied forces for use in the control of gripper manipulation. This particular tactile sensor was designed and built by Mr. Karsten Weiß for the *HERMES* mobile robot project [Porto and Science 1998].

An algorithm that can discriminate between types of contact surface and recognize objects at the contact stage is also proposed. A technique for recognizing objects using tactile sensor arrays, and a method based on the quadric surface parameter for classifying grasped objects is described. Tactile arrays can recognize surface types on contact, making it possible for a tactile system to recognize translation, rotation, and scaling of an object independently.

The author also describes a new model-based approach to building a contact state observer. The observer uses contact force and position measurements, and prior information about the task encoded in Strain Quadric Composition [Petchartee 2007a], to determine the current normal force and shear forces. Quadric surfaces can be used to represent multiple principal strains at a contact point. An application of strain quadric composition showed some correlated results of strains can be interpreted by tactile sensors [Petchartee 2007a].

## TABLE OF CONTENTS

TITLE PAGE .....	I
ABSTRACT .....	II
TABLE OF CONTENTS .....	III
LIST OF FIGURES.....	VI
LIST OF TABLES .....	V
PRINCIPAL ABBREVIATIONS .....	VI
ACKNOWLEDGMENTS .....	VII
CHAPTER 1: INTRODUCTION	
1.1 Motivation.....	1
1.2 Task and goals of the work .....	2
1.3 Result requirements .....	4
1.4 Organization of the Dissertation .....	6
1.5 Statement of Problem .....	8
1.6 Related Work .....	11
1.7 Major Contributions of This Dissertation .....	15
CHAPTER 2: RELATED WORK	
2.1 Robotic tactile sensing .....	18
2.2 Sensing technologies and Analysis techniques .....	21
2.3 Sensing and manipulation .....	32
2.4 Sensing global shape .....	33
2.5 Control Systems .....	34
CHAPTER 3: SYSTEM OVERVIEW	
3.1 System Configuration .....	35
3.2 Force Sensor Design .....	43
3.3 Tactile Sensor Design .....	45
3.4 Electronics Circuit Design .....	48
3.5 Software Integration .....	53
3.6 Sensor Behavior .....	55
CHAPTER 4: THE NEW TACTILE SENSOR AND ITS PERFORMANCE	
4.1 Performance Matrix .....	59
4.2 Experimental Setup .....	61
4.3 Performance Test .....	64
4.3.1 Force Sensor Characteristics .....	64
4.3.2 Tactile Sensor Characteristics .....	78
4.3.3 Tactile Performance .....	83
4.4 Summary .....	86
CHAPTER 5: EXPERIMENTS AND APPLICATIONS FOR OPTIMIZATION GRASPING FORCE	
5.1 Introduction to Optimization Grasping Force .....	88
5.2 Experiment Overview for Optimization Grasping Force .....	90
5.3 Experiment Setup for Optimization Grasping Force .....	95
5.3.1 Process .....	95
5.3.2 Experiment Model .....	104
5.3.3 Real Experiment .....	121
5.4 Analysis of result .....	125
5.5 Statistic Tested Results .....	130
5.5.1 With dead weight .....	130
5.5.2 With acceleration sensor .....	136
5.6 Conclusions .....	140

CHAPTER 6: EXPERIMENTS AND APPLICATIONS FOR TOUCH IDENTIFICATION

6.1 Introduction to Touch identification .....	142
6.2 Experiment Overview for Touch identification .....	143
6.3 Experimental Arrangement for touch identification .....	148
6.3.1 Process .....	148
6.3.2 Experiment Model .....	150
6.3.3 Real Experiment .....	155
6.4 Analysis of result .....	164
6.5 Conclusions.....	169

CHAPTER 7: SUMMARY AND OUTLOOK

7.1 Summary of Results .....	170
7.2 Review of Contributions .....	173
7.3 Future Works .....	174
7.4 Problem Solution .....	176
7.5 Conclusions.....	183

REFERENCES.....	185
-----------------	-----

<b>List of Figures</b>		
<b>FIGURE</b>	<b>TITLE</b>	<b>PAGE</b>
3.1	<i>ATHENE</i> Robot	35
3.2	Hardware Configuration 1	36
3.3	Hardware Configuration 2	37
3.4	Software Architecture	40
3.5	Software Operation	42
3.6	Operating principle of the tactile elements	44
3.7	Array of electrodes as planes for force measurement	44
3.8	Model for tactile sensing	47
3.9	The sampling circuit	49
3.10	Details of each side assembled into the finger	49
3.11	Details of finger components	50
3.12	The circuit diagram	51
3.13	The Controller Unit	52
3.14	Finger Screen	53
3.15	Single Side Screen	54
3.16	Material Behavior	56
3.17	Sensing Complexity	58
4.1	The impulse tester	61
4.2	The 3-axis test bench	62
4.3	The noise compression	65
4.4	Hysteresis curve	67
4.5	Temporal response	68
4.6	Data from pressing on a tactile element	69
4.7	Sensitivity and Resolution	70
4.8	The relationship between force and resistance	71
4.9	The time variant data	73
4.10	Calibration of Nonlinear models vs. original data	76
4.11	Single tactile response to lateral scans	79
4.12	Frame of image	81
4.13	Accuracy of point source localization using weighted average	82
4.14	Threshold filtered sensor output	83
4.15	NURBS surface interpolation	85
5.1	Grasp-Lift-Replace Experiments	92
5.2	Grasp-Optimize-Replace Experiments	93
5.3	A set of test objects	93
5.4	Tracking the localized contacts by centroid determination	96
5.5	The center of force	99
5.6	Ball Grasping	101
5.7	Algorithm to find cycle of signal	102
5.8	Memory queue for the routine to find cycle	103
5.9	Dynamic model	109
5.10	(a), (b) Object prehension, (c), (d) area of contact deformation and pressure distribution	111
5.11	Slip displacement	115
5.12	Geometry of the problem	118
5.13	Distributions of shear tractions	119

5.14	Minimum prehension force determinate by increasing the applied force	121
5.15	Minimum prehension force determinate by decreasing the applied force	123
5.16	Explanation of algorithm used to measure slip	125
5.17	Explanation of algorithm using the least force in object manipulation	129
5.18	Statistical experiments	131
5.19	Standard deviation of experimental results	133
5.20	The GOR experiment evaluated with the acceleration sensor	136
5.21	Flowchart of the GLR experiment evaluated with the acceleration sensor	137
5.22	The GLR experiments evaluated with the acceleration sensor	138
6.1	Quadric Surface in the experiments of Object Identifications	146
6.2	Fitting Accuracy	157
6.3	Eigenvalue trajectories of quadric parameter with their invariant of any transformation of the surface	160
6.4	Noise Tolerances	165
6.5	Windows of Margin	166
6.6	Mixed threshold	167
7.1	Graph showing the relationship between the PWM values sent to the robot and the resulting forces	176
7.2	Graph showing the lowest PWM values able to move the grippers	177
7.3	Solutions to gripper threshold	178
7.4	Speed of communication protocols and devices	180

**List of Tables**

<b>TABLE</b>	<b>TITLE</b>	<b>PAGE</b>
1	Implementations of array sensors and their densities in units per square millimeter	18-20
2	Performance Matrix Validation	59-60
3	Experiment1 Results	134
4	Procedure to evaluation eigenvalue trajectory	159
5	Statistic error of classification	168

## PRINCIPAL ABBREVIATIONS

<b>ADC</b>	Analogue to Digital Convertor
<b>COM</b>	Common Object Model
<b>DLR</b>	Deutsches Zentrum für Luft- und Raumfahrt e.V.
<b>DLL</b>	Dynamic Link Library
<b>DOF</b>	Degree of freedom
<b>DSP</b>	Digital Signal Processor
<b>ESD</b>	Electrostatic discharge
<b>FE</b>	Finite-element
<b>FSR</b>	Force Sensing Resistor
<b>GLR</b>	Grasp-Lift-Replace Experiments
<b>GOR</b>	Grasp-Optimize-Replace Experiments
<b>KMITL</b>	King Mongkut's Institute of Technology Ladkrabang
<b>KMITNB</b>	King Mongkut's Institute of Technology North Bangkok
<b>LaPACK</b>	Linear Algebra Package; provides routines for solving systems of simultaneous linear equations, least-squares solutions of linear systems of equations, eigenvalue problems, and singular value problems.
<b>LMS</b>	Least mean square.
<b>MAE</b>	Mean Absolute Error
<b>MRG</b>	3-D shapes coding using multiresolutional graphs.
<b>MOBP</b>	Momentum modification to backpropagation
<b>MSE</b>	Mean Squared Error
<b>NN</b>	Neural network
<b>NURBS</b>	Non-Uniform Rational Basis Spine
<b>PTF</b>	Polymer-thick film
<b>PVDF</b>	Polyvinylidene fluoride
<b>PWM</b>	Pulse Width Modulation
<b>QR</b>	A decomposition of a real square matrix into an orthogonal matrix and an upper triangular matrix.
<b>RBF</b>	Radial Basis Function
<b>RMS</b>	Root Mean Square
<b>SQC</b>	Strain Quadric Composition
<b>SQL</b>	Structured Query Language
<b>SVD</b>	Single Value Decomposition



$E$	Modulus of elasticity, the ratio of stress and strain, Newton/m <sup>2</sup>
$E_v$	The experimental result presents with mean and standard deviation
$E(x, y, z)$	Electric field, units of volts/m
$F$	The prehension force, units of Newton
$F_N(t)$	The fluctuating normal force, units of Newton
$F_x, F_y, F_z$	Shear force in x-direction, y-direction and z-direction respectively, units of Newton
$F_n$	Normal forces on the normal contact point $n$ , units of Newton
$F_t$	Contact friction forces perpendicular to the normal force, units of Newton
$F_G(t)$	The fluctuating friction force, units of Newton
$G$	Shear modulus, the ratio of shear stress and shear strain, Newton/m <sup>2</sup>
$M_G$	The weight of grasped object, units of Newton
$M_x, M_y, M_z$	Moment about x-axis, y-direction and z-direction respectively, units of Newton-meter
$c_a, c_s$	A damping constant and associated damping respectively, units of Newton.sec/m
$d(\zeta)$	The small difference in distance located at $\zeta$ meter, unit of meter
$d_i$	The deviation of measurements.
$\bar{d}$	The mean deviation of measurements.
$e_z$	The eccentricity parameter of the ellipsoid contact model, units of meter
$k_a, k_s$	Spring stiffness and normal contact stiffness respectively, units of Newton/m
$p_0$	The peak contact pressure, units of Newton/m <sup>2</sup>
$p(x, y)$	The pressure distribution function, units of Newton/m <sup>2</sup>
$q, Q$	Shear stiffness under the action of a line load, unit of Newton/m
$q(\zeta)$	Shear stiffness distribution, unit of Newton/m <sup>2</sup>
$s, S$	Direct stiffness under the action of a line load, unit of Newton/m
$s(\zeta)$	Direct stiffness distribution, unit of Newton/m <sup>2</sup>
$v(x), u(x)$	Surface displacements
$\bar{x}$	The average or mean value of measurements.
$y_{ie}(t), \dot{y}_{ie}(t)$	An excitation in different derivation, unit of meter and meter/sec respectively.
$y_p(t), y_c(t)$	The complementary and particular solution of differential equation, unit of meter.

$\beta$	The ratio of the deformation and the degree of force in the contact with polymeric materials, unitless
$\gamma_{ij}$	The shear strain along the $i$ axis that applies on the $j$ side of the cube, unitless
$\epsilon$	Electrical permittivity, units of Coulomb <sup>2</sup> /N.m <sup>2</sup>
$\epsilon_i$	The normal strain in the $i$ direction, unitless
$\epsilon_{ij}$	Strain which the component along the $i$ axis that applies on the $j$ side of the cube, unitless
$\kappa$	The buck modulus, the ratio of an average pressure at a point inside solid and the resultant fractional change in volume, unit of Newton/m <sup>3</sup>
$\mu$	Modulus of rigidity, the ratio of the shear stresses and shear strains, unitless
$\mu(x, y)$	Average dynamic coefficient of friction, unitless
$\mu_i$	Instantaneous coefficient of friction, unitless
$\mu_k$	Average kinetic coefficient of friction, unitless
$\nu$	Poisson's ratio, the ratio of transverse contraction strain to longitudinal extension strain in the direction of stretching force, unitless
$\rho$	Material charge density with the units Coulomb/m <sup>3</sup>
$\sigma$	The standard deviation of measurements.
$\sigma_v$	The local plastic pressure, units of Newton/m <sup>2</sup>
$\sigma_{ij}$	Stress which the component along the $i$ axis that applies on the $j$ side of the cube, units of Newton/m <sup>2</sup> , for examples; $\sigma_{xy}, \sigma_{yx}, \sigma_{yz}, \sigma_{zy}, \sigma_{zx}, \sigma_{xz}, \sigma_{xx}, \sigma_{yy}$ and $\sigma_{zz}$ .
$\sigma_{rr}$	Stress at the polar coordinates $(r, \theta)$ , units of Newton/m <sup>2</sup>
$\tau_{ij}$	Shear stress, units of Newton/m <sup>2</sup> for examples; $\tau_{xy}, \tau_{yx}, \tau_{yz}, \tau_{zy}, \tau_{zx}$ and $\tau_{xz}$ .
$\tau_{r\theta}$	Shear stress at the polar coordinates $(r, \theta)$ , units of Newton/m <sup>2</sup>

## ACKNOWLEDGEMENTS

The research and writing of this dissertation required the assistance and guidance of many people whom I would like to thank.

First and foremost, I would like to thank my supervisor, Professor Dr. V. Graefe and Professor Dr. Gareth Monkman, for their guidance, advice and support during the period of my Ph.D. study. I have benefitted greatly from his strong scientific background, his outstanding insight on all issues of sensors, grasping and dextrous manipulation, and their constant encouragement in the face of sometimes slow progress. Their hard work and style of scientific pursuit have helped me to learn how to be a good researcher and will continuously influence me in the years to come. From them I gained an excellent understanding of control engineering, a subject that I now feel at least competent in. I am indebted to them for his many suggestions and corrections to this dissertation.

I would also like to thank all of those people, my past and present colleagues. I worked with during the course of this research, in particular Günther Hofbauer and Anton Pröls. It gives me great pleasure to thank Professor Dr. - Ing. H. D. Ließ who provided invaluable instructions and help in the behavior of tactile sensors.

I would also like to thank Professor Somkiat Mongkon of KMITNB for pointing out the solution to the linear elastic plane strain problem, on which this dissertation is based. I also thank Professor Kobchai Dejhan of KMITL for the suggestion to analyze the electric field of sensor materials and investigate event classification. I would like to thank Dr. rer. nat. Wolfgang Schätzl for reading through the dissertation and giving many good comments. I do appreciate Professor Dr. Manukid Parnichkun of Asian Institute of Technology for his kind help on my research motivation during my graduate study.

I express my gratitude to Mr. Thamnoon Julmanichoti, the senior executive vice president of The Communications Authority of Thailand for supporting and accepting me for the oversea's study.

Finally, I owe huge gratitude to my family: my parents, my brothers and my sister provided the love, understanding and support that I needed most during the course of my graduate studies. This work is dedicated to them.

## CHAPTER ONE

### INTRODUCTION

#### 1.1 Motivation

There has been increased interest in the application of robots in manufacturing because of their flexibility and programmable sensitivity in manipulating a variety of object shapes. Moreover, sensors applied to robots should allow intelligent slip sensing and precise gripping during manipulation. In most factories, robot manipulators are designed in the form of parallel jaw grippers generally called end-effectors.

The motivation for many sensor based studies has been triggered by the need to mitigate the limitations of parallel jaw grippers. When equipped with tactile sensors, these grippers are more effective than traditional grippers as they are capable of encircling objects with the least possible force necessary to prevent slippage or premature release. However, to be able toprehend objects with different weights, robots must have excellent force control capacity, particularly when manipulating fragile objects or in cases where the coefficient of friction between object and gripper surfaces is low. This places high demands on both spatial and temporal sensor parameters making real-time operations necessary. To achieve this the robot must be capable of identifying the physical characteristics, including the surface nature, of the object. It must also be able to estimate the objects weight in order to generate an appropriate control force for secure acquisition of the object without fear of damage.

Nicholls' research survey [Nicholls 1989, 1992] on tactile-sensor technology indicates that despite rapid developments in the industry, the advent of robotic manipulators having sensitivity comparable to that of human hands has still far to come. Therefore, there has been ongoing research to develop guidelines for solving such problems, resulting in the availability of several new tactile-sensor designs. Some designs are capable of sensing only the contact between the object and the sensor surface, and merely the presence or absence of contact. Other more complex designs

have the capacity to generate information, for instance, about the size and shape of the object together with the force distribution on the tactile sensor surface.

According to [Crowder 1998], simple touch sensors are able to measure the sense of touch or force at a certain contact point between object and sensor surfaces and are thus only capable of determining the presence or absence of contact. In comparison, tactile sensors are capable of measuring the sense of touch as a force distribution on the sensor surface which can be used further to analyze the characteristics of the contact, such as the object shape.

## **1.2 Tasks and Goals of this Study**

From the above motivation, the present study aims at researching, designing and applying an improved version of tactile sensors capable of sensing different kinds of information. The tactile sensors under investigation must have a simple design and yet possess a flexible interface to a robotic system. In addition, repair must be uncomplicated, and the acquisition of materials easy.

In the experiments to show the capacity of the proposed tactile sensors, a robot called *Athene* is used. The robot is programmed to analyze the tactile image data recorded from tactile sensors and then to classify the object shape under any transformation invariance. The first series of experiments illustrate the robot's optimized grasped capability.

- 1.) Upon gripping the object, the robot lifts the object while adjusting the control force to the minimum before the occurrence of slip.
- 2.) The object is prehended between the robot fingers above the surface.

Prehension forces are then reduced until the first occurrence of slip is detected and the applied force noted as the minimum retention force. This shows the sensor capacity to detect the onset of incident slip. In the second experiment, four different shapes of objects have been used to test the robot's ability in recognizing contact surfaces with the proposed method. The experiment in this study proposes a surface

recognition algorithm that determines the types of contact surfaces by fusing information collected by the tactile sensor system. This algorithm can recognize and localize 3-D objects using a 2-fingered robot hand, on which tactile sensor arrays are mounted.

### 1.3 Resulting Requirements

Since there have hitherto been no theories explaining the real requirements of tactile sensors for robots, the mechanism and operation of the tactile sensors in this research are studied in comparison with humans and their grasping behaviors. Although this is an effective technique in developing tactile sensors for robotic manipulation, the characteristics and requirements of the tactile sensors will be determined by their applications. These are presented below:

1. The sensors must be sensitive to an external force. The sensitivity partly depends on the physical characteristics and the materials from which the sensors are made. Provided that the sensitivity of the materials are identifiable, materials selection can be in accordance with the object to be prehended. Violation of this, i.e., using highly sensitive tactile sensors to lift heavy objects or using insensitive sensors to lift light objects, causes two problems – namely that the sensors will not sense the force lower or higher than certain predefined values. Generally, the sensitivity of the sensor should be appropriate to the weight of the grasped objects.
2. The tactile sensor measurements must be stable and repeatable and hysteresis must be low. Calculation of deviations in linearity between applied and sensed forces is not necessary as several techniques can be used to compensate for many kinds of known non-linearity.
3. Because of their intended industrial applications, the tactile sensors should be robust. However, they should not cause damage to parts, tools or equipment.

[Omata and Terunuma 1992] have mentioned that most tactile sensors lack the capability of sensing certain forces exclusive to humans such as the shear force at the finger tips, the contact surface characteristics, the object stiffness and flexibility. Nicholls [Nicholls 1992] has a similar view and adds that tactile sensors used for robotic grippers must consist of at least two types of sensors. The first type must be able to locate the contact position and to characterize the force distribution between

the object and the grippers. The second type must be able to track some types of mechanical reaction during manipulation, such as unexpected movement or slip.



## 1.4 Organization of the Dissertation

This dissertation is divided into eight chapters. Chapter One discusses the motivations behind the study, the tasks and goals, the expected results, Statement of the Problem, and the resulting requirements. It also outlines the brief content of each Chapter.

Chapter Two reviews the present and past research related to this dissertation. It summarizes the existing technologies used for developing tactile sensors, and discusses their strengths and weaknesses. In addition, the gripping and force-sensing mechanism, and the system used to govern force-control experiments are presented.

In Chapter Three, the robot, tools and equipment used in the experiments are detailed. Then the computer system used to control the robot, the program structure and operations, and the experimental objects are described. This chapter also presents the set of tactile sensors and their components, and the program used to interface with the grippers. It concludes with information about the capacity of the tactile sensors in sensing normal force and shear force on the sensor surface.

In Chapter Four, the operating principles of the tactile sensors, their electronic components and materials are elucidated. In addition, the calibration and characteristics of the tactile sensors developed are described. Noise, sensor linearity, hysteresis and measurement resolution, including the temporal resolution, of the sensor elements are also discussed. The shape of force distribution on the tactile sensor surface during gripping is the last topic of this chapter.

Chapter Five presents experiments and applications. The first section of the Chapter describes optimization of grasping forces from the robot gripper. The second section discusses real experiments, mathematical proofs and statistical results.

Chapter Six discusses contact surface classification methods using tactile data. The first section reviews the experiments used for contact identification. The second section provides details of the experiment model for contact classification. The last section describes real experiments and their results.

In Chapter Seven, all the experimental results including the problems solved by the findings from this dissertation, and issues for further research are discussed. They are separated into sections: summary of results, review of contributions and problem solution.

## 1.5 Statement of the Problem

Generally, when robots manipulate objects, they must do so with a predefined grasping force. By contrast, humans are skilled at manipulating objects with a grasping force maintained only slightly above the minimum required to prevent slipping. They can estimate the weight and friction properties of an object by looking at it and using knowledge based on previous experience. As they grasp and lift the object, they make use of dynamic or “fast-acting” receptors in the skin that respond to small, localized slip that is precursor to gross sliding of the object [Johansson and Westling, 1990], [Srinivasan et al. 1990].

Those receptors enable them to reach a better estimate of the contact friction conditions and thus maintain the normal/tangential force ratio with a margin of safety depending on the task, material and texture of the object being handled. Accurate knowledge of the coefficient of friction is particularly important for gentle manipulation and prehension which is subject to sliding. When performing fine manipulation with fragile objects, it is essential that the grasping forces be maintained between the minimum required to prevent slippage and the maximum before damage occurs. When a pre-determined slip is to be maintained during retention the current and accurate knowledge of frictional conditions is essential to prevent the object from unexpectedly accelerating or ceasing to slide.

Although it is evident that humans benefit from the ability to continually adjust their grasping forces based on incipient slip sensing, comparatively little has been done to provide such capabilities for robots. It is therefore desirable to provide robots with a counterpart to the human ability to obtain continuous and accurate updates of the friction coefficient. A number of efforts have been made over the years to develop sensors that can detect the onset of slip [Cuttino et al. 1988], [Dario et al. 1984], [Dornfeld and Handy 1987]. With varying degrees of success, these sensors are able to detect when an object has begun to slip. However, they all require motion of the grasped object before being activated. In other words, for these sensors to send a signal, major sliding must already have begun, and consequently there is little time to increase the prehension force before significant object motion occurs.

The development of robotic systems capable of operating in unstructured environments to replace human operators in hazardous or inaccessible locations relies on the use of sophisticated sensors capable of discriminating and detecting incipient object slippage for precise and secure object grasping. Normal touching forces, shear forces, or sliding forces in the plane of the contacting surface play an important role in robot sensing and manipulation of objects. To safely grasp an unknown object, an intelligent robot gripper needs to detect the forces in the gripping direction and in the gravitational direction. Thus, a robot gripper should be composed of three-axis force sensors which can detect the forces  $F_x$  (x-direction force),  $F_y$  (y-direction force) and  $F_z$  (z-direction force) or six-axis force sensors which add the capability of detection in  $M_x$  (moment about the x-axis),  $M_y$  (moment about the y-axis) and  $M_z$  (moment about the z-axis).

Surface tractions or stresses acting on an internal material are typically decomposed into three mutually orthogonal components. One component is normal to the surface and represents direct stress. The other two components are tangential to the surface and represent shear stresses. Direct stresses tend to change the volume of the material and are resisted by the body's bulk modulus (which depends on the Young's modulus and Poisson's ratio). Shear stresses tend to deform the material without changing its volume and are resisted by the body's shear modulus. Defining a set of internal datum planes aligned with a Cartesian coordinate system allows the stress state at an internal point  $p$  to be described as relative to  $x$ ,  $y$ , and  $z$  coordinate directions. Since each point in the body is under a static equilibrium (no net force in the absence of any body forces), only nine stress components (3 direct and 6 shear stresses) from three planes are needed to describe the stress state at a point  $p$ . These nine components can be organized into the matrix:

$$\begin{bmatrix} \sigma_{xx} & \tau_{xy} & \tau_{xz} \\ \tau_{yx} & \sigma_{yy} & \tau_{yz} \\ \tau_{zx} & \tau_{zy} & \sigma_{zz} \end{bmatrix}$$

where shear stresses across the diagonal are identical (i.e.  $\tau_{xy} = \tau_{yx}$ ,  $\tau_{yz} = \tau_{zy}$ , and  $\tau_{zx} = \tau_{xz}$ ) as a result of static equilibrium (no net moment). This grouping of the nine stress components is known as stress tensor (or stress matrix). The subscript notation used for the nine stress components have the following meaning:  $\sigma_{\psi\eta}$  is the stress on the  $\psi$  plane along the  $\eta$  direction. Direction of the surface normal upon which the stress acts is  $\psi$  whereas direction of the stress component is  $\eta$ .

## 1.6 Related Work

[Mark 2000] has summarized the history and the current state of the art in tactile sensing and analyzed why past predictions for the exploitation of the technology have not been realized. In the 1970s, despite a great deal of robotic activity, very little research on tactile sensing was conducted. Some good ideas were put forward, but the few devices reported were primitive, for example, adding transducers to detect movement in compliant robot components or detecting contact through force feedback.

By contrast, the 1980s were a period of growth and exploration. A great variety of device designs, transduction methods, and sensing physics were examined during this period. The main transduction methods investigated included resistance and conductance, capacitance, piezoelectric and pyroelectric, magnetic, magneto electric, mechanical, optical, ultrasonic, and strain gauges. A typical device consisted of a surface pad with a linear or rectangular array of scalar-valued sensing points.

Despite the findings of the Harmon survey [Harmon 1982], tactile sensing has not made any significant contribution to real applications in factory settings. Commercial sensors just became available, and there was market potential for low-cost, robust, accurate and repeatable sensors that could easily be integrated into robotic systems. The technology was beginning to mature with the advent of commercial devices, and so it was expected that tactile sensors would be integrated in factory-based robotic systems in the near future [Nicholls and Lee 1989].

In the 1990s, sensors were often silicon-fabricated with tougher and more durable designs. Many new and different materials were examined, and much was learned about the complexities of friction control in human fingers. Systems that could alter the characteristics of a soft contact surface showed promise for future devices, and elastic contact layers have been used in so many tactile sensors.

To date, a variety of tactile sensors have been presented on the basis of various principles such as variation in electrical capacity and resistance, piezoelectric and magnetic effects, and etc. [Raibert and Tanner 1982], [Hackwood et al. 1983], [Dario et

al. 1984], [Novak 1989], [Yamada and Cutkosky 1994], [Hakozaki and Shinoda 2002]. They have played an important role in sensing the friction coefficient [Bicchi et al. 1989] or an object surface condition [Howe 1990]. In particular, the tactile sensors have attracted greatest anticipation for improving manipulation because a robot must detect the distribution of not only normal force but also tangential force applied to its finger surfaces [Ohka et al. 1994]. Material and stability recognition capabilities are advantages of a robotic hand equipped with the three-axis tactile sensors [Takeuchi et al. 1994]. Also, in a peg-in-hole scenario, a robot can compensate for its lack of degrees of freedom with the optimum grasping force allowing an object to move between two fingers using a measured shear force occurring on the finger surfaces [Borovac et al. 1996].

In an attempt to detect the onset of slip signals that occurred before major motion of the object, [Howe and Cutkosky 1989] developed a dynamic tactile sensor for use with soft robotic fingers. Grasp force control based on beginning slip detection was tested by Tremblay, [Tremblay et al. 1992]. Finally, [Howe 1992] has found that skin acceleration sensors can be used with a force reflecting master slave manipulator, thereby permitting a human operator to determine not only how hard the slave gripper is grasping, but also when the grasping force approaches the minimum required to prevent slippage.

Several designs of three-axis force cell have been reported to use magnetic effects [Hackwood et al. 1983], variations in electrical capacity [Novak 1989], [Hakozaki and Shinoda 2002], piezoelectric PVDF film [Yamada and Cutkosky 1994] and a photo-interrupter [Borovac et al. 1996]. Since constitution of the three-axis force cell is more complicated than that of single-axis force cell, it is difficult to develop a three-axis tactile sensor composed of many three-axis force cells. Consequently, the number of elements in the aforementioned three-axis tactile sensor was insufficient for acquiring the spatial distribution of tactile information. It is not required that each component sensor of a three-axis force sensor has the same rated output to accurately detect forces. The six-axis force moment sensors developed in [Yabuki 1990], [Hatamura et al. 1989], [Ono and Hatamura 1986], [Kim et al. 1999], [Kim 2001], [Kim 2000], [Kim 2003] are not suitable for use in an intelligent robotic gripper due to their

low accuracy caused by interference error and size. The lack of any widespread application of tactile sensing is partly due to the difficulties mentioned and also to the lack of availability of commercial sensors with suitable configurations and characteristics.

Typically, tactile sensors do not directly measure the force generated by contact with an object, but instead measure strain in an interposed compliant skin which is a rubber-like medium used for sensor protection and to confer a more stable grasp.

Many array sensors employ a protective cover made from an elastic material which gives mechanical compliance assisting the grasping process and increasing the robustness of the device. However, this configuration raises a serious difficulty known as the inverse tactile transduction problem. When an object is pressed into the surface of an elastic layer, the stresses that will be generated down at the sensing points can be calculated from the material properties and the surface shape. This is called forward analysis. In inverse analysis, the changes on the surface from the sensed data gathered remotely through the elastic medium are computed.

Unfortunately, this does not give rise to a unique solution, as there is no one-to-one correspondence between the stresses deep within an elastic material and those that are applied normal to the surface. In other words, a given pattern of sensory values may be caused by many different physical patterns on the surface. This is known as an ill-posed problem and cannot be solved by direct analysis. It can be seen that elastic materials act as a low-pass filter, only transmitting large-scale spatial patterns and attenuating any fine detail. A useful illustration of the inversion problem and its ill-posed nature is presented in [Nowlin 1991].

Hence, essentially what is required is the solution of the elastic field inverse contact problem. Here, the distribution of forces acting on a boundary of the sensor itself should be inferred from spatially discrete knowledge of the stress field over a surface inside the sensor. Great importance is also given to the measurement of rapid changes in tangential shear force to provide early warning of object slippage. Detection



of incipient slippage which should be accomplished and codified rapidly for prevention of actual slipping is based on fast scanning of the sensors in the contact area.

The mathematics for this problem, known as the tactile inverse problem, has received much attention, and there are several ways to deal with such problems. Recent sensors capable of detecting texture, stress changes, the various stages of dynamic slip, and other temporal contact events have been produced. By using several complementary sensors with different response rates, an integrated system can process a range of contact features for a given sensing problem. Also, while compliant materials have essential properties for some tactile tasks, it has been shown that rigid contact must be established if dynamic properties of objects are to be sensed through tactile means [Ellis et al. 1994].

## 1.7 Major Contributions of This Dissertation

This dissertation describes a new type of tactile sensor and an improved version of the dynamic tactile sensing approach that can provide a regularly-updated and accurate estimate of applied force for use in the control of manipulation. The sensor performs similarly to the human tactile receptors described by [Johansson and Westling 1987]. When the finger is pressed against an object, it compresses to conform to the surface of the object.

In addition, the studies showing continuous adjustment of force to stabilize gripping, particularly during motion, have been reviewed. This prehension force adjustment occurs simultaneously with, or slightly ahead of, fluctuations in load forces. They may therefore be seen as anticipatory, and it is argued here that a key purpose of research in manipulation should be to understand the integration of sensory motor information in building an internal model of the object and the effector system in order to support such anticipation.

A strategy by which a controller can repeatedly and accurately estimate the pre-slip at the contact point between a gripper finger and an object has also been developed. This information is further used to control the grasping force. The results can show by using tactile sensors detect the beginning of slip and normal and tangential forces at the robot-gripper. This approach is similar to responses reported in the physiology literature for human subjects [Johansson and Westling 1987].

Moreover, this dissertation presents a scheme by which a manipulator can use dynamic tactile sensing to detect when it is about to lose hold of a grasped object and can take preventive measures before major sliding occurs. By detecting localized slippage on the gripping surface preceding major slip, the controller can modify the grasping force to prevent the object from further slipping. Also, by monitoring normal and tangential forces at the contact when these "incipient" slip signals occur, the controller has the capacity to obtain an accurate estimate of the applied force, which can then be used during the manipulation task.

For the processing of tactile signals, the use of image-processing techniques is emphasized in the study. Many have been derived from computer vision research and applied to static images from array sensors. Some statistical methods are adapted for the extraction and recognition of features. Segmentation methods using edge extraction, threshold, filtering and boundary growing are all employed. Geometric measures and the method of moments are also used. Moreover, for the proposed techniques, the importance of dynamic events is recognized, and sensors have been developed for detecting stress changes, slip and other temporal contact events.

The developed tactile sensor has been integrated with a robot-gripper. A system to measure the pattern of the object surface by using the tactile inverse problem proposed and evaluated in this research has been developed. The study also introduces the mechanical filter effect depending on touch motion.

From the experiments in this study, a contact recognition algorithm which determines the types of contact surfaces by fusing information collected by the tactile sensor system is proposed. This algorithm can recognize and localize 3-D objects using a 2-fingered robot hand, on which tactile sensors are mounted.

This dissertation describes and proposes enhancements to the proposed tactile sensor capable of detecting both normal and tangential forces. A method to estimate the six-axis force from the quadric surface of the contact areas by taking into account the first contact surface displacement caused by a normal force has been designed. A series of calibration experiments using a manipulator-mounted tactile sensor and a commercial six-axis force sensor have been conducted to evaluate the component of force and determine the behaviors included in the contact area.

Subsequently, the tactile sensor is mounted at the end of a robot manipulator touching hard object specimens such as rigid balls. From the experimental data, the tactile sensor can detect not only normal forces but also tangential forces, including the case when a ball being rotated, pushed and/or pulled. However, tangential sensitivity variations resulting from the behavior of the electric field in tactile sensor elements can also be found.

The main contributions of this dissertation are listed below. Although some of them have been achieved in other experiments, their co-occurrence is relatively rare. More importantly, a simultaneous presence of all contributions has not yet been accomplished.

- Adaptive algorithm exploiting the minimum force for an object manipulation;
- Understanding of the behavior of the new tactile materials for contact classifying applications and successful results;
- Proposed model for the interaction force in the new tactile sensor, evaluated model and the study of its impact on touch encoding to derive six-axis force sensing;
- Study of the impact of threshold values on control of the gripper and the solution of this problem;
- Innovative design taking into account the test environment to maximize the flexibility of robot control.

## CHAPTER TWO LITERATURE REVIEW

### 2.1 Robot tactile sensing

Chapter Two presents a literature review of research conducted on tactile sensor-oriented methodologies for robotic manipulators. Much of the work has been prompted by industry's need to understand this area in order to increase the efficiency of robotic manipulators in manufacturing.

Previous studies in the field have been compiled by [Nicholls and Lee 1989] and [Nicholls 1992]. Among these, of particular interest are implementations practical for robotic manipulation, a list of which is provided in the table below. The table includes information on their density of cells per mm<sup>2</sup> and size of arrays which have been built.

	Transducer principle	Author/Research Group Implementation	Density Cells/mm <sup>2</sup>	Size of Array
1	Piezoelectric	(Dario 1982) (Howe 1989) (P. Dario et al. 1983) (Patterson 1986) (R. D. Howe et al. 1993) (Gaetano et al. 1998) (Y. Yamada et al. 1998) (Hyungtae Kim et al. 2002) (Atkinson 2003) (Todorova 2004) (Krishna 2004)	28.44	8 x 8  5 x 5 15 x 15

2	Piezoresistive including Strain gauges	<p>(Tamai 1982)  (Wong 1985)  (Buttazzo 1986)  (Tise 1988)  (Patterson et al. 1986)  (Speeter 1988, 1990)  (Friedrich 1995)  (Daniel Castro 1997)  (Fiorillo 1997)  (Sugiyama et al. 1990)  Tactile Matrix Sensor,  JRA Technology Ltd.  (Model400, Interlink  Electronic, Inc., Camarillo,  CA 2001 )  (Nicholas J. Droessler  2001).  (Claire M. Seguna 2000)  (C. M. Seguna, M. A.  Saliba 2001)  (Lomas 2003)  (Noda 2006)</p>	<p>1.58  40.96  4  0.16  1.77</p>	<p>16 x 16  16 x 16  32 x 32  4 x 4  8 x 8  12 x 12  5 x 5</p>
3	Thermal	<p>(Monkman and Taylor,  1993)  (Yuji 2002)  (Yamamoto 2005)</p>	0.25	
4	Ultrasonic	<p>(Hutchings et al. 1994)  (Ando and Shinoda  1995,2002)</p>	0.31	<p>16 x 16  2 x 2</p>

5	Magnetic/Inductive	(Checinski 1985) (Luo 1985) (Vranish 1985) (Patterson 1985) (Hasegawa 2004, 2005) (Murayama2005)		
6	Capacitive	(B.L. Gray 1996) (E. Nicolson 1995) (Castelli 2002) (Fan-Gang 2004)		8 x 8 8 x 8 8 x 8
7	Electrochemical	(De Rossi 1989) (Masato 2006)		
8	Opto-electronic	(Rebman 1985) (King 1985) (Mott 1985) (Begej 1988) (Winger 1988) (Jenstrom 1989) (Schoenwald 1992-1997) (Maekawa et al. 1992b) (Bertholds 1987) (Eghtedari 1989) (Yamada 2002) (Ohka 2005) (Rossiter 2005) (Mazid 2006)	0.08	10 x 10  4 x 4

Table1. Implementations of array sensors and their densities in units per square millimeter.

As can be seen from table 1, the commonest sensors used in tactile arrays are of the piezoresistive types. They tend to be of small size, fast response and their ease of fabrication and integration makes them ideal.

## 2.2 Sensing technologies and Analysis Techniques

Many physical principles have been exploited in developing tactile sensors. In most cases, development is largely application-driven. It should be recognized that operation of touch or tactile sensors to a great extent depends on the materials of the object being acquired. For its strengths and weaknesses to be analyzed, a particular design needs to be considered in terms of its application. Since parallel-jaw robotic manipulators with flat internal sensors are capable of grasping either round or flat objects and are a simple application used in most industrial environments, robotic manipulation of this type is the topic of this research study.

From the designs listed above, the works of [Fearing 1990], [Maekawa et al. 1992], [Russell 1987], and [Speeter 1988] were indicated to be well-suited for flat-finger geometry. Among these, Speeter's tactile sensors achieved the highest sensitivity with the minimum sensed force of only 0.3 Newton. In comparison, Fearing's design had the sensitivity with the minimum sensed force of 0.5 Newton. The optical wave-guide design of [Maekawa et al. 1992] had the same resolution as that of [Fearing 1990]; however, it could provide only information on contact area and net force, but not pressure distribution.

Piezoelectric properties are used for the development of transducers which convert kinetic energy into electrical energy. Crystalline materials which exhibit piezoelectric properties are used to make the elements used as tactile sensors. However, there are also polymeric materials which exhibit piezoelectric properties. These have the advantages of robustness and flexibility to externally applied forces. Among several types of polymeric materials, polyvinylidene fluoride (PVDF) is frequently selected for use in sensors because of its low cost and good mechanical properties. It is characteristically supplied in sheet form in varying thicknesses between 5  $\mu\text{m}$  and 2 mm. A thin layer of metal is attached to both the upper and lower sides of the sheet so that it can collect the charge and permit electrical connections to be made. Although not piezoelectric in its raw state, PVDF can be made piezoelectric by heating in an electric field. In addition, it can be molded. Hence, PVDF has a number of benefits, including its property to be used as an artificial robot skin.



A few research studies have been conducted on use of tactile sensors on objects in motion. In their experiments, [Bajcsy et al. 1986] attached a plastic “fingernail” to the rear of robot fingers comprised with small measurement units called ‘piezoelectric’ elements, which responded to variations in surface height as the nail pressed against an object. It may be possible to analyze the signal from this sensor to find details of the surface finish; nevertheless, because the nail does not form part of gripping surface of the finger, the signal generated may not be an actual representation of variations in the object surface. As a result, this sensor cannot be practically used for robotic manipulation.

Similarly, [Patterson and Nevill 1986] has developed an induced vibration sensor capable of recognizing small shapes and textures. For these types of sensor, large areas of piezoelectric film were excited by vibration induced in a ridged rubber skin when the sensor slides against a surface. Because of complicated interactions between the sensor and the test surface, the analysis is difficult. For instance, signals vary greatly even with minute movements of the test object. However, repeatable results may be obtained, and the sensor is capable of identifying the test object from among a list of candidates provided that other conditions are controlled and pattern-recognition techniques on the power spectrum of signals are used.

Piezoelectric materials in the polyvinylidene fluoride (PVDF) family, a type of polymeric materials, can be used to develop transducer arrays of tactile matrix sensors, particularly large ones. These materials have become popularly used because of their unique properties, two of which are that they can be used to develop force sensors with the thickness of only 5 mm and they have high sensitivity to minute external forces.

[Canepa et al. 1998], for example, used PVDF materials in developing tactile sensors capable of sensing incipient slip between the object and the surface of tactile sensors. This was made possible by information on the normal and shear stress delivered by PVDF arrays. Following the work of [Howe and Cutkosky 1993], [Dario et al. 1984] used film-like PVDF materials to develop tactile sensors with high flexibility and very high sensitivity. After that, their sensors were further developed so that they could identify the characteristics of the grasped object surfaces, making their research

well known in the field [Patterson and Nevill 1986]. Moreover, Dario et al. used the film-like PVDF to develop stress-rate sensors which were then applied in examining conditions during prehension thus increasing further the effectiveness and activeness of their robotic manipulator. It may be claimed that they are the very first researchers who used PVDF materials to develop active tactile sensors.

As discussed earlier, PVDF materials used in developing tactile sensors have an advantage over other types of materials in that they can be developed with a very high degree of thinness and measurement resolution. In addition, they are very cheap and moldable. The most recent technology using PVDF materials is 'phase-array transducer' which has a much more complicated design than other tactile sensor arrays. This transducer is expected to receive more popularity in applications in the future.

What follows presents the drawbacks of using PVDF in developing tactile sensors compared with other types of materials. This is based on the summary of [Carlson 2000], [Lee and Chu 2005] and [Najarian et al. 2006]. The first drawback of PVDF is unequal response rate from each sensor. This is because each sensor is of a different size, resulting in its different response rate despite an equal external applied force. An even greater different rate will be found if the PVDF materials are from different manufacturers. The second drawback is its fragility when compared with other types of materials used for developing tactile sensors. Thus, applications of sensors made from PVDF materials risk easy damage. The third drawback of using PVDF is phase-array electronics are scarce. At present, there is only one distributor of this device. Hence, the selling price is relatively high. However, several companies are interested in producing phase-array electronics, so this limitation may soon be resolved. The next drawback is difficulty of material modifications before applications as each sensor has its own response rate. Besides, it has unequal degree of non-linearity. The solution to these problems is to sort the materials according to their response rate.

In recent years, researchers have found some new techniques for designing and applying tactile sensors. One successful commercially available product is the

Force Sensing Resistor (FSR) which has been developed by Interlink Electronics. The Resistor is a semiconducting polymer-thick film (PTF) device which exhibits a decrease in electrical resistance with any increase in applied mechanical force to the active surface. The FSR has similar applicational properties to a load cell or strain gauge, but the technology and sensitivity are more comparable to that of the semiconductor strain gauge.

A force sensing resistor is a piezoresistive polymer, whose electrical resistance changes in a predictable manner following the application of a mechanical force to its surface. It is normally supplied as a polymer sheet with a sensing film applied by screen printing. The sensing film consists of both electrically conducting and non-conducting particles suspended in matrix. The particles are of submicron size, and are formulated to minimise temperature dependence, improve mechanical properties and increase surface durability. Applying a force to the surface of the sensing film causes an improvement in the conductivity between the conducting electrodes, and hence reducing the electrical resistance of the film. However, in addition to its good sensitivity to small external forces the FSR does exhibit a small degree of temperature-dependence. Though flexible, there are limits to which it can be bent to fit the necessary radius of curvature of a robot gripper finger [Seguna and Saliba 2001].

Strain gauges have also been widely used in tactile-sensor development. A strain gauge when attached to a surface will detect a change in the length of material as it is subjected to an external force. It can be manufactured from either resistive elements (foil, wire, or resistive ink) or semi-conducting materials. A typical resistive strain gauge consists of a resistive grid bonded to an epoxy-backing film. A semi-conducting strain gauge is fabricated from a suitable piece of doped silicon. In this case, the mechanism in resistance change is the “piezo-resistive effect”. Semiconductor strain gauges can several hundred times more sensitive than wire strain gauges but suffer from slight non-linearity and higher temperature dependence. When used for robotic tactile applications, the strain gauge is normally used in two configurations: as a load cell, where the stress is measured directly at the point of contact; or with the strain gauge positioned within the structure of end-effectors.

Less frequently used technology includes thermal techniques whereby the flow of heat to or from the object can be measured. Typically, a current flowing through a thermal sensor (resistance thermometer or thermistor) causes it to heat which in turn results in an increase in electrical resistance. Contact with an object causes heat to flow from the sensor into the object material thus resulting in a lowering of temperature and a subsequent reduction in resistance. Such devices tend to be slow, however Peltier elements or infra-red pyrometers which deliver better temporal characteristics have also been used [Monkman and Taylor 1993]. The use of a small Peltier heat pump allows the construction of a much faster-acting thermal sensor. The heat pump is sufficient for many VR simulation purposes, because the human thermal comfort zone lies between 13 and 46 °C and the working range of heat pump is 10-65 °C [Burdea 2003].

Ultrasonic tactile sensors are based on instantaneous localization of acoustic emissions caused by touch and/or contact movement. One method uses a sensor structure which consists of an ultrasonic emitter on the flexible sensor-body and a sound-sensing matrix embedded at the center of the body. Any points on the sensor surface work as emission sources when touched and the body transmits the waves inwardly. The matrix works as a wideband acoustic emission transducer which is capable of detecting arrival directions of acoustic waves, packet by packet. This means it has to resolve and localize a series of ultrasonic emissions caused by touch and slip. The second method employs ultrasound to measure the thickness of an elastomeric pad. The sensor uses a thin rubber pad that is deformed when an object is depressed into it. The amount of deformation depends on the magnitude of the force applied to the object and the stiffness of the rubber. Beneath this rubber pad is a two-dimensional array of ultrasonic transmitters and receivers that are used to measure the thickness of the rubber pad. A tactile sensor with a number of elements (arranged as an array) has to measure thickness of the elastomeric pad through the use of ultrasonic pulse-echo ranging. The strength of the echo pulse depends upon the acoustic properties of the rubber pad and the material contacting the pad. This pulse amplitude is not measured but only the time-of-flight of the pulse.

[Ando and Shinoda 1995] describe a tactile sensor based on ultrasonic emission. Their system consists of a flexible spherical fingertip and a sound sensor at the center of the fingertip. Contact points act as emission sources and the sensor works as a direction-sensitive, wideband acoustic emission transducer. This sensor can distinguish multiple contacts but errors in position estimation of the contacts are as large as several millimeters. In order to realize this type of mechanism it is necessary to solve two important problems: 1) What kind of ultrasonic emissions appear by touch, and are they detectable? 2) How can the multiple wave packets be resolved and localized instantaneously? Based on work [Hutchings 1994], for either no object contact or contact with a metal object, large echo signals are produced. Also, the echoes produced by many plastic materials, liquids, and biological soft tissues can be undetectably small since their characteristic acoustic impedance is close to that of the covered material (elastomeric pad). Air trapped in the cells of the elastomer has a detrimental effect on its ultrasonic reflection characteristics and the elastomer used must have a relatively constant coefficient of friction.

Magnetic-based sensors have also been used in industry. There are two approaches to the design of touch or tactile sensors based on magnetic transduction. Firstly, movement of a small magnet by an applied force will cause the flux density at the point of measurement to change. Detection of magnetic field changes is achieved either by a Hall element or a magneto-resistive device. Secondly, the core of a transformer or inductor can be manufactured from a magneto-resistive or magneto-elastic material of which magnetic characteristics are modified when subject to a change in the external physical force. This material will deform under pressure and simultaneously cause magnetic coupling between the transformer windings and the coil's inductance. That is the external force will result in an inductance change. Although the field intensity of this type of sensors follows an inverse relationship leading to a nonlinear response, this can be easily linearized by mathematical processing. The major disadvantage lies in its size and complexity which makes the production of large arrays difficult and expensive.

Capacitive based sensors are another technology popularly adapted as tactile sensors. These types of sensor rely on applied forces which either changes the

distance between two plates or the effective surface area of a capacitor. As a result, the capacitance of the tactile sensor at a specific elemental position will change. In such a sensor, the two conductive plates are separated by a dielectric medium. The higher permittivity of the dielectric increases the dynamic range which its elasticity provides an effective return spring mechanism. To measure changes in capacitance, a number of techniques can be applied, the most popular one being use of a precision charge source. Another technique is to use elements of the sensor as part of a tuned or LC circuit and measure changes frequency.

Because of the ability to manufacture very small elements, capacitive sensor arrays have found recent cost effective application in fingerprint recognition systems. Their applicability to robotics is somewhat limited in that they provide only binary images over relatively small areas.

Research work on other types of tactile sensors was well summarized by [Nicholls and Lee 1989]. Among those, capacitive tactile sensors are relatively reliable, easy to construct and inexpensive. Three capacitive tactile sensors using capacitive-strain measurement techniques were developed based on the earlier design of [Fearing 1986]. Nonetheless, they had a slow response rate, i.e., exhibited a much larger time delay than that found in other types of force sensors such as Son's design [Son 1996]. This is due to several factors, most notably the time required to scan and process array information, the time required to compute velocity commands, and the time consumed in transmitting commands to the host PC. A significant problem with capacitive sensors is hysteresis [Boie 1984], which cannot be compensated for computationally. However, when compared with other types of tactile sensors, it can be said that capacitive tactile sensors have escalated the performance of robotic manipulation in the field of sensor-oriented technology.

Developments in electrochemical micro sensors is mainly concentrated on chemiresistors and potentiometric micro sensors. Classification of electrochemical micro sensors follows directly from Ohm's law: *potentiometric* from measurement of potential, *amperometric* from measurement of current, and *chemiresistors* from measurement of resistance. The schematic of a chemiresistor consists of a pair of

contacts deposited on an insulating substrate and a selective layer whose conductivity is modulated by the interaction with the electrolyte. The response signal is obtained by applying a constant current and measuring the resulting voltage difference at the electrodes. The chemical modulation of the signal may occur in the bulk of the selective layer, at its surface, or interface with the insulating substrate or at the contacts. The mechanism is relatively simple but the exact origins of the signal are often difficult to determine. Because of this uncertainty, the interpretation of the response in terms of the concentration of the electrolyte is complicated. All of these factors and their unpredictable combinations make the rigorous interpretation of the chemiresistor results quite difficult.

Potentiometric sensors derive the analytical information from an explicit relationship between the potential of the indicator electrode and the concentration in the sample. Because the potential of a single electrode cannot be measured a second, so-called reference electrode is introduced. The macroscopic potentiometric on-selective electrodes for liquid or gas measurements represented the largest group among all chemical sensors. The reasons which make potentiometric sensors particularly suitable for miniaturization is that the magnitude of the signals do not depend on the size of the sensing area. However, the power of the measured signal is very small, and its measurement requires a high-input impedance amplifier. Potentiometric sensors have only limited usefulness due to their vulnerability to changes of buffer capacity of the sample and its adverse effect on individual reactions (J. Janata 1989).

Optical technology has also been widely applied in the development of a wide range of tactile sensors. The operating principles of optical-based sensors fall into two classes: *intrinsic*, where the optical phase, intensity, or polarization of transmitted light is modulated without interrupting the optical path; *extrinsic*, where the physical stimulus interacts with light external to the primary light path. Intrinsic and extrinsic optical sensors can be used for touch, torque, and force sensing. For industrial purposes, the most suitable ones are those which require the least optical processing. For example, detection of phase shift using interferometry is not considered a practical option for robotic touch and force sensors.

There are also other optical technologies employed in developing optical-tactile sensors. For instance, 'photo-elasticity' is a phenomena where externally applied stress results in changes in an optically-transparent material. The polarization of light transmitted through a photo-elastic medium subjected to an applied external force undergoes rotation. This results in changes in effective light intensity when the outgoing light is passed through a plane polarizer.

Photo-elastic sensors are of considerable importance in measuring the degree of slip of the object being gripped. The force sensitivity is determined by a spring or elastomer, and the sensor can be constructed with source-receiver fiber pairs embedded in a solid elastomeric structure. The intensity of received light is a function of distance, and hence applied force. The amount of light transmitted to the receiver is determined by the applied force which changes the thickness of the clear elastomer. By using a number of matrices of transmitter-receiver pairs, the tactile image at the contact points can be determined. Although the optical fibers described are solely for transmission of light to and from the sensor, they can also be used to develop tactile sensors.

Two major drawbacks of many simple optical-tactile sensors are their size (too large to be attached to robot grippers fingers), and their operation and data processing (which is often too complicated for use in industrial environments). Despite these, a suitable design based on internal-state micro-bending of optical fibers can be a solution. Micro-bending is a process of light attenuation in the core of fiber when a mechanical bend or perturbation (of the order of few microns) is applied to the outer surface of the fiber. The degree of attenuation depends on the fiber parameters, which include the radius of curvature and spatial wavelength of the bend.

Like capacitive arrays, optical sensor arrays in the form of back-illuminated CCD cameras with light reflective elastomeric coverings have also found recent application in fingerprint recognition systems. Likewise, their applicability to robotics is similarly limited.



Use of materials with defined force-resistance characteristics has also received considerable interest in touch and tactile sensor research. The basic principle of these types of sensor is electrical resistance or conductivity measurement between two points on a conductive elastomer or foam. The majority of sensors use either semiconducting polymers or elastomers consisting of carbon-impregnated rubber. The resistance of elastomers changes in accordance with the applied external force resulting from the deformation of elastomers which alters the particle density. The majority of industrial analogue tactile sensors are based on the principle of piezoresistive sensing. This is due to the simplicity of their design and interface to robotic systems.

In conclusion, the choice of transducer, modality, and passivity will depend largely on the sensor application. A combination of these sensor techniques can yield highly reliable information for a wide range of applications. Areas of most interest include contact location, contact force, local shape, slip and vibration direction. In dexterous end-effectors, the force and relative motion between the grasped object and the fingers also needs to be controlled. This can be done by using a set of sensors capable of determining the magnitude, location, and orientation of the force at a contact point in real-time. Attaching miniature force sensors around the robot fingers to enable a kinesthetic sense equivalent to that found in humans is one approach.

In Chapter Three, tactile sensors developed for robotic manipulation using piezoresistive principles are proposed. Materials used for developing tactile sensors used in this research consist of elastomeric foam which is well known for its mechanical compliance. Foam is generally used to wrap fragile objects like glass, but the type used in the present study is that used for containing electronic devices because of its electrostatic discharge properties. Hence, it is sometimes called ESD foam.

Foam is normally made from artificial rubbers or similar polymers, which can be classified into polystyrene, neoprene, polyethylene, polyester-based polyurethane, and others. The most used ones are polyethylene and polyurethane, and the materials are thus called polyethylene-based foam (PE-Foam) and polyurethane-based foam

(PU-Foam) respectively. These foams are used to surround the fingers of robot grippers and can be molded or bent into any desired shape.

The tactile sensors proposed in the present study work by measuring a change in electrical resistance. To sense the force distribution exerted on the tactile sensors by object contact, part of the surface of the compliant material is covered with a grid of electrode pairs, and the resistance between the electrodes of each pair is measured. In other words, the resistance change is a result of the pressure on the foam - which consequently retracts. This type of sensors allows an easy construction of a tactile image of good resolution, depending on the designed density of grid arrays.

Due to their simplicity of design and interface to robotic systems, for this research, a sensor prototype of this form was built. Experimental analysis of its behavior demonstrates both its feasibility and its limitations.

From the above discussions, it would be reasonable to rely on most important features used in designing tactile sensors, e.g.

- 1) capability in measuring the magnitude, direction and point of action of the external force applied on the finger body,
- 2) lightness in weight so that they cause no errors during fine control of finger joints,
- 3) high sensitivity to sense external forces (including normal and shear forces),
- 4) good dynamic range and reasonable spatial resolution of at least 2 mm with fast response of at least 100Hz,
- 5) low hysteresis and temperature drift,
- 6) enough compactness to be housed in a finger body and
- 7) good linearity is desirable, though some degree of non-linearity may be tolerated.

### 2.3 Sensing and manipulation

The amount of force between the robot gripper required to retain an object is a good representation of interactions between a robot and its environment. Success in controlling the force depends on the application of force-measurement materials.

Robotic manipulation requires well defined and orderly steps in which the conditions of touch between the robot fingers and the grasped object are precursors to reducing errors in the prehension position. Although each step varies with movement and the order of movement which can be pre-determined, it is also subject to the pattern of sensing reaction during contact. As there are several alternative patterns to a single reaction, a degree of decision-making must be made.

The objective of using tactile sensors for robotic manipulation lies in that a robot is able to lift an object from its existing position to a higher one, then move it in other directions, and finally place it at a given destination. All these require that the force sensors be able to identify characteristics given by an objects surface.

One of the problems involved is manipulation. There have been numerous research studies conducted on active manipulation, but none have successfully yielded tactile sensors capable of identifying the characteristics of the prehended object and hence the strategies required to retain it. The next problem concerns the properties of the object surface, including both geometric and weight factors. These must be characterized for robot analysis and processing during the prehension and retention sequence. This is further complicated by the fact that different types of tactile sensors require different analytical and processing algorithms.

It has been mentioned earlier that robotic manipulation requires well-defined and orderly procedures. One of the papers showing these features was the experimental work of [Howe 1990], concerning the pick and place of an object of previously unknown weight. In their research, tactile sensors were attached to the robot fingers, and thus the degree of slip and slip acceleration could be identified during robotic manipulation.

The research was divided into five stages, including the pre-contact stage, the manipulation stage, the optimization stage, the unloading stage, and the post-contact stage. Each stage had its own explanatory theories and function-control procedures. The completion of each stage was signalled by different 'events'.

Event-driven manipulation programming as in the above has been employed in several studies under different names. For instance, [Brooks 1985, 1987] used the term 'presumption architecture' in his research. [Howe and Cutkosky 1989] explained 'event' as sensing measurement which occurs during robot or robot-part movement, and this was applied in their algorithm to drive gripping. Later, [McCarragher and Asada 1993] used the term 'transitions to drive an assembly algorithm' in their research.

## **2.4 Sensing global shape**

Arrays consisting of 16 x 4 tactile sensor elements, mounted on the inner sides of the gripper fingers, have been used in experiments for this research. Consequently, during prehension of an object, both sides will retract, depending on the shape of the object. The force distribution on both sides of the tactile sensors will be in accordance with the shape of the object. To achieve discreteness in force distribution and enable identification of the global shape of the prehended object, a Non-Uniform Rational Basis Spine (NURBS) has been developed which allows interpolation of the force distribution on the sensor elements. As a result, the three-dimensional information derived will yield a more precise representation of the grasped object [Piegl and Tiller 1997].

However, there are applications for contact classification and shear and moment force sensing in chapter six and seven where quadric surfaces will be used for the presentation of object geometric features independent of the resolution of the tactile sensor. The quadric surface approach is a simple, yet adequate, method for the proposed tactile sensor as the dimension of the tactile array (16x4) cannot represent a complex object surface.

## 2.5 Control System

An expert system is a system which employs human knowledge stored in a computer to solve problems that ordinarily require human expertise [Turban 1992]. The system simulates judgment and behavior of a human or an organization that has expert knowledge and experience in a particular field. Typically, such a system contains a knowledge base consisting of accumulated experience and a set of rules for applying the knowledge base to each particular situation described by the programming codes. Sophisticated expert systems can be enhanced by addition of information to the knowledge base or to the rule base.

In Chapter Four, strategies that enable an expert system to adapt to, or learn from, interactions with object manipulation and object approaching will be described. It is assumed that a relatively primitive computer-based adaptive capability can be of significant value in a problem-solving environment in which a computer is used as a collaborative decision-support tool. Because of its capability to support rule-based programming and object-oriented design, the Microsoft Visual C++ (VC++) Version 6.0 and SQL database have been chosen as an expert system tool for this project.

## CHAPTER THREE

### SYSTEM OVERVIEW

In this Chapter, the task and the whole system including the basic hardware structure and supporting software for robot control and experiment will be described. The basic idea, design, construction and software integration of the tactile sensors are discussed.

#### 3.1 System Configuration

In this research, *ATHENE* (shown in Figure 3.1) was used. A 6-DOF articulated arm with 2-finger grippers, 2-DOF on waist and stereo vision system enabling the robot to move in 3D dimensions is mounted on the mobile platform. There are tactile sensors covering the surface of the 2-finger grippers on all four sides and their tips. The tactile sensors are used to sense force and moment data during prehension operations.



Figure 3.1: *ATHENE* Robot

The service robot *ATHENE* has been designed to operate in indoor environments like offices and warehouses. It has 1.95 meters in height and can reach and grasp from normal-sized tables. In the tactile module, the analog-digital converters (ADC) are coupled to a 16-bit microprocessor via multiplexers. The tactile controller is equipped with a CAN-bus interface and mounted onto the gripper module. The sensor module is plugged into the CAN-bus and the power supply cord of the manipulator- It can be

handled like an additional module, i.e., the sensor data can be read through the CAN-bus interface of the PC. The robot consists of:

- 1) A robot arm with seven degrees of freedom (DOF) and kinematics similar to human arms;
- 2) Parallel jaw grippers with tactile sensors;
- 3) A dual color-CCD stereo camera head with two degrees of freedom (DOF), controlled by software, to provide visual feedback to the robot;
- 4) An image acquisition system with two PCI bus frame grabber boards (IC-P2M) manufactured by Imaging Technology Inc.;
- 5) A computer network and a microprocessor network.

The *ATHENE* robot is a *Centaurus* with the mobile platform having three wheels. The single front wheel is the control wheel (for driving and turning), and the two rear wheels are passive wheels. Above the mobile platform are the mechanics of the 6-DOF manipulator. This consists of the waist, the shoulder, and the right hand at the tip of which the tactile sensor is installed. The neck of the robot has 360-degree rotation and can tilt. Its eyes comprise of two cameras, each of which can move to the left, right, up and down.

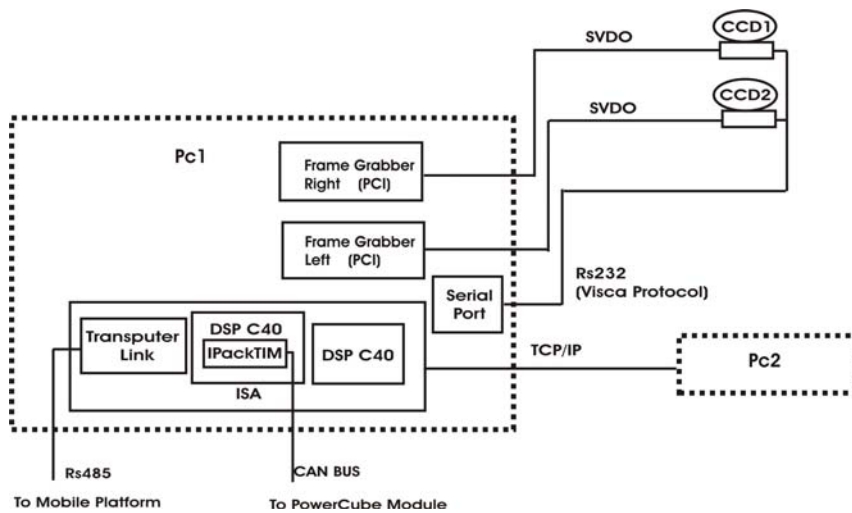


Figure 3.2: Hardware Configuration 1

From the hardware configuration above, the system consists of two computers connected by TCP/IP Protocol. One computer is the PC2, in which no special hardware is installed. Its function will be discussed later. The other is the PC1, which directly controls all the operating mechanisms of the robot.

The primary mechanisms are the two robot eyes which can pan and tilt according to signals transmitted to them from the computer through the serial port using the VISCA protocol, which is a special characteristic of this type of camera. The Super Video (SVDO) signals from both cameras are connected to the two frame grabbers. The hardware operation sensing the visual signal is controlled by the processing unit in its corresponding computer.

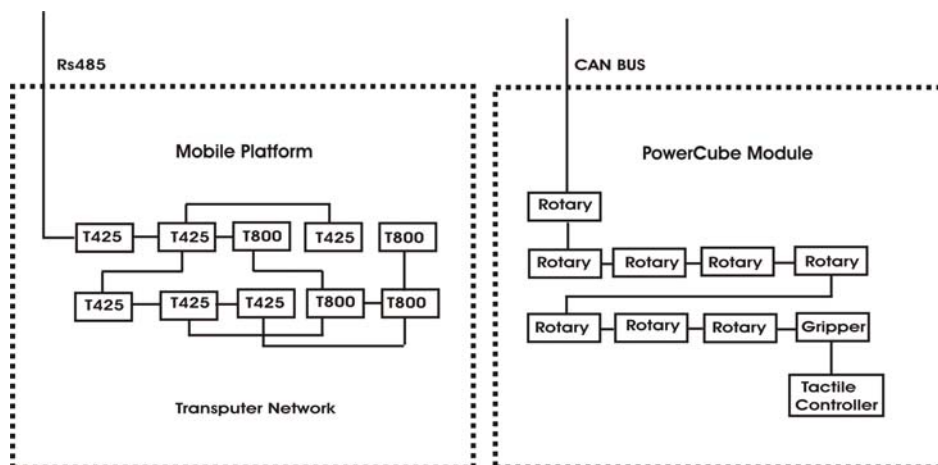


Figure 3.3: Hardware Configuration 2

The secondary hardware consists of the arm controller, grippers, tactile sensors, and the neck. These components receive control signals from the CAN-bus in the form of CAN-Protocol data transmission. The processors of this computer consist of three types. The first one is the processor of the computer itself. The second are two 32-bit 40MHz digital signal processors (DSP), manufactured by Texas Instrument and connected to the computer processor through the PCI bus. The connection between these two processors is through their ports. One of the processors is installed with the IpackTim CAN-module functioning to transmit data using the CAN-Protocol.



Commands are sent from the computer processor through the first and then second DSP via the CAN-module to the CAN-bus and finally different modules of the robot-arms including the tactile sensors.

The final hardware mechanism is the mobile platform which has a large number of 8-bit microcontrollers (Transputers). In controlling the mobile platform, commands are sent via the DSP to the first Transputer CPU in the set. From the above, the processors in this control set include:

- 1) Intel Pentium IV CPU, which controls programming operations on the PC1 and the PC2;
- 2) DSP processors, of which the control programs are loaded on the PC1 only during operation;
- 3) Transputer CPU, which, like DSP processors, are loaded on the PC1 only during operation;
- 4) Microprocessor on the tactile controller (whose control programs have been written and developed before being burnt on EPROM of the tactile controller) which commence their function when energy is distributed to the robot. This is an additional 16-bit 20MHz microprocessor.

It should be noted, however, that all programs in each processor function independently and consist of sub-programs which examine their communication with other processors. As such, the central processor will be responsible for data transmission and transfer from one processor to the others. Different processing programs have different compilers, which can be summarized as follows:

- 1) TLINK C compiler used on the Transputer CPU in the mobile platform;
- 2) Parallel C compiler used on the DSP processors;
- 3) Tasking C compiler used on the microcontrollers of the tactile controller;
- 4) Microsoft Visual C++ used on the two PC's.

## System Software for Robot Control

The software structure for robot control consists of two parts. Their relations are shown in Figure 3.4.

Each part functions on different computers. On the PC1, the MISSION software retrieves data from the two cameras of the robot using the frame-grabber hardware. The image data are processed and stored in the database engine operating on the PC2. These image data include the current object image data and robot-gripper image data. These two pieces of data are processed to enable successful approach and prehension. In addition, the MISSION software stores data from the tactile sensors in the database, and controls all robot movement.

The software operating on the PC2 is the BrainThread, which also connects to the database. It uses data from the database for robot operational decision making. Another parallel program operating with the BrainThread is MATLAB, which performs mathematical processing. Because of its speedy operation enabled by its optimized relations to the processors, the program is used for some types of calculation. When the BrainThread software performs certain calculation tasks, the data will be transmitted to the MATLAB software, which processes and stores the results. Both types of software are connected by a "wrapper". Wrappers are a type of software, or more specifically, "glueware" that is used to attach together other software components.

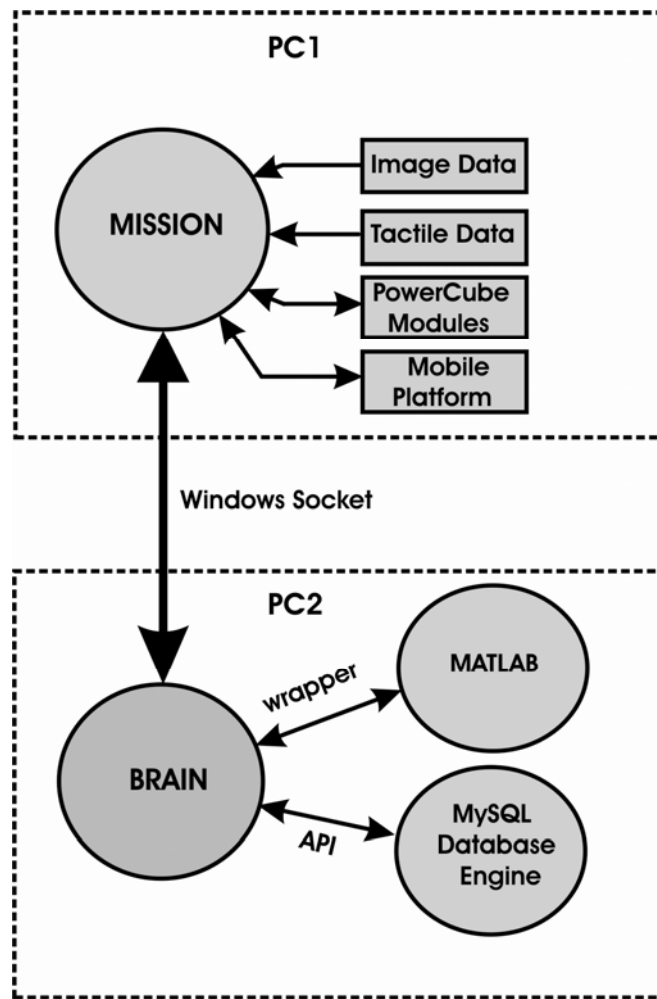


Figure 3.4: Software Architecture

All software operations are shown in Figure 3.5. Operations start when data from the left and right eye images stored in the database table are processed. Data in both tables show the image contour points potentially belonging to the object, robot grippers, or other objects not to be identified by the robot. Data in all tables in the database are stored in rows which represent moments of acquisition. They are also stored in columns, sometimes called attributes, which represent different types of data. Data in the left and right image tables are used when the robot is approaching the object.

The data in Tactile Image A and B are used when the robot has already prehended the object and starts to gauge the force required to retain it. The A and B of the tactile image tables represent the data from each side of the tactile sensors due to the fact that the robot has parallel fingers, both of which make contact with the object

surface on object acquisition. Each column in these tables shows the data from every sensor element of the corresponding tactile sensor.

The TacEvent table shows special data reported by the tactile sensors such as slip, center of force etc. The data in Joint1 table, Joint2 table etc., show each joint angles history. All the data above will have time-variability characteristics which can be compared to the temporary memory in the human brain.

The CMD table stores commands to control parts of the robot, including image recording, data storing and tactile-sensor reading. The commands programmed for this table emanate from the BrainThread program.

The file system has different files which store data on robot control with certain patterns. This is an important feature for several reasons. To begin with, some situations have certain patterns and are frequently used by the robot. There may also be some commands which momentarily perform a number of robot controls. These commands will be stored in the file system in order that the BrainThread sub-programs can read data directly from it. Only data inappropriate for operation will be modified after data in the file has been read to the BrainThread. This file system can be compared with the long-term memory found in the human brain.

The whole process of software operations can be explained as follows: The robot starts reading data from the image tables or the tactile sensor tables, depending on the task it is performing. With data on joint angles, the robot is capable of controlling the movements of its grippers to successfully perform the task commanded. When the command is repeated or part of the command is similar to other commands, the BrainThread will read such command from the file system. The command inappropriate to the task can be resolved at this stage. The BrainThread is also capable of storing its operation status in the form of state variables.

The command desired will then be stored in the CMD table. After that, the BrainThread will send an event message to the MISSION software processor in the PC2 to read the command from the CMD table in order to control robot functions.

In the opposite direction, the MISSION software will send an event message back to the BrainThread to signal the completion of the task. The whole process will then be repeated. The BrainThread is capable of storing more than one command in the CMD table enabling the robot to perform more than one type of task. Moreover, for every movement of the robot, joint positions will be stored in their respective tables.

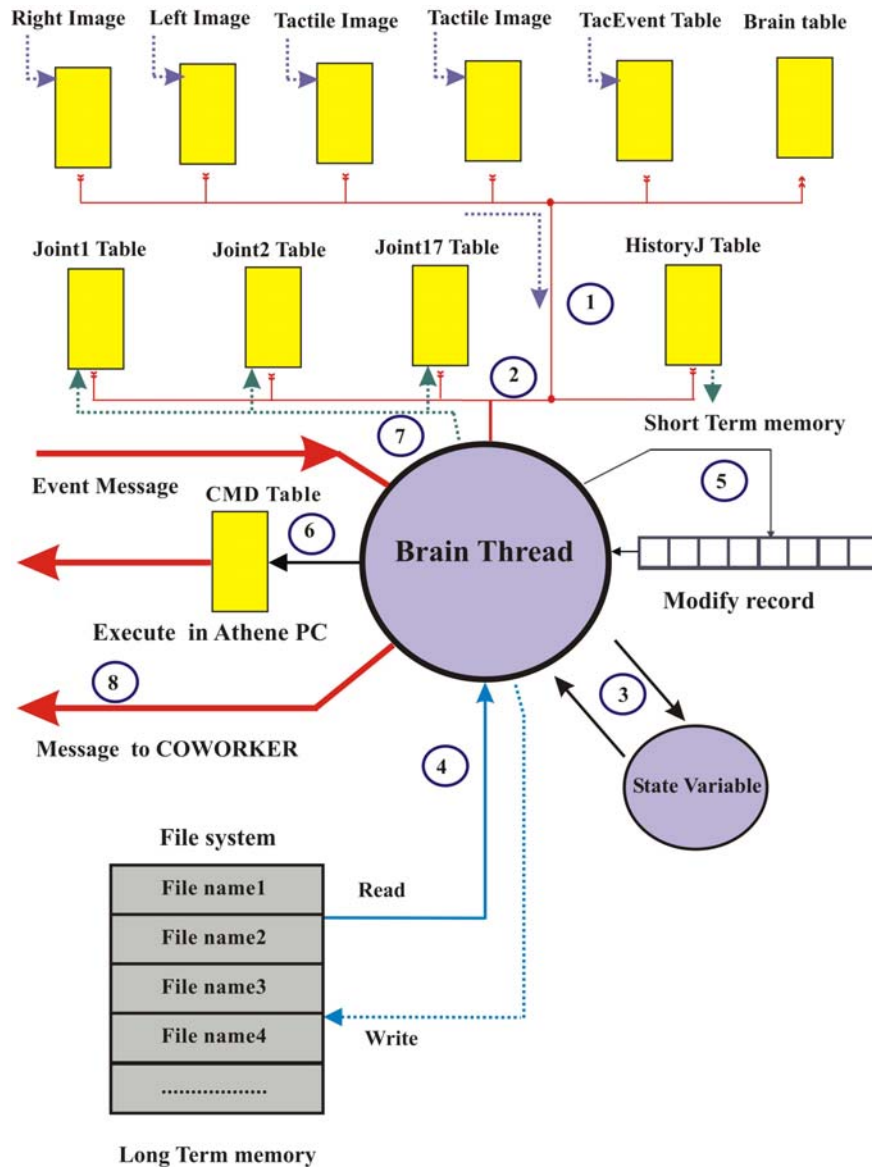


Figure 3.5: Software Operation

### 3.2 Force Sensor Design

In this section, the principle of operation and the design of the tactile elements are discussed. The material used for this research is a soft, deformable surface made from electrically conductive foam, which detects continuous pressure with excellent sensitivity and resolution. The conductive foam is 3-mm thick. The underlying physical phenomenon behind the sensors is that of the variable resistance, whereby the resistance of the foam decreases with an increase in the applied pressure. The analysis of the structure of the conductive foam can help in understanding this phenomenon.

There are many types of polymer foam: polystyrene, neoprene, polyethylene, polyester-based polyurethane, polyether-based polyurethane, and others. Each is a synthetic plastic with very desirable properties: malleable, deformable and capable of returning to its original shape (good elasticity). However, polyethylene-based (PE) foam and polyurethane-based (PU) foam are the most readily commercial available conductive foams. The conductive foam used in this research is a material with a surface resistivity of greater than  $1 \times 10^2 \Omega/\text{square}$  and less than  $1 \times 10^5 \Omega/\text{square}$ . Concepts of surface resistivity can be found in many books and standards [ASTM Standard D 257-99, ESD STM 11.11-2001, IEC 61340-5-1 Standard, Heaney 1999].

Conductive foam is normally a composite material comprising an electrically insulating PU-Matrix doped with an electrically conductive material such as graphite. The bond between the foam material and the conductor is a physical bond, which means the graphite particles are not chemically bonded with the foam polymer, but are embedded in the matrix. The resistance measured between two electrodes on the same side of the conductive foam (one tactile element) is derived from electrical conductivity through a number of conductive paths. In the quiescent state the foam has a resistance of about  $1\text{M}\Omega$ . When compressed, the resistance drops to around  $50\Omega$ . These values are measured using the size and shape of electrodes which have been designed specifically for this project, for example: circular electrodes of 1 millimeter diameter arranged on the same ground plane (See figure 3.7). Any kind of mechanical perturbation exerted on the

sensor surface will induce elongation and/or compression, which rapidly increases and/or decreases some conductive paths.

If many tactile elements are arranged in a rectangular grid, an image of the applied force field or the force distribution may be obtained.

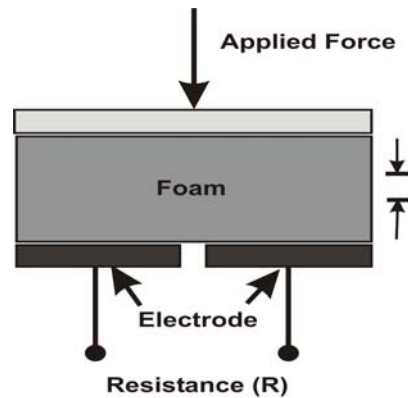


Figure 3.6: Operating principle of the tactile elements

As shown in figure 3.7, the inner electrodes are arranged in an array and surrounded by the ground plane or common electrode.

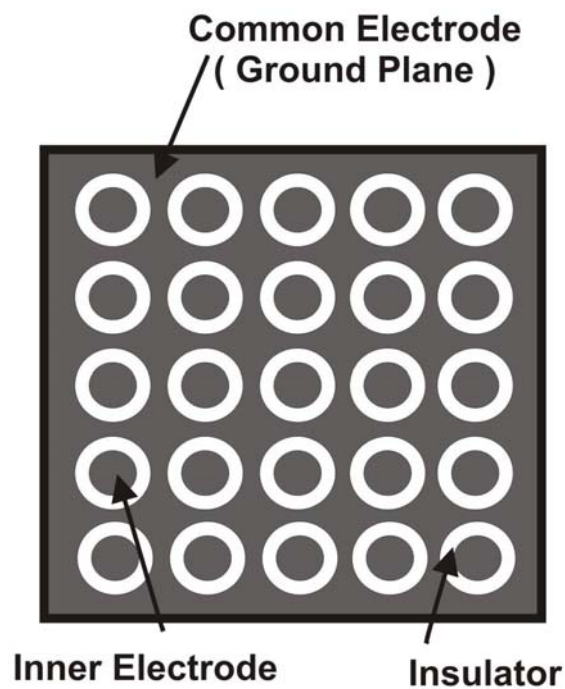


Figure 3.7: Array of electrodes as planes for force measurement

### 3.3 Tactile Sensor Design

To create a tactile sensor from a basic force sensor, a number of procedural issues on the design of a usable tactile sensing system must be addressed. System parameters such as the number of tactile elements, the density of arrays, the sensor-scanning speeds are strongly interdependent. The sensor's performance is dictated not only by the quality of the individual tactile elements, but also by how the tactile elements are integrated. The spatial resolution of the tactile array is a function of the proximity of individual sensors to one another.

Consequently, this research has begun with the formulation of a conceptual model, which includes the essential ingredients of a general tactile sensing system. This model is used to explore various system designs and their respective trade-offs.

Figure 3.8 schematically illustrates the conceptual model of the tactile sensing system used in this research. The functional divisions naturally fall into a pyramid form, with the more computationally intensive processes occurring at the upper end of the pyramid and the more functionally rigid processes residing near the bottom. The vertical connections between elements are bi-directional or unidirectional, permitting data to flow downwards for addressing purposes and upwards for signal use by higher subsystems. This structure can be easily applied for the development of manipulator control, which is also typically hierarchical in nature [Albus 1981]. Clearly, this architecture is by no means unique to tactile sensing or manipulator control systems. Other researchers have presented similar models for multi-sensor integration [Albus 1983], human cerebellar function [Malchior et al. 1984], automated production [Snyder 1985], and many other applications. The advantage of using a hierarchical structure is that complex processes can be systematically decomposed into sub-processes, which can be implemented at desired levels of complexity.

The model is divided into six levels. In the first level of the model is transduction of contact data, which may involve complex measurements such as the detection of normal force and shear force as well as their spatial derivatives at the contact surface.



However, the transducers used in this research are simply intended to indicate contact with an object. Much of the previous interest in tactile sensing has been focused on transduction, and past research results provide a rich foundation from which to draw.

The second level, multiplexing and transmission of tactile data, involves the interrogation of sensors and the preparation of collected information for serial transmission. Critical trade-offs exist between the operating speed and the number of electrical wires in a conduit. Contact data from many tactile elements must be transferred to the controller at a rate sufficient for tactile information to be successfully used in dynamic end-effector control. Since conduit routing and fatigue will be a major problem to the systems success, the system should be designed to minimize the number of data conductors used.

The third level, tactile data selection, reduces the amount of data that must be transmitted from the robot gripper by selecting which sensors or sensor patches should be interrogated. In very simple tactile systems with relatively few transducers, compromises may not be necessary. In more expansive systems, however, sensor selection will be a necessity. Sensor selection will be predetermined to automatically respond with contact events, or modulated in anticipation of upcoming interactions planned by the controller.

The fourth level, preprocessing, is strongly dependent on the type of transduction array used and can range from elaborate processing schemes to detect geometrical features such as edges or holes, to merely data scaling for transmission to the controller. The selection of a particular transduction and preprocessing scheme strongly influences the reliability, size, and mechanical behavior of a tactile array. Initial choices are important since they will later impose bandwidth constraints on data access by higher levels.

The fifth level, tactile data interpretation, forms a dynamic, tactile "map" of contact interactions and may also perform computations, which enhance contact features. This level of data will be placed in a format useful to the next level of the system.

At the sixth level, control, the algorithm for grasp and manipulation are implemented. At this level, tactile parameter such as sensor density, resolution, and localization are particularly important, since information must be sufficient to allow reliable control of desired complex tasks.

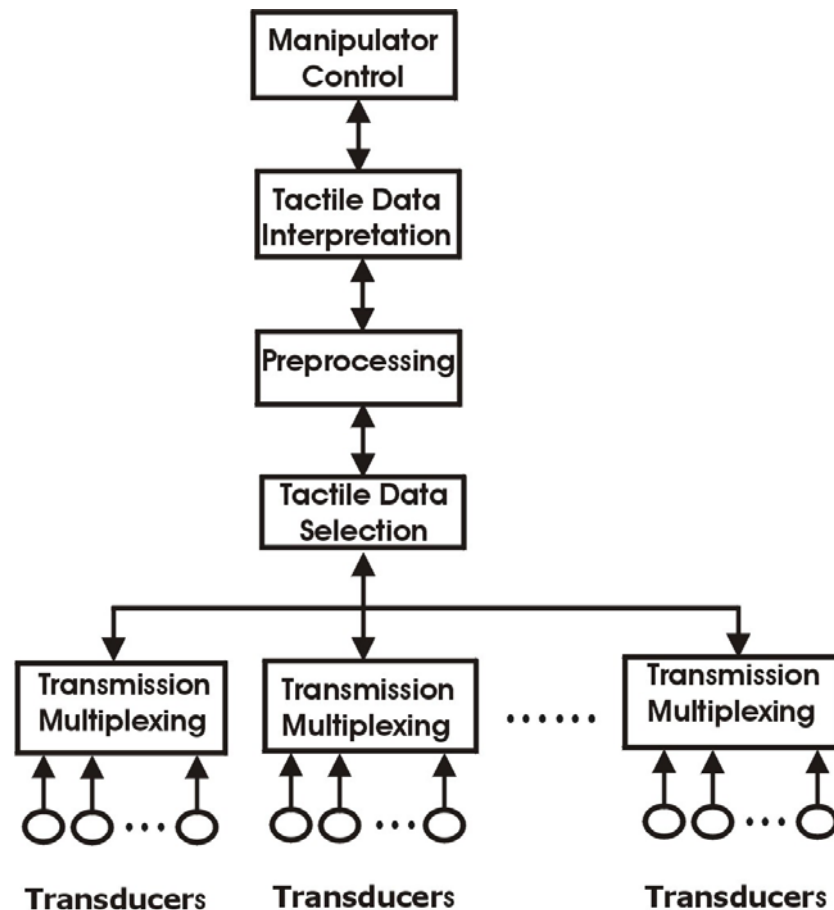


Figure 3.8: Model for tactile sensing

### 3.4 Electronics Circuit Design

As discussed earlier in 'Force Sensor Design', the operating principle of this type of tactile sensor is to measure a change in electrical resistance. From Figure 3.7, each tactile element will have two electrodes. One electrode from each tactile element will be connected to a common substrate or ground plane. The other electrodes will be connected in series with a fixed resistance to the voltage source.

The voltage measure points are above the joints of each tactile element. The R value will be related to the surface resistivity of the conductive foam. That is, the R value will determine the voltage drop across the tactile-elements under normal conditions. In other words, the value of the fixed resistance is so chosen that when no force is applied to the foam surface, the voltage across a tactile element should be approximately 80% of the supply voltage  $V_+$ . The decrease in voltage across a tactile element (from 80% to 0% of  $V_+$ ) is due to compression of conductive foam under tactile pressure, whereas the increase in voltage across the tactile element (from 80% to 100% of  $V_+$ ) is due to elongation or expansion of the conductive foam under shearing or traction forces.

The voltage across the tactile elements will decrease when a compressive force is exerted on the foam because of the resulting increase in conductivity. On the other hand, the voltage increases as a result of a tensile force. Such increases are noticeable notable despite the minimal size of expansion of the foam.

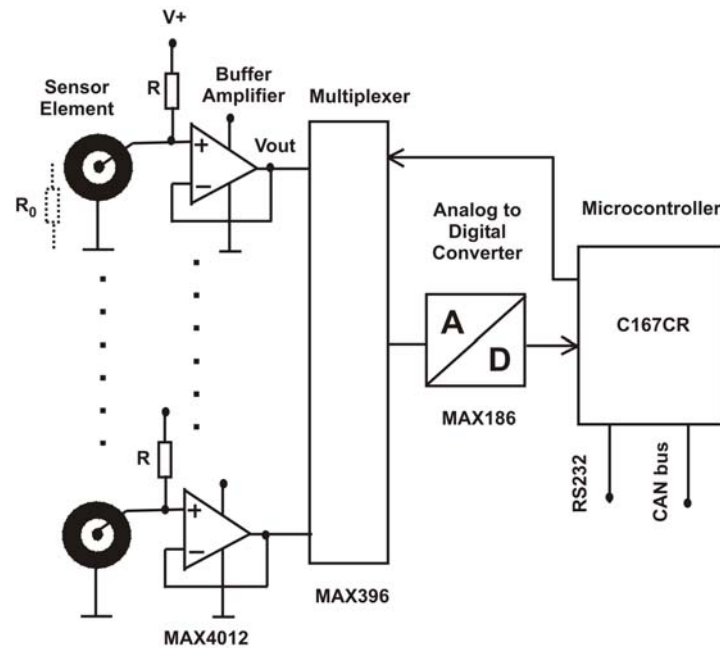


Figure 3.9: The sampling circuit

The analog-digital converter (ADC) is used with successive approximation on all input channels from sensor electrodes. In order to reduce the number of ADC chips, MAX396 16-channel analog multiplexer chips for the controller units of the finger sensors are used.

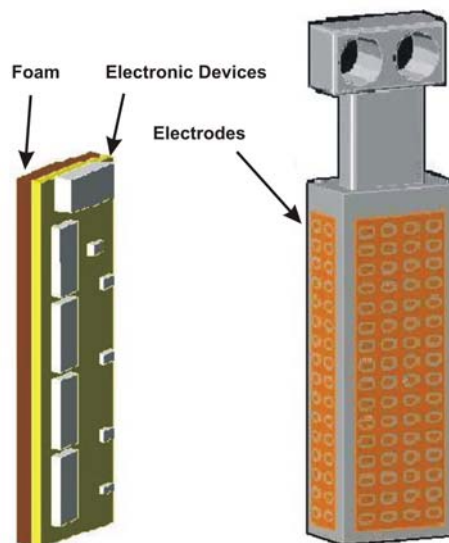


Figure 3.10: Details of each side assembled into the finger

Each side of the fingers consists of three layers. The first layer, the epoxy layer, is used to protect the semiconductor devices from excess force and collision. The PCBs (printed circuit boards) with epoxy are glued to an aluminum core. The second layer is the PCB layer with the inner electrodes connected to an electronic circuit through an epoxy layer and to the topmost, the foam layer which is glued to the rear of the PCB. Illustrated in Figure 3.10 is a designed fingerplate for a device which takes advantage of this pressure measurement property. The arrangement of layers in this way enables the robot fingers to measure deformations by measuring changes in the electrical conductivity of the foam as the surface of the fingers is deformed.

The fingers are covered by 3-mm thick conductive foam. Each finger consists of many tactile elements. Each side of the fingers is designed to measure the force at one specified location. Electronic devices to drive each tactile element are located very closely to each tactile element in the finger segment. This allows signal processing to be brought as close to the sensors as possible or even to be integrated with the sensors. The width of the fingers is 20 mm, their length is 55 mm excluding an aluminum core and they have a thickness of 12 mm.

The tactile sensors have been developed with the following specifications: One finger consists of two 16x4 cells, two 16x2 cells, and 6x2 cells, making up the total 408 cells for the two fingers.

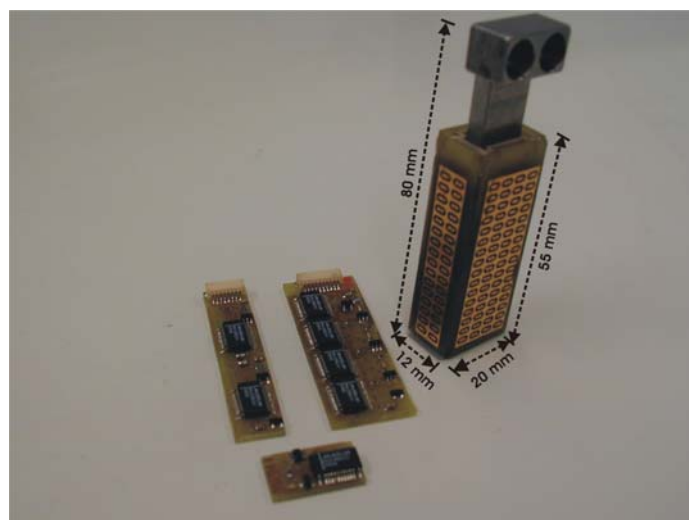


Figure 3.11: Details of finger components

The controller facilitates three essential functions: data collection, manipulation and communication. The C167 microcontroller equipment is housed in the controller unit with a 20 MHz clock. One of the main advantages of this system board is flexibility of the memory configuration. The main memory on the board is arranged in two continuous areas with I/O port (communication channel), and both can be accessed as 8-bit or 16-bit words. An internal RAM chip is also included which can be accessed with zero wait state by the microcontrollers. For this application, both external and internal memories are used and the entire main memory is configured and accessed as 16-bit words. In this model, 128Kx16 SRAM external RAM was made available. This microcontroller also has a 2Kx16 flash memory which contains codes that allow transfer of application programs from the PC host to the board. The flash memory is accessed at power-up or reset so that the board can be used in embedded stand-alone real-time applications.

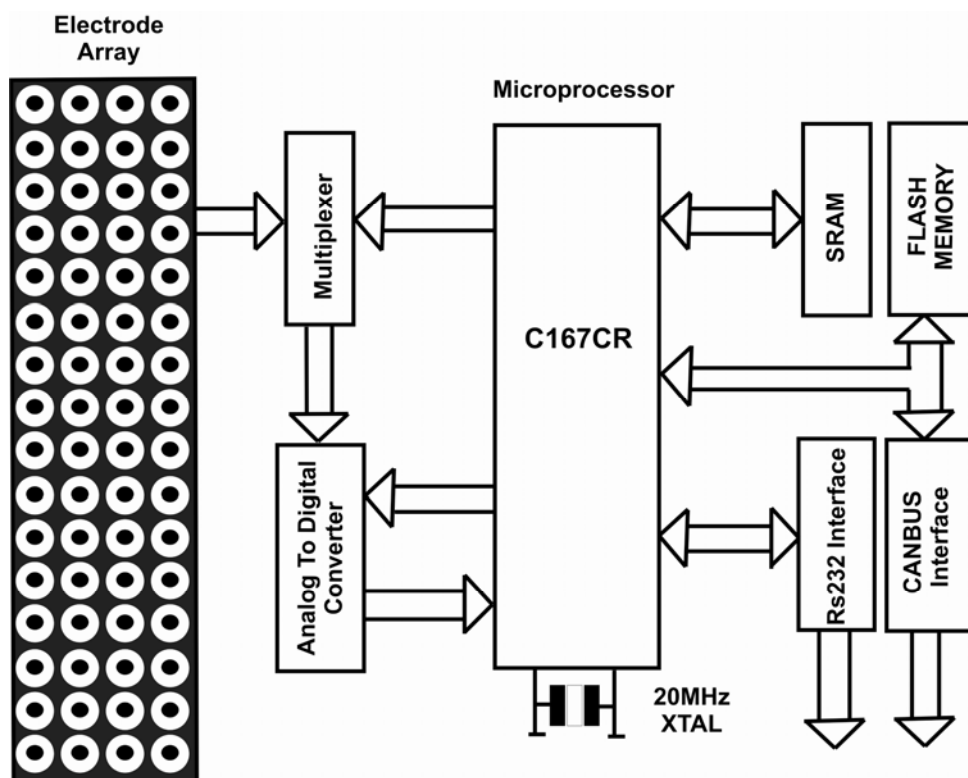


Figure 3.12: The circuit diagram

The controller unit has two PC host interfaces: RS232C and CAN-bus. A fast CAN interface is provided by the C167 chip. Several software-configurable registers are also mapped into the chip's I/O location.

These resources allow bi-directional interrupts (communication requested signal) between the controller board and the PC host. The analog-to-digital (ADC) module consists of quad-channel ADC chips with successive approximation on all input channels with sampling frequencies up to 10 KHz. The inputs are limited to a range of zero to +5 Volts and so input voltages from every tactile element must be within this range. The sampling timing is synthesized fully by the software. No interrupts are used, so the sampling timing is jitter free.

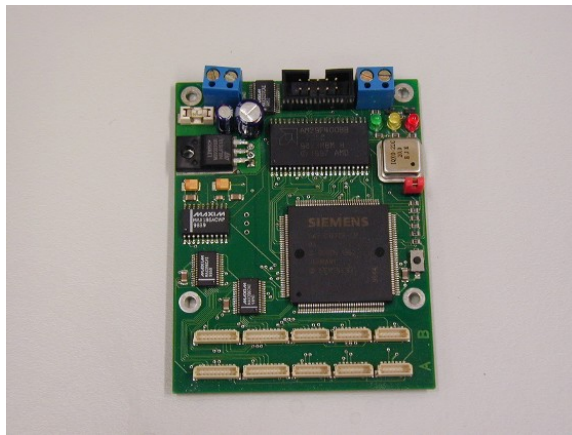


Figure 3.13: The Controller Unit

### 3.5 Software Integration

The software integration of visual modalities has been achieved in an efficient manner by creating a unified data structure for geometrical properties of objects and by programming with multi-threading techniques. When displaying a visual image, the update rate is approximately 100 Hz which appears continuous. The first main screen, shown in Figure 3.14, is Finger Screen, which is adapted for the shortcut viewing of the finger sensors. Each area corresponding with the electrodes is arranged in such a way that they easily recognize the existence of the physical finger sensors. Since graphic environments are often identical, it will be advantageous if the graphic specifications are similar. That is, the whole area of the finger as well as its different plates can be seen on the screen, as shown in Figure 3.14.

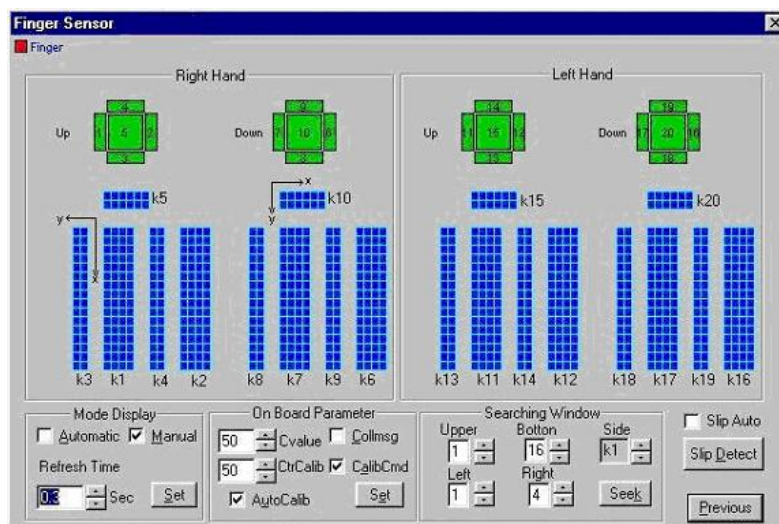


Figure 3.14: Finger Screen

The two requirements for software integration are real-time rendering and data transfer speed. In order to satisfy both requirements and to optimally use the power of the computer processor, the visual thread and the communication thread need to be separated. That is, the two threads are run at the same time. The visual thread is updated at 100 Hz while the communication thread is connected to the tactile controller at 256 Kbits/sec.



Since the two threads are running simultaneously, there is always a chance of conflict between their access to shared memory, i.e. when one thread is writing data to the memory and the other thread is reading from the memory. In order to avoid this problem, these two threads need to be synchronized. The easiest way to do this is to use critical sections. In Visual C++, there are four types of synchronization objects: critical sections, semaphores, mutexes, and events. Technically, the first three are all instances of general semaphores. When one thread wants to access the shared data, it will check first if the other threads are accessing the same data. If the operating system indicates that the shared memory is not being used, one of the other threads can access the data. On the other hand, if the operating system indicates that the shared memory is currently being used, the thread that is accessing the memory must wait until the other one is completed.

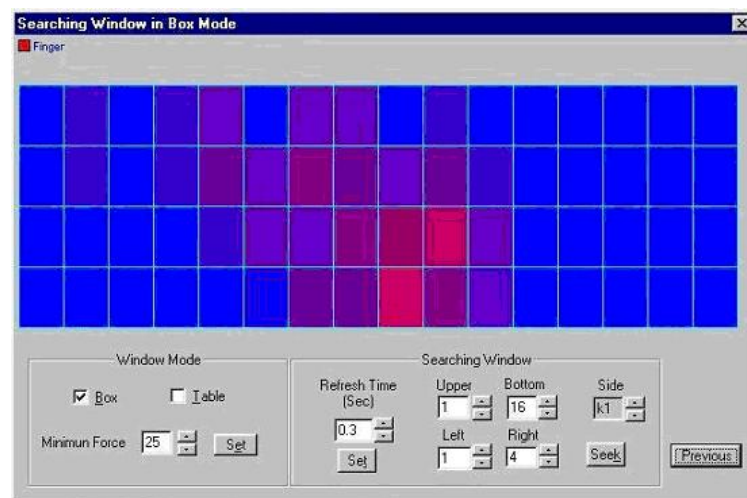


Figure 3.15: Single Side Screen

### 3.6 Sensor Behavior

This type of sensor has been designed and build by [Weiß and Wörn 2004, 2005] to measure finger forces. However, integration with the robot fingers and software development has been done as part of this research. This tactile sensor measures the pattern of deformation beneath the fingers, which changes when a force is applied to the fingers. This pattern can then be used to predict finger forces. Normal forces, shear forces, and even changes in finger postures have all been shown to result in different deformation shapes. In conclusion; a new tactile finger sensor containing a 2D array of detectors is described in order to understand how normal forces and shear forces can be sensed. Normal touching forces, shear forces, or sliding forces on the plane of a contact surface play an important role in robot sensing and manipulation of objects.

Before describing the detailed operating principles of the tactile sensors, the tactile sensor layout will be presented. The figure below shows the side-cut picture of the tactile sensors. The uppermost part is the 3 mm-thick conductive foam. The conductivity measured by the electrodes is distributed under the foam. There are 64 points to measure the resistance which disperses evenly over the conductive foam surface. All the electrodes are connected through the multiplexers to the ADC. Some electronic circuits will be installed below them, as shown in the figure 3.10. Between the sets of electrodes and electronic circuits lies a layer of epoxy material acting as an insulator. The force exerted on the tactile sensors will usually be in a downward direction.

Figure 3.16 exhibits only one side of the robot finger after tactile sensor installation. A robot finger has five sides (four sides on the finger shaft and one side of the fingertip). Normally, a measurement of resistance requires two electrodes, which in this case are the 64 electrodes and the common ground plane.

There is an analytical mathematical model which provides the complete field distribution inside the tactile material. Using the Ansoft Maxwell 2-D field simulator, the electric field's characteristics and static responses are calculated which are shown in figure 3.16.

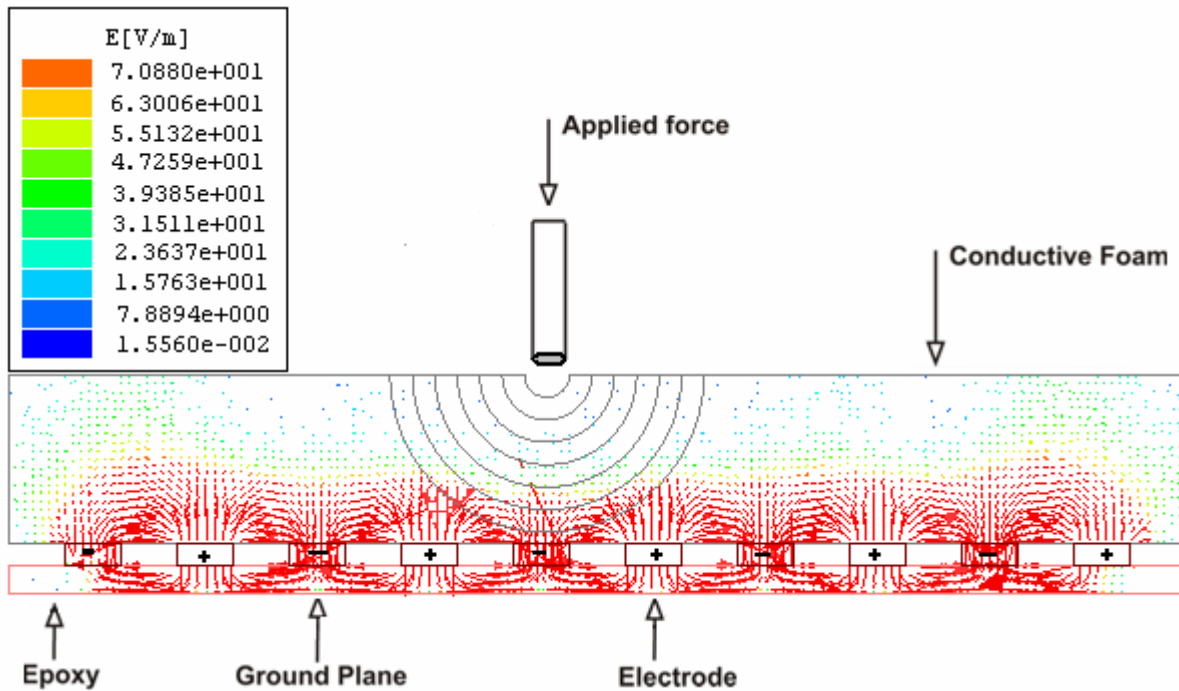


Figure 3.16: Material Behavior [Ansoft Maxwell 1997]

The following section describes the material behaviors of the tactile sensors and why the conductivity changes upon an application of force. However, complex mathematical models will not be used. From the figure 3.16, the parts with + are the electrodes connected to the conductive circuit. The parts with - are electrodes commonly connected to the ground plane. The direction of current flow will be dependant on the three dimensional electrical field in an isotropic material.

Conventionally, a current flows from + to -. If the electrodes and the ground plane are on the same plane level, then the electrical field will flow perpendicularly from the electrodes and flow back perpendicularly onto the ground plane. In figure 3.7 and figure 3.16, the electrodes and the ground plane do share the same horizontal plane. Hence, the vector field will take a divergent shape, and a symmetrical distribution can be observed. However, when the material is pressed on the top, pressure distributions are formed. The area underneath the applied epression results in a high pressure, while the pressure of the surrounding areas decreases.

The volume under the tactile sensor surface in figure 3.16 corresponds to a downward difference pressure distribution on the material, and has a symmetrical characteristic. However, the electrical field lines inside the material are no longer symmetrical. The conductivity values read from the electrodes will have a data distribution that corresponds to the curvature of the tactile surface under pressure.

On measuring the resistance at the tactile elements, the analysis of the electric field has to be carried out by using Poisson's equation, which requires certain boundary values. In addition, measuring the resistance under pressure will also depend on the analysis of the material behaviour for both pre-deformation and post-deformation.

In some part of the electrical field analysis, the potential distribution  $V = V(x, y, z)$  in the material for a uniform charge density can be given in Cartesian coordinates by Poisson's equation:

$$\frac{\partial^2 V}{\partial x^2} + \frac{\partial^2 V}{\partial y^2} + \frac{\partial^2 V}{\partial z^2} = -\frac{\rho}{\varepsilon} \quad (1)$$

where  $\rho$  = material charge density (depending on pressure) with the units Coulomb/m<sup>3</sup>. and  $\varepsilon$  = electrical permittivity. Material analysis concerning  $\rho$  and  $\varepsilon$  will be discussed in chapter7 where the concept of the stress/strain quadric and its applications will be introduced. The electric field  $E(x, y, z)$  is defined as  $E = -\nabla V$  or

$$E(x, y, z) = -\frac{\partial V}{\partial x} \mathbf{x} - \frac{\partial V}{\partial y} \mathbf{y} - \frac{\partial V}{\partial z} \mathbf{z} . \quad (2)$$

The ground plane (-) is connected to the ground and maintained at  $V = 0$ . The voltages at the electrodes of the tactile elements show some variations (i.e. the voltages are dependent on potentials calculated by the voltage dividers formed by R and R<sub>0</sub> as shown in figure 3.9). From the above equations and the boundary conditions, calculations must be carried out using Finite Element software. In practice, determination of electrical resistance is achieved through voltage measurements, as shown in figure 3.9.

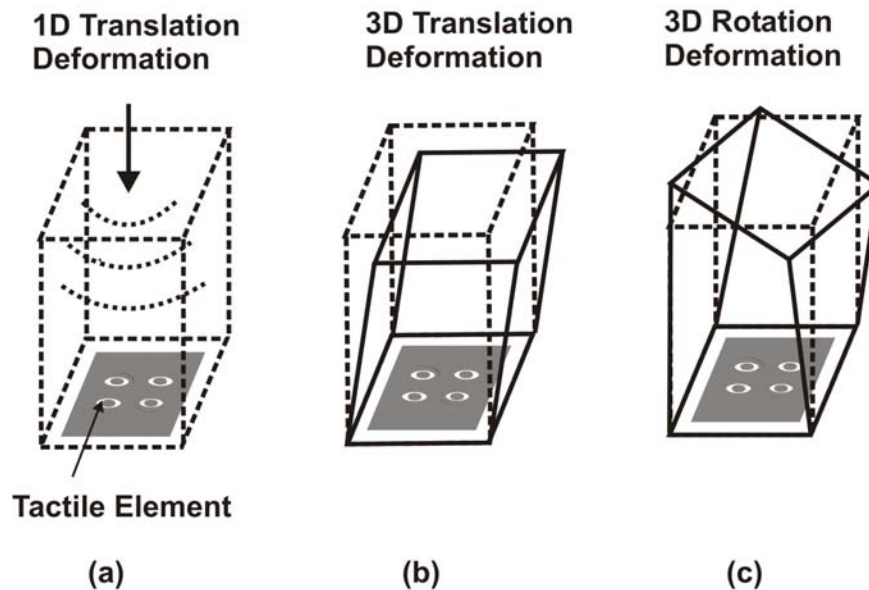


Figure 3.17: Sensing Complexity

Figure 3.17 shows the behavior of a cubic section of the sensor upon the application of a downward pressure. In figure 3.17a, when the tactile surface receives a vertical indentation causing a force distribution in the lower part of the foam content and the area surrounding the center of the force, the force then increases the conductivity in that area. The area with the highest conductivity is at the center of pressure, while the surrounding areas also show increasing conductivities, though to a lesser extent than in the center. In figure 3.17b, the object pressing on the sensor surface moves without slip. It can be seen that the foam cube diverts in a certain direction depending on the direction of object movement. The diversion caused by pressure on the foam occurs in three dimensions resulting from shear forces. Figure 3.17c occurs when the object pressing on the tactile sensor is rotated with the center of rotation different from the center of force, which is caused by force applied to the surface. In this case, the foam cube distorts three-dimensionally as well. Both 3.17b and 3.17c yield extremely complicated computations in this respect.

## CHAPTER FOUR

### The New Tactile Sensor and Its Performance

#### 4.1 Performance Matrix

The tactile sensor design has been tested in order to determine its ability to detect tactile information. A number of experiments have been conducted to explore the following parameters: hysteresis, temporal resolution, sensitivity, linearity and time variance, spatial resolution, localization, shape determination from force distribution, and surface fitting. The experiments together with their procedures are summarized in the table below, and further details are discussed in Section 4.3: Performance Tests.

	Parameters	Experiments and Procedures
1	Hysteresis	An experiment to measure hysteresis was conducted by exerting forces on a particular tactile element, using an indenter - a 3-mm diameter cylinder with an evenly cut surface. The indenter was also used for all the other experiments. Force was increased from zero to three Newton with increasing strain being continuously measured and recorded. Then the force was reduced from three to zero Newton with reducing strain being similarly measured and recorded.
2	Temporal resolution	Two experiments were conducted to test this parameter. In the first experiment, the indenter was used to create a 1-mm deep indentation on a tactile element. The indentation was maintained for one second and then released for one second. This process was repeated. However, the time spent for pressing and releasing was reduced to half the previous time after every successive ten seconds. In other words, the frequency of indentation was doubled every ten seconds. In the second experiment, the indenter was used to create a stable force on a tactile element for 1.5 seconds. The data from the beginning of the indentation until the end of the process were recorded.

3	Sensitivity	An experiment was conducted to find the relationship between the tangent of the data curve from the ADC and the displacement in order to ascertain sensitivity. Data was collected while the indenter was used to indent to different depths on the tactile surface.
4	Linearity and time variant	Two experiments were conducted. One experiment was conducted to test linearity - the relationship between the resistance measured from a tactile element and the force exerted on it by the indenter. The other experiment was conducted to test time variance - the resistance of the tactile sensor which varies with time during which a constant force is maintained.
5	Spatial resolution	This measurement was achieved by applying force on different tactile elements along a particular 16 element row. The ADC data from the eighth location resulting from each pressing event were measured and graphically plotted.
6	Localization	This parameter refers to the ability to localize contacts on the tactile sensor surface. Two experiments were conducted to test this. In the first experiment, the indenter was used to apply force to the tactile sensor surface before being horizontally displaced to other positions whilst maintaining the depth of displacement. The second experiment was conducted by using the indenter to press different positions on the tactile sensor surface with all the data being recorded to determine the center of force representing the contact points.
7	Shape determination from force distribution	This was an experiment to determine the force distribution on the tactile sensor surface while objects with different shapes were being pressed against it. Black and white colors were used to show 2D areas which did and did not experience force.
8	Surface fitting	The same sets of objects as used for testing parameter seven were also used in this experiment. However, this resulted in 3D data.

Table2. Performance Matrix Validation

## 4.2 Experimental Setup

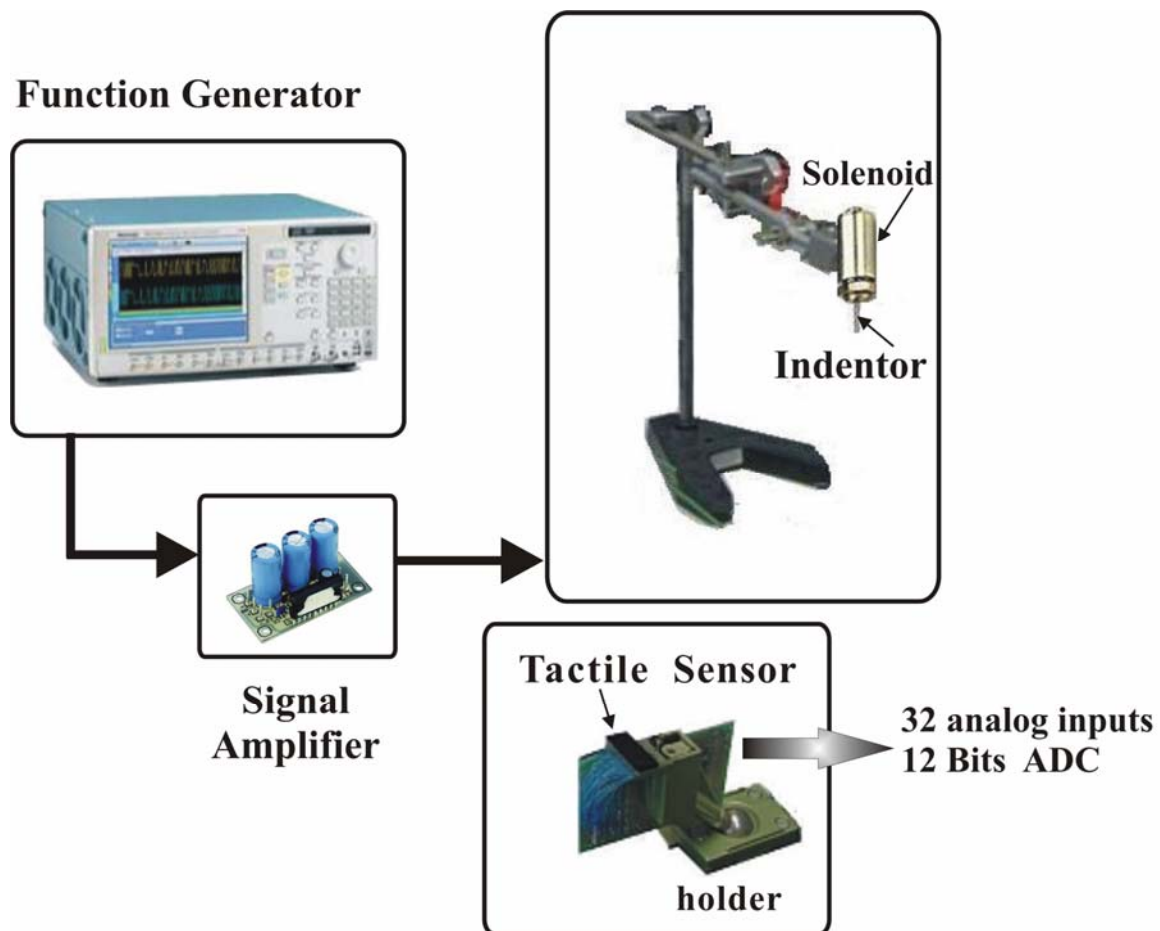


Figure 4.1: The impulse tester

Two sets of experiments were conducted to determine the tactile sensor parameters and the equipment used was chosen accordingly. Included in the first set of experiments were the experiments in which the impulse tester was used to create impulses on the tactile surface. For example, the experiment conducted to test the second parameter in Table 2. The equipment used for this one consisted of a function generator and an impulse tester. The impulse tester, the equipment at the tip of which the indenter was installed, used a solenoid to generate the force required for pressing the indenter on the tactile surface. The frequency of indentation was increased or decreased by programming on the function generator. The signal from the function generator will then be amplified by an amplifier before driving the solenoid. The solenoid forced the indenter to move in the vertical direction and



pressed upon the tactile surface. The degrees of pressure were controlled by the amplifier and the function generator while the depths of indentation were adjusted according to the height of the arms. To apply a constant pressure, the function generator had to program supplying a direct voltage to the solenoid.

The tactile surface contained 64 tactile elements arranged in a 4x16 array. For the reason of convenient measurements, all tactile elements were connected to external test points. The signals measured at specific test points were able to be divided by electrical resistors measured by a multimeter, or the shapes of those electrical signals were to be measured by an oscilloscope.

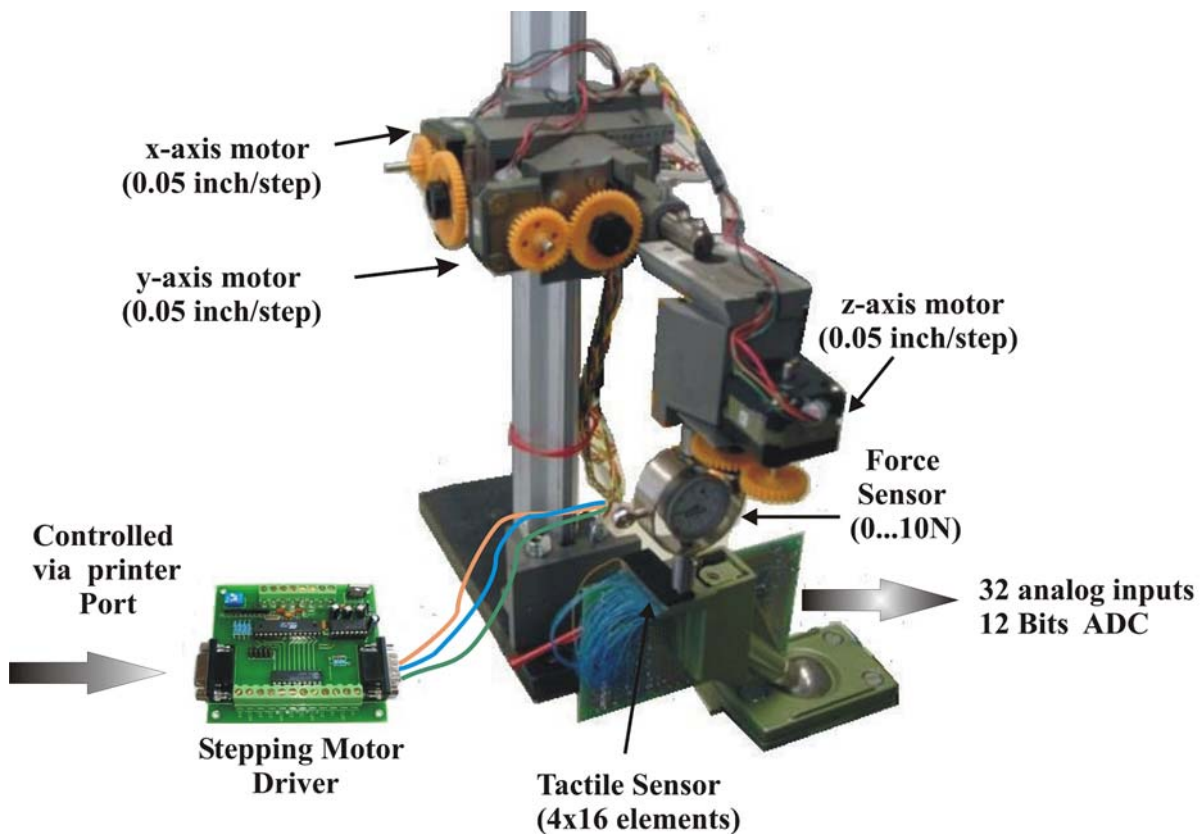


Figure 4.2: The 3-axis test bench

Included in the second set of tests were experiments which required the horizontal displacement of the indenter to different positions on the tactile sensor surface. A special tester employed force from the computer controlling the stepping motors through the stepping motor driver. Its tip was capable of three axes of precise movement. For each axis, the control resolution was one-twentieth of an inch per

step of the movement. The commercial force sensor was equipped with indenter through the tip of the z-axis. This was the indicator of the pressure applied by the z-axis motor. On the other hand, the depths of indentation were also marked on the sliding ruler. Then, it was able to gauge the vertical distances by counting the applied steps into the z-axis stepping motor. The signals measured from the tactile sensor were able to be measured for its electrical signals by an ADC card. The pressure distribution or the whole electrical signals of the tactile array were simultaneously measured with 32 analog inputs, at a 12-bit measurement resolution and a sample rate of 640 Kbit per second.

### 4.3 Performance Test

This Section is divided into three parts. In 4.3.1: Force Sensor Characteristics, electrical noise, thermal response, hysteresis, temporal resolution, sensitivity, and linearity and time variance are discussed. In 4.3.2: Tactile Sensor Characteristics, spatial resolution and localization are presented. In 4.3.3: Tactile Performance, shape determination from force distribution and surface fitting are described.

#### 4.3.1 Force Sensor Characteristics

##### Electrical noise

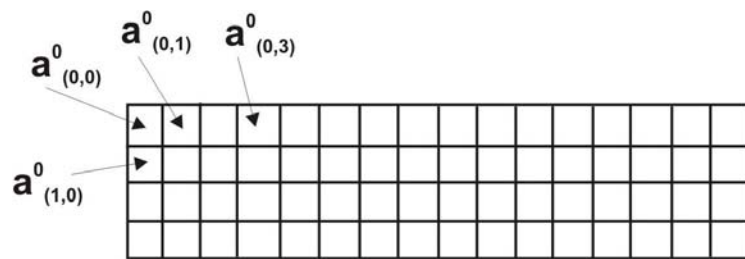
Electrical noise from the tactile sensor in the form of interfering signals is a very important factor which must be taken into account before data from the tactile sensor can be used. There are three main causes of noise. First, the contact between the foam and the electrodes was not electrically or mechanically perfect because the foam was simply glued to the electrodes at the back of the PCB. Secondly, the foam started to degenerate after extended periods of use; for instance, its ability to stretch and yield reduced. As a result, the voltages around the used area became different along the foam surface. It was very difficult to solve this problem using software based compensation methods. The only realistic solution was to replace the foam.

The third cause of noise resulted from the processing of the foam which involved mixing graphite particles with polymeric particles in the foam. However, this did not produce a chemical bond of the two elements. The resultant conductance was merely through the graphite particles from the electrodes to the ground plane.

In order to reduce the noise, four lower bits of each sampling data from the ADC were simply neglected hence the signal contain only 8 relevant bits, and a filter was used to compress the noise. The simplest noise reduction method was a low pass filter achieved by the “sliding method” or “box filter”. Instead of using the mean value, a specified factor ( $C_f$  : compression factor) was used as a divisor. Data from

each tactile element was replaced by the summation of its local neighbors divided by the compressed factor. This method chose a local neighborhood to smooth the data derived from the tactile array.

The compression factor was selected by observing raw data from the ADC. For calculation, each data from the tactile element could be part of two different lines. The one chosen for smoothing was the middle taxel. One disadvantage of using this method was that sharp edges and secular highlights might be diminished or lost. Using a threshold value ( $F_t$ ) as a reference it was possible to restore some of the lost sharpness. By this method, taxels which contain levels higher than the threshold value were set to a new value (filler value), and taxels which contain levels lower than or equal to the threshold value were set to the original value.



$$a^0_{(0,0)} = \frac{2 \cdot a^0_{(0,0)} + a^0_{(0,1)}}{C_f}$$

$$a^1_{(m,n)} = \frac{a^0_{(m,n-1)} + a^0_{(m,n)} + a^0_{(m,n+1)}}{C_f}$$

$$\text{If } (a^1_{(m,n)} > F_t) \text{ then } a^0_{(m,n)} = a^1_{(m,n)}$$

Figure 4.3: Noise compression

$a^0_{(1,2)}$  is old data from the tactile element at row 1 and column 2.

$a^1_{(2,3)}$  is new data (filler value) from the tactile element at row 2 and column 3.

## **Thermal response**

This characteristic does not depend on the properties of the tactile sensor itself but on the material covering the tactile sensor. According to the properties specified by the manufacturer, temperature change does not influence the measurement of force-resistance relationship if it remains within the range of 0° to 120°C. The magnitude of an actual change in the force-resistance relationship is not predictable outside this range. In addition, the material used in this type of tactile sensor responds only to a force stimulus not to other external stimuli, radiation, and in particular, electro-magnetic fields. For these reasons, additional information for purposes of temperature compensation was not required.

Furthermore, our conductive-based tactile sensor was encapsulated, enabling accurate, stable, and reliable operation. The sensor's conductive foam consisted of both electrically-conductive and non-conductive particles suspended in a polymer matrix. The particle sizes were of the sub-micron order and were formulated for minimal temperature dependence, improved mechanical properties and increased surface durability.

## **Hysteresis**

Hysteresis represents the historical dependence of physical systems. If an object is pressed on the sensor surface, the surface will deform. When the pressure is released, the surface will be restored. The absence of these characteristics exhibits hysteresis, which is caused by the loss of absolute energy from the system. Hysteresis correlates with the resilience of the rubber: the higher the resilience, the lower the hysteresis.

Hysteresis is calculated from a stress-strain curve. Hysteresis is the difference between the loading energy and the unloading energy, whereby energy values are determined by calculating the area under the test curve. In this experiment, the sensor was loaded incrementally from 0 to 3 Newtons and then back down to the no loading condition to determine the extent of the hysteresis. This piece of data was

shown by plotting the force of the probe versus the sensor output. In Figure 4.4, the lower curve represents the sensor output for an increasing applied force and the time to increased force is in 1 minute. The upper curve represents a decreasing force and the time to decreased force is also in 1 minute. The difference between the curves is the hysteresis, which was 8.2 % of the total response. This difference lies within the noise range of the system. Thus, it should be possible to reduce the effect of hysteresis down to an acceptable level by compensation in software.

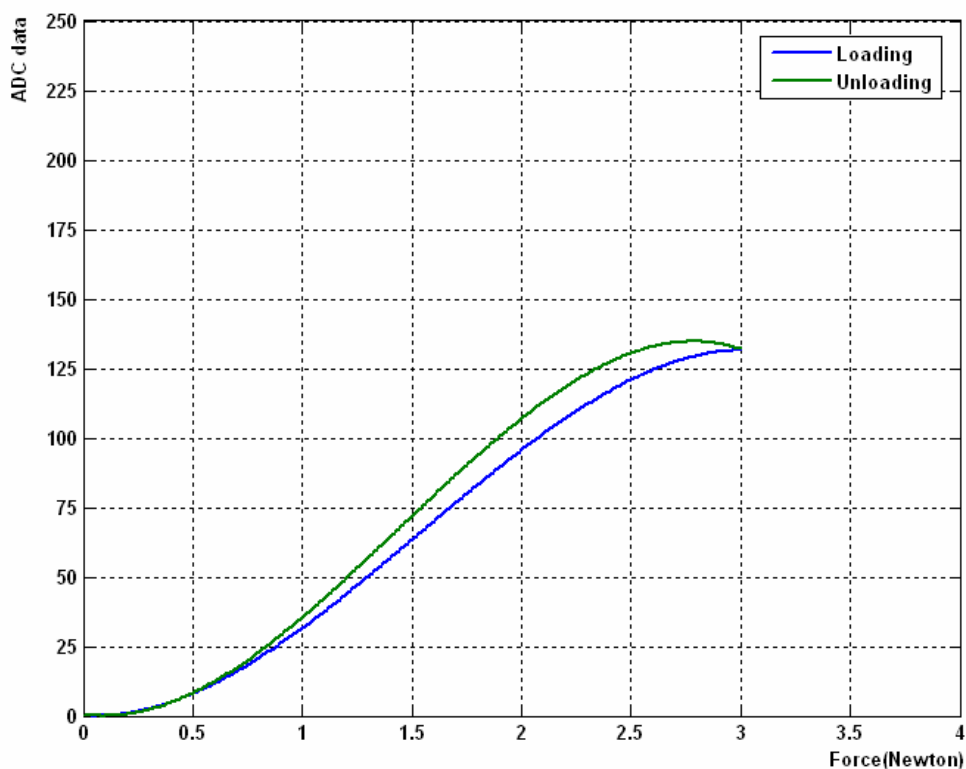


Figure 4.4: Hysteresis curve:

(lower curve: increased force in 1 minute; upper: decreased force in 1 minute)

### Temporal Resolution

This section discusses the resolution of the tactile sensor capable of processing temporal resolution. In the first experiment, the indenter was used to press on the tactile sensor surface to test the response. The 1-mm deep indentation was maintained for 1 second and repeated every 2 seconds. The data were recorded and plotted on the graph in figure 4.5 where the horizontal axis is time and vertical

axis the ADC data above the particular tactile element. The time used to maintain the indentation and repetition time were reduced to half after every ten seconds; in other words, the indentation frequency was doubled every ten seconds. This was to test the frequency of pressure at which the tactile sensor would or would not respond.

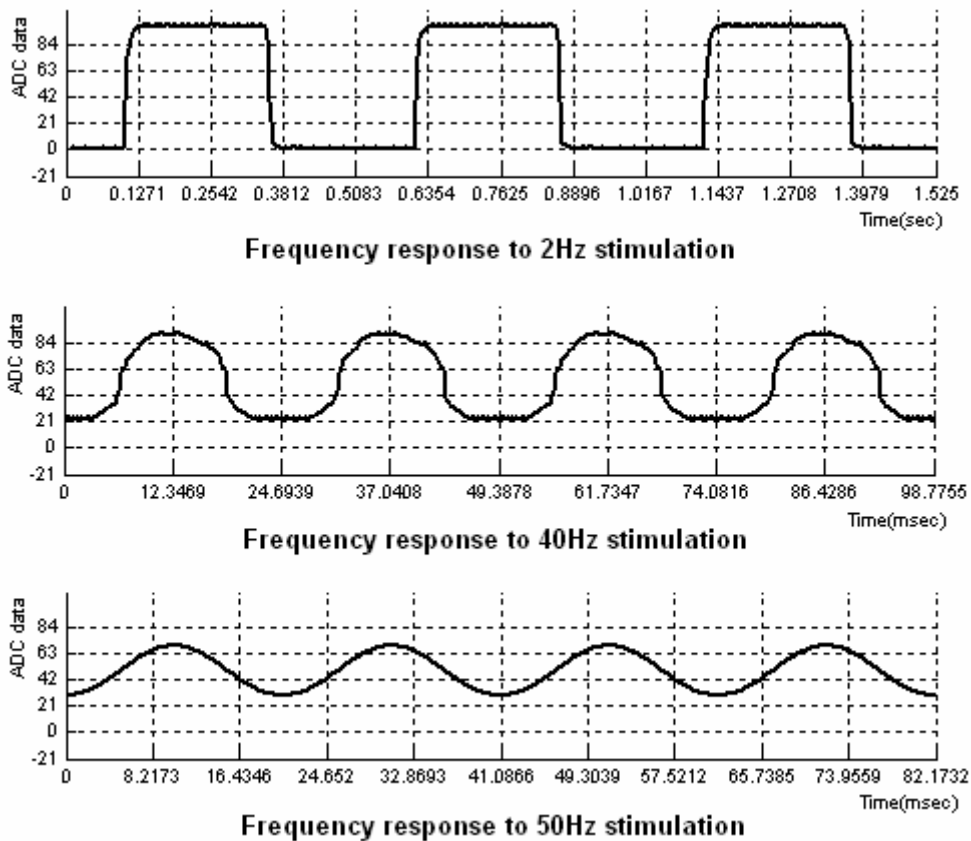


Figure 4.5: Temporal response

Theoretically, the test methodology above would yield square-wave signals. In practice, however, square waves were not apparent. This could be attributed to the physical behavior of the material. With a high indentation frequency, the ability to restore to the quiescent state was reduced resulting in a rounding of the waveform. From the graph in figure 4.5, the data becomes unstable at the frequency of 40Hz and diminished completely at 50Hz.

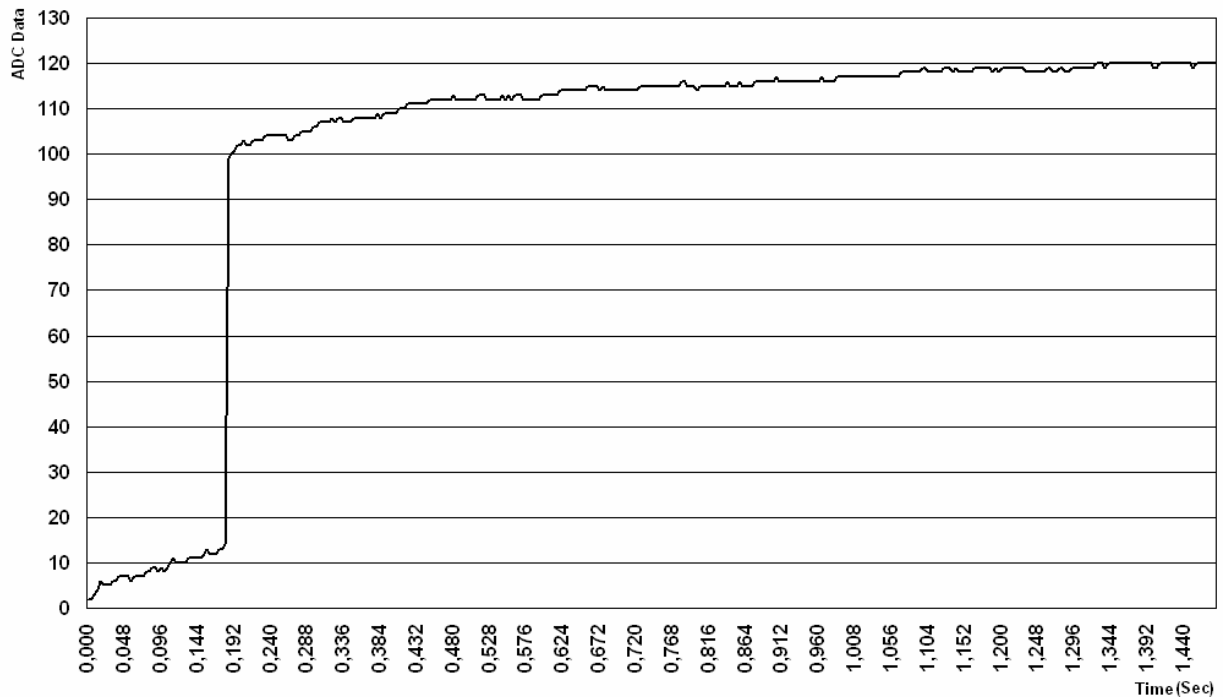


Figure 4.6: Data from pressing on a tactile element

The second experiment to test the temporal resolution was conducted by maintaining a 1-mm indentation on the tactile sensor surface. While a constant force was being applied for 1.5 seconds, no noise spikes were observed at the start of the applied force. In fact, a square wave is not apparent in the presence of any other kinds of external force disturbance because of the gradual decrease in resistivity. In addition, the polymer behaves like a low pass filter in the presence of an external force disturbance. In this way, the conductivity increases and decreases slowly. As the transitory time is finished, the system elasticity tends to restore the foam to the quiescent state and the resistance returns to the original value.

### Sensitivity

One of the most important performance criteria is pressure sensitivity. This can be defined as the relationship between the tangent of the data curve from the measured voltages and the displacements. To evaluate the sensitivity of the sensor, the relationship between measured voltages and the displacement pressing on a specific tactile element was measured.



This was equal to the change of measured voltages in Figure 4.7 divided by the change of the displacement amplitude. From the slope in this Figure, the sensitivity was 1.6 volts per millimeter.

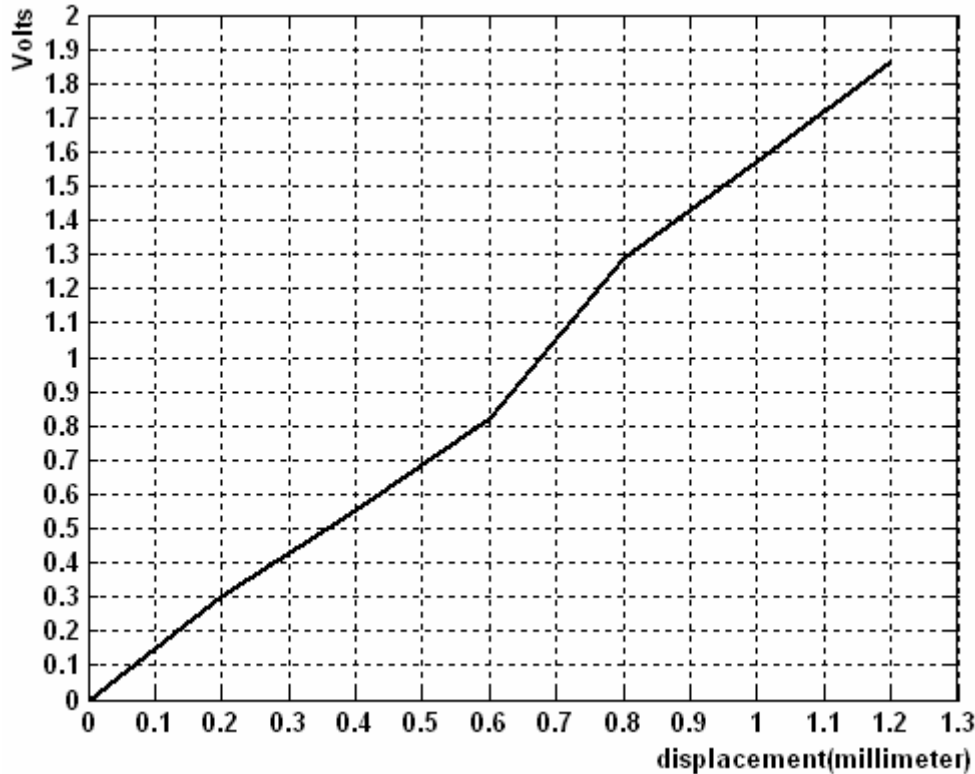


Figure 4.7: Sensitivity and Resolution

Sensor response was affected by the applied force and the force distribution as well as the tactile sensor. The problem is that the response per force unit area varies over the applied area. That is, as the area of an applied stimulus of constant pressure changes, the sensor output also changes. The response variation subject to stimulus size was due to both mechanical and electrical properties. If the tactile sensor consisted of discrete force sensing elements that had no connection to one another, there would be no cross-talk. However, since the tactile sensor in this research had interconnecting components in them, elastomeric covers and mechanical connections became a significant factor. On the other hand, the sensor-scanning electronics was not an obstacle in determining the response per force unit area because it could read a particular cell without ambiguity.

### Linearity and Time variance

Figure 4.8 shows variations in the contact resistance when forces are applied to the tactile sensor surface. In the experiment, a 3-mm x 20-mm x 55-mm piece of foam was placed on a flat surface. Then the indenter was used to depress the foam. Forces of 2, 4, 6 and 8 Newtons applied to the foam surface yielded resistances of 650K $\Omega$ , 250K $\Omega$ , 100K $\Omega$  and 50K $\Omega$  respectively as shown graphically in the force-resistance relationship of figure 4.8.

The response was monotonic, although not perfectly linear, when the forces were small between 0 and 4 Newtons. The measured values showed that this tactile sensor had a high sensitivity in this range and a lower sensitivity to increasing forces outside this range.

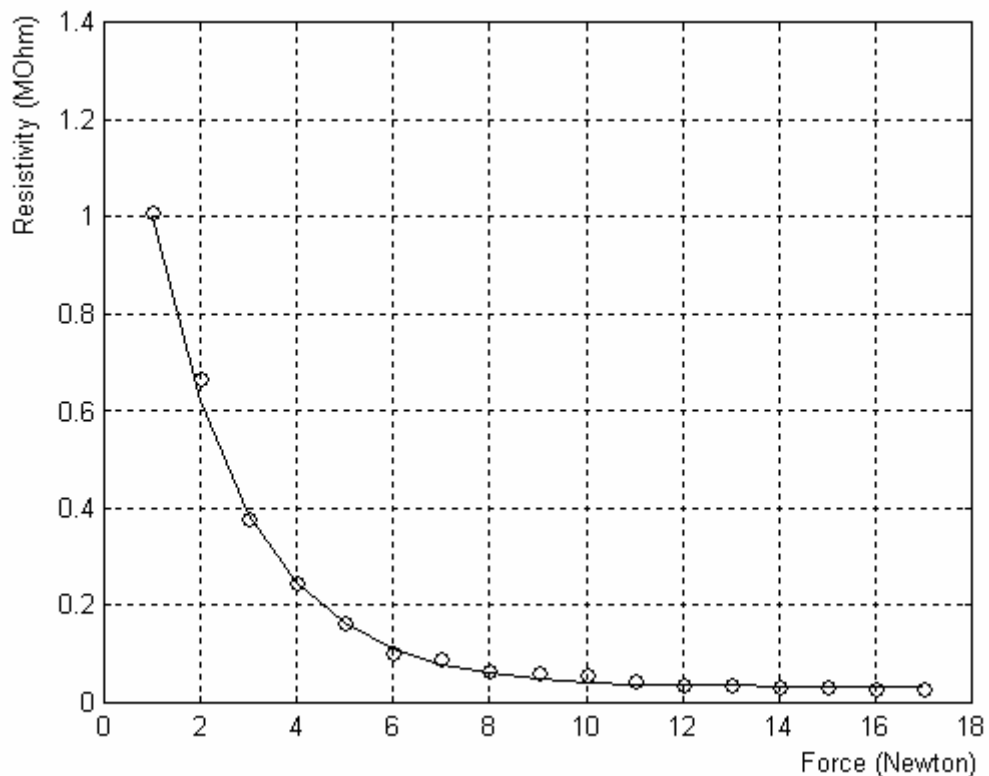


Figure 4.8: The relationship between force and resistance

The advantage of smooth and continuous curves is the applicability of computational methods in fitting mathematical equations to the curve.

We found that there is a well-defined mathematical relationship between the range of applied force and the values returned by the tactile element.

From the graphical trend line shown in Figure 4.8, we see that the relationship between an applied force and the returned sensor value obeys the formula:

$$R = (1.579e^{-0.449(F/N)} - 8.365 \times 10^{11} \times e^{-32.34(F/N)}) \Omega \quad (3)$$

where R is the value returned by the tactile element and F is the force (Newton) applied to the tactile surface. The coefficients, 1.579 and  $8.365 \times 10^{11}$ , have the units  $\Omega$ , while 0.449 and 32.34 have the units  $\text{Newton}^{-1}$ .

Temporal variation of data from the tactile sensor is another important factor which needs to be discussed. The graph in figure 4.9 shows data collected from the tactile sensor array during actual gripping of a metal cuboid. The plane of the tactile sensor array was parallel to that of the object. The graph lines with different colors represent data from different tactile elements. The right hand section of the figure provides a description of the relationship between the colors and the positions of the tactile elements. For example, R2C7 indicates the tactile element in the second row of the seventh column. From figure 4.9, it can be seen that signals sensed by tactile elements may change, although the force on the tactile surface remains stable. The ADC data increased with time within the first second, after which they became stable.

Although differences in the height of each line reflect different sizes of force exerted on each tactile element, this is not a major problem. It can be seen from figure 4.9 that each line has increasing height or differently increasing rates during the first few seconds, i.e., non-symmetric, which is a more serious problem. In conclusion, this type of sensor may generate non-linear and time-variant signals as well as different variants in each tactile element.

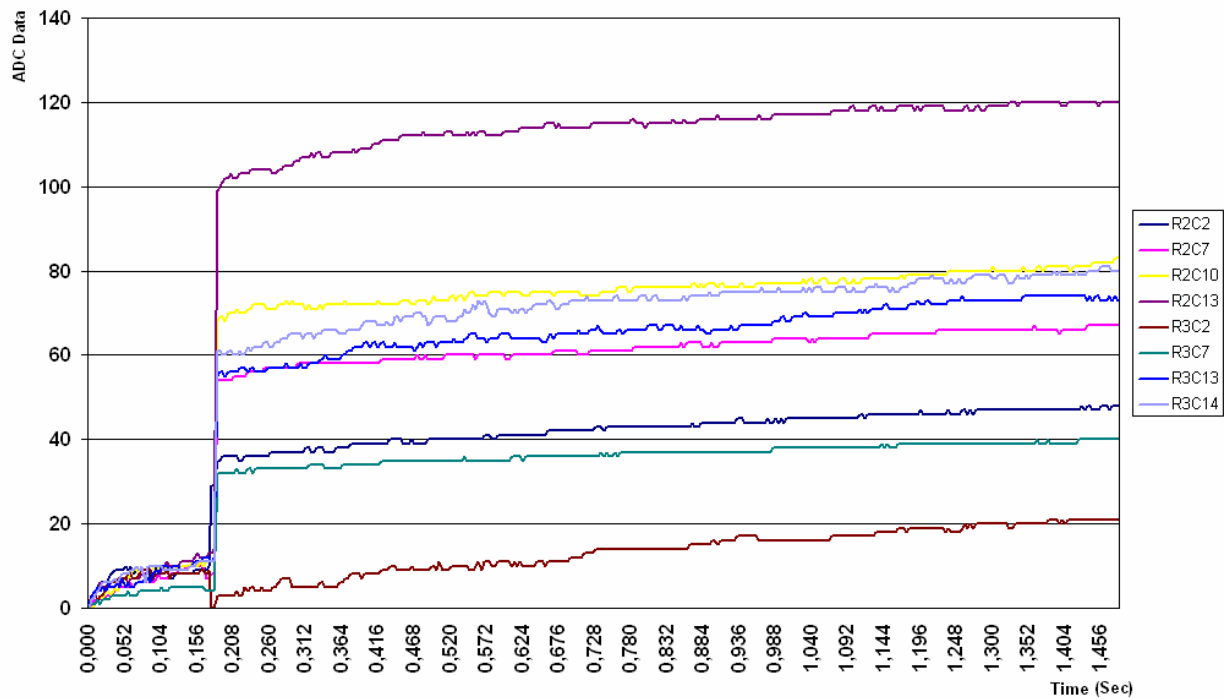


Figure 4.9: Time variant data

These sensor elements have a markedly non-linear profile with changes in concentration. Calibration models have been investigated in order to differentiate between static and time-variant signals. They are also used as a compensation method to describe the interactions between the analyses and real data from sensors for exploratory studies and calibration. In the selected scenario, they can be used to predict, and compensated for, time-variant signals within the first one to two seconds after making contact with the object. When calibration within a range of a few samples has been carried out, the constants pertaining to the model will be evaluated. Because field data are collected and manipulated (computed) over a period of time without laboratory calibration somewhat greater data errors are expected. To partially compensate, the field data is corrected using a nonlinear interpolation between successive laboratory calibrations. The objectives of this section are: 1) to apply a non-linear calibration model to correct the tactile sensor; and 2) to monitor sensor performance whilst it is in use.

Calibration is a specific type of inverse prediction where  $f(t_0)$  is an unknown value, but is noted in one or more further observations.

It does not affect the point estimates and does not affect the construction of intervals. Data for calibration problems come from a calibration sample of “known”  $t_i$  values, which are used to produce responses,  $f(t_i)$ ,  $i=1,2,\dots,n$ . As a starting point in the analysis, we assume that the variability in  $f(t)$  for the analysis sample is similar to that for the calibration sample.

It has long been popular to use linear regression and least-squares polynomial fitting for the determination of instrumental calibration graphs. It is simple to compute and in the case of normally distributed uncorrelated random errors, it is probably optimal. However, there exists a weak alternative which, in some circumstances, may not be preferred, such as in our case. Direct search methods extend their uses to a much larger and more general class of functions.

The way in which the unknown parameters in the function are estimated, however, is conceptually the same as it is in linear least-squares regression. Direct search has been used as a linear regression method to determine the inner linear relationship between the dependant  $f(t)$  and independent variables  $t$  using a number of principal components. This adaptation uses of a direct search technique known as the Nelder-Meade algorithm. It does not attempt to approximate any gradients or other partial derivatives. It is quite effective on small problems involving only a few variables which can also be handled by functions employing optimization methods.

For the search method, we use the Nelder-Meade direct simplex search. This search has the advantage that it has memory and can go back to previous search candidates and thus is less likely to get “stuck” in a search. Unlike many other search procedures, it does not require the generation (by analytic or numeric means) of derivatives. Like most searches, it works best at low dimensionalities. We have found it to be a good robust searcher for this type of problem compared to other searchers we have used. The software is implemented by defining an objective function that is to be minimized. Like all search program, this function has a number of stopping conditions. These include the objective function reaching a minimum as defined by a tolerance and within a maximum number of iterations. Alternatively, successive

iterates may differ by less than a specified tolerance. Note that successful searches do not mean that the global minimum has been found.

A nonlinear model is any model of the basic form:

$$y = f(t, \beta, \lambda) + \varepsilon, \quad (4)$$

where the functional part of the model  $f(t, \beta, \lambda)$  is not linear with respect to the unknown parameters,  $\lambda$  and  $\beta$ . The method of least squares is used to estimate the values of the unknown parameters. The models to meet two criteria are of practical importance: the function is smooth with respect to the unknown parameters and the least-squares criterion used to obtain the parameter estimates has a unique solution.

The following model for the calibrated tactile data is proposed:

$$f(t, \beta, \lambda) = \beta_1 e^{-\lambda_1 t} + \beta_2 e^{-\lambda_2 t}. \quad (5)$$

For the purpose of tracking and correcting this non-linearity, we have devised a four-parameter calibration function and corresponding linearization function which characterizes the sensor elements response over the first few seconds after the object has made contact with the tactile surface.

For the purposes of illustration, consider determining the best-fit curve  $f(t) = \beta_1 e^{-\lambda_1 t} + \beta_2 e^{-\lambda_2 t}$  given a small dataset and using uniform weighting to simplify the model. Real calibration would associate an error estimate with each calibration point and weigh them inversely proportional to their error estimates. Least-squares fitting is derived from minimizing the expression:

$$\chi^2 = \sum_{i=1}^N [f(t_i, \theta) - f(t_i)]^2 \quad (6)$$

The alternative method of robust calibration is called minimum 1-norm. It has the distinct advantage that it emulates more closely the techniques used by a trained analyst – drawing a line by eye through the data which minimizes the absolute deviation between the calibration points and the line. It has the same number of points above and below the fitted line. Minimum 1-norm is derived from minimizing the expression:

$$m = \sum_{i=1}^N |f(t_i, \theta) - f(t_i)| \quad (7)$$

We will consider Figure 4.9 with a proposed nonlinear model calibrated over a few seconds of concentration range using the same time sequence from 0.2 to 1.4 seconds.

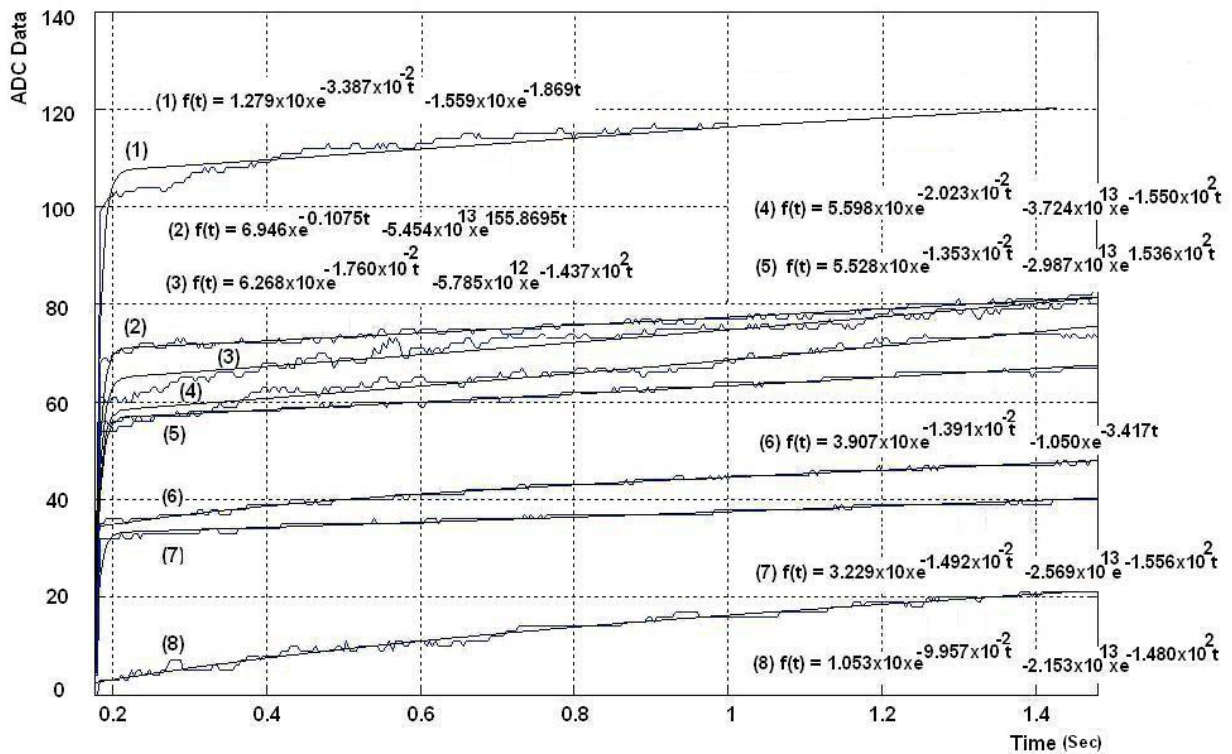


Figure 4.10: Calibration of Nonlinear models vs. original data

Based on Figure 4.10, all calibrations are accurately determined and, from moderate to high concentrations, give quite similar results. It is clear that the

proposed calibration is accurate for the values near the real data that correspond to the minimum 1-norm retaining accuracy over the calibrated range.

A model parameter is determined by fitting a function to the experimental data using least-squares minimization. Models will be applied to corrected and linearized sensor values for all tactile elements concerned. The linearization process is illustrated in Figure 4.10 for a set of sample data collected after contact with the object. The values of  $\lambda$  and  $\beta$  are progressively approximated after the correction process on a few samples of data. The parameters  $\lambda$  and  $\beta$  therefore provide an index of a sensors non-linear properties, which can be recorded to track conditions and to correct field data using post-processing.



### 4.3.2 Tactile Sensor Characteristics

#### Spatial Resolution

The spatial resolution of the sensor is limited by the space between the tactile element center and the elastomeric properties of the protective material covering the fingerplate. For a sensor that records just the surface normal force, a point source should be detected by only one or more cells directly in contact with the stimuli. Besides, spreading to and blurring from adjacent cells should be minimal because a sharp sensor response gives more details of the tactile force outlines of the object.

Figure 4.11 shows the response of a single tactile element when the indenter was used to scan a straight line across the surface. By pressing the indenter to a depth of 1 mm on the tactile surface, the data were measured and collected from the eighth taxel located in the middle of the fingerplate. The tactile response changed with the indenter position due to underlying continuum mechanics of the foam media. It showed the peak forming of signals around the area of contact. This was because the distance between tactile elements was constantly 2 mm. From this, the indentation depth could be determined to be about 1 mm.

The number of contacts included 16-grid points with their centroid at the eighth point measured from a coordinate located at the middle of the fingerplate. It can be seen from figure 4.11 that the tactile sensor could discriminate between simultaneous contact points whose distance was at least 2 mm. This means if there are any contact points whose distances are less than 2 mm apart, the tactile sensor will sense them as one contact point.

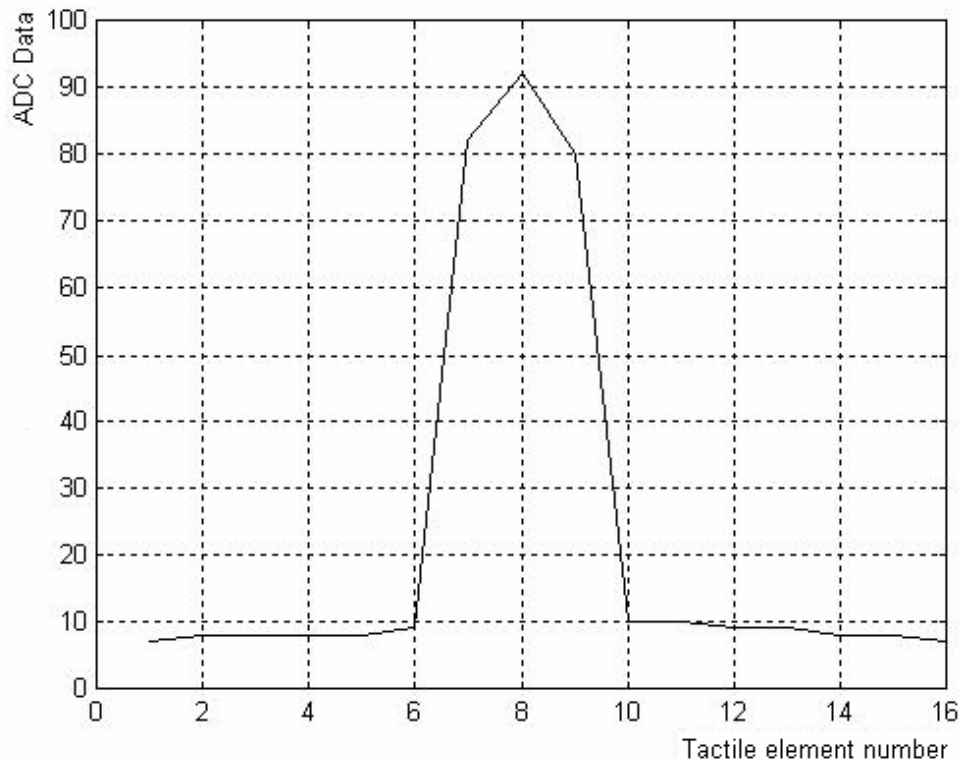


Figure 4.11: Single tactile response to lateral scans

In some cases, however, it may be useful to vause the propagation of strains caused by contact points between adjacent tactile element sites. This is not an effect from the normal force of contact points but a side effect resulting from the nature of an elastic material and a surface tension caused by the deformation of contact points. Experiments involving this phenomenon have been introduced during previous research studies. Fearing and Hollerbach [Fearing and Hollerbach, 1985] showed theoretically how strain sensors placed below a tactile surface could be used to extract the angle of inclination. Their experiments also adapted an elastomeric material covering the strain sensor array. The spatial effect caused by the covered material lead to an increased sensitivity of nearby sensor elements.

## Localization

Tactile localization is the ability to locate a contact point on a tactile surface that has just been touched. Generally, the ability to locate the stimulus site accurately increases as the density of tactile elements increases. In this experiment, the indenter was pressed on the tactile surface to depth of 2 mm. A captured frame of the tactile data is shown in figure 4.12. The frames were recorded at the exact moment at which contact began. The number in the image represents the ADC data at the contact region on the tactile sensor.

To understand the distribution of the displacement field in the contact area, frame 1 and frame 10 were compared, as shown in lowest part of the picture. These two frames were 9 frames apart with 90 msec time difference and about 17 mm of object movement. All the objects moved to the left, and the region bounded by the circle in the upper panel moved to the corresponding region in the middle panel. From a three-dimensional reconstruction of the tactile data, the portions of the surface in contact with the indenter could be estimated. The tactile sensor was able to detect multiple areas of contact, and the minimum inward displacement that could be detected was 0.1 mm.

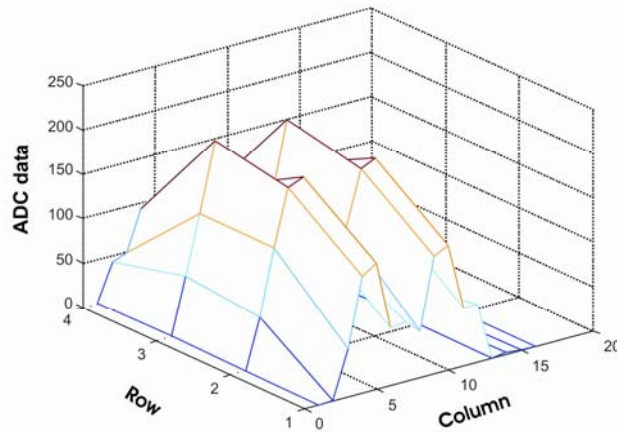
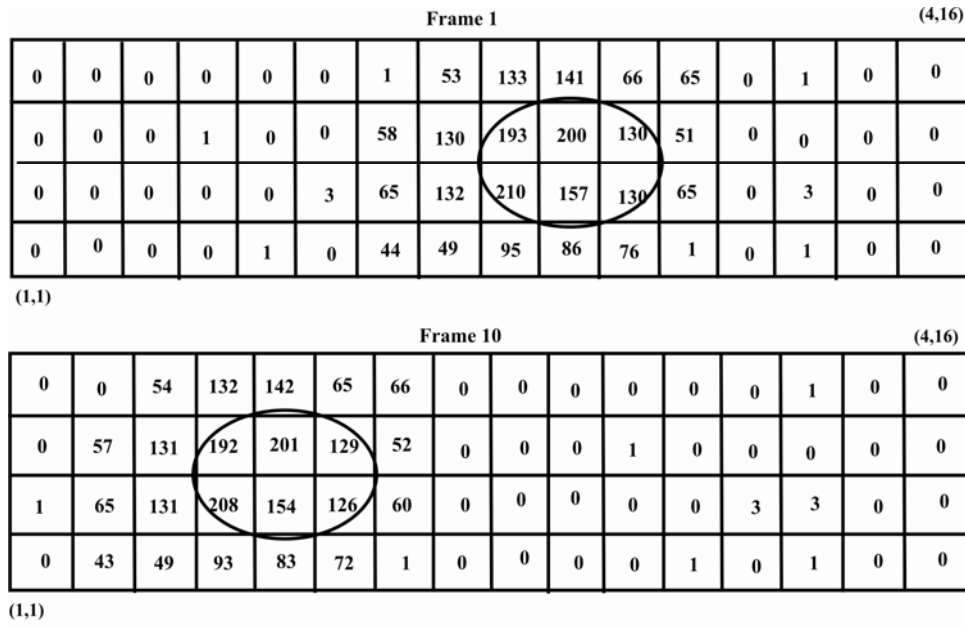


Figure 4.12: Frame of image

To identify the location of contact points, it is necessary to use a realistic method that requires some computing power. The basic one is the center of force, which is defined in the same way as a moment around the axis. The method is called weighted averaging. The location of the indenter can be more finely located by the weighted averaging of the response of neighboring elements, based on the following relationship:

$$\mathbf{x} = \frac{\sum_{j=1}^m \sum_{i=1}^n (f_{(i,j)} \mathbf{x}_i y_j)}{\sum_{j=1}^m (\sum_{i=1}^n f_{(i,j)} y_j)}, \mathbf{y} = \frac{\sum_{j=1}^m \sum_{i=1}^n (f_{(i,j)} \mathbf{x}_i y_j)}{\sum_{i=1}^n (\sum_{j=1}^m f_{(i,j)} \mathbf{x}_i)} \quad (8)$$

where  $x$  and  $y$  are the expected location of the indenter, and  $x_i$  and  $y_i$  are the grid location of a sensor unit  $(i, j)$ , and  $f_{(i,j)}$  its output. The results are shown in figure 4.13, which compares the locations predicted from the above formula (represented by dots) to the actual indenter positions set by the  $x$ ,  $y$  stage (represented by circles).

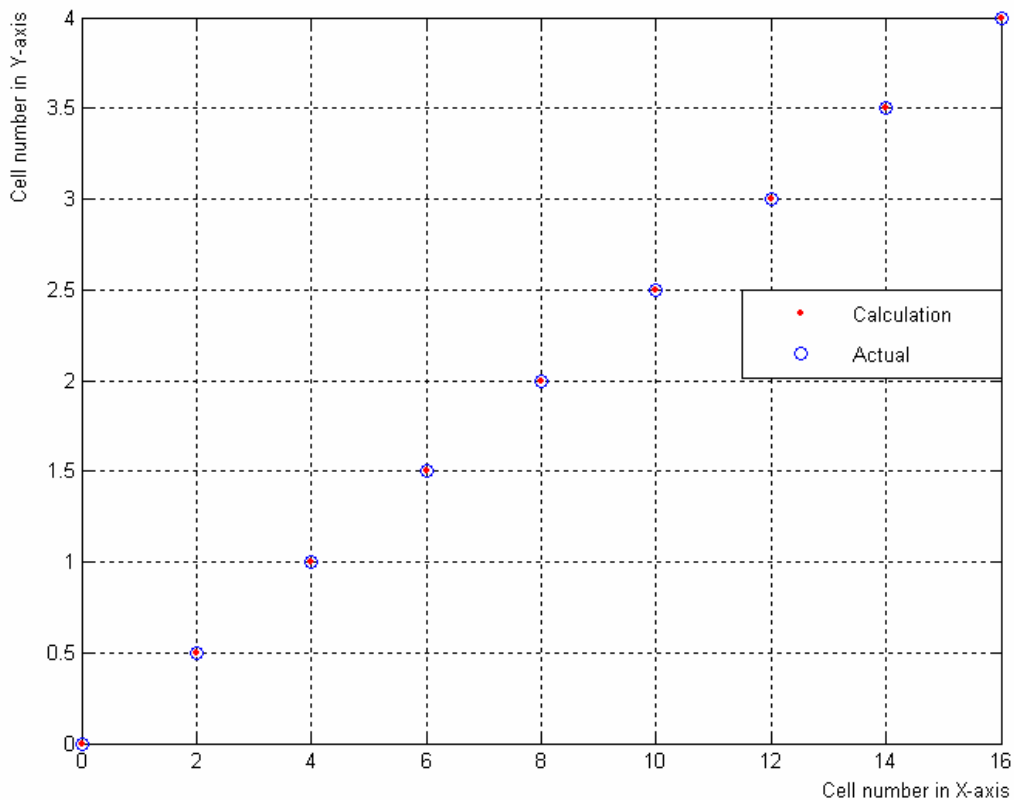


Figure 4.13 Accuracy of point source localization using a weighted average

Figure 4.13 shows that the expected location of the indenter using the weighted averaging method and the actual location of the indenter were always the same; in other words, the estimation was 100 percent correct. Consequently, this method can be used to define the contact location of object acting on the tactile surface.

### 4.3.3 Tactile Performance

#### Shape Determination from Force Distribution

The shape of an object can be determined by pressing it against the tactile sensor and recording the resultant data profile. This ability is especially desirable when a visual inspection is impossible, such as when a manipulator end-effector obscures the view. The spatial resolution results of the previous section indicate that the sensor shape-discrimination ability should be good. To verify this, several small objects were pressed against the tactile surface, and the data outputs recorded. Figure 4.14 shows threshold filtered binary versions of the sensor output for these objects. The response is shown in this form to demonstrate the outline of the objects.

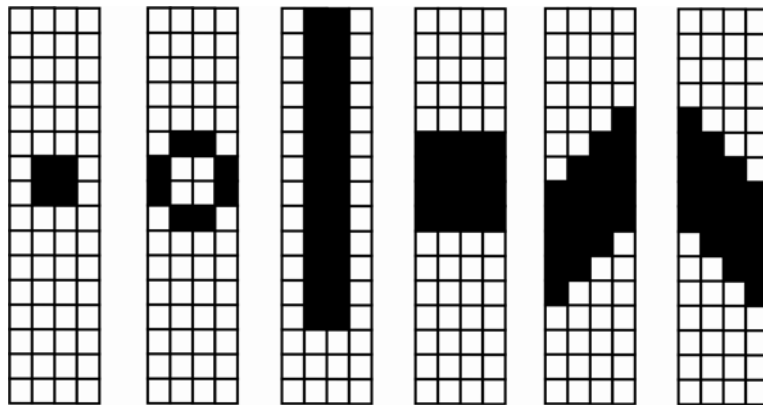


Figure 4.14: Threshold filtered sensor output

From left to right: a ball, a ring, and a cylinder pressed on the tactile surface;  
a rectangular cube pressed on the tactile surface at different angles

Data from the tactile arrays are used to show the force distribution at the robot finger to forecast the shape of contact points. Figure 4.14 exhibits the two-dimensional shapes of the object grasped between the robot fingers, using the 'binary threshold' techniques. Tactile elements with ADC values above the threshold value are represented as black, whereas those below with ADC values below the threshold value are in white. The pictures in the first three columns of figure 4.14, from left to right, represent a ball, a ring and a cylinder. Those in the last three were

derived from a cuboid being pressed against the tactile sensor surface at different angles.

### **Surface fitting**

The previous section discusses only two-dimensional shapes of objects using the threshold corresponding to each tactile element. In this section, the signal from each tactile element will be interpolated at the surface to examine the model fitting between the tactile element and the shape of the object under prehension.

There are many techniques available for the construction of three-dimensional surfaces which correspond to data arranged in array format, such as Spline Surface, Basier Surface, Polynomial surface, and NURBS Surface as defined in section 2.4, etc. For all these techniques, constructing surfaces from discrete data requires interpolation. However, with the NURBS method the parameter from the surface will have special properties not found in other techniques [Piegl and Tiller 1996]. That is, the parameter yielded by the NURBS technique undergoing rotation, translation, scaling, and projection represents the actual force on the surface. Consequently, parameter data from the tactile sensor during prehension can be compared with similar data in order to determine whether it is the same object despite different positions and orientations on the tactile sensor surface, or if several objects with different sizes have similar shapes.

The first sample of the surface generated by the NURBS technique is shown in figure 4.15. It was recorded during the prehension of a ball by the robot. The figure consists of two planes of the tactile sensor surface. The program illustrating the surface of the object was executed on the PC2, which used data from the database engine which stores data from the tactile sensor.

In the figure, tactile force images are shown. The data are displayed using three dimensional plots. The height of each pair of images corresponds with the tactile element data output. The first image at the far left is derived robotic prehension of a ball. The second image represents a toroidal ring of approximately

1.4 cm diameter. The third image is that of a cylinder. The final three images show the tactile surfaces when a metal cuboid was pressed against it at different angles. In all cases, variations in the pixel height along an object's edges resulted from variations in pressure distribution during indentation of the object against the sensor surface.



Figure 4.15: NURBS surface interpolation  
(NURBS = Non-Uniform Rational Basis Spine)



#### 4.4 Summary

Due to the cyclic application of forces experienced by the tactile sensor, the resistive medium within the foam will migrate over a period of time. Additionally, the foam will become permanently deformed, leading to permanent deformation of the sensor. This causes the sensor to have a poor long-term stability. As a result, the sensor must be replaced after extended periods of use.

Hysteresis in a tactile sensor may not necessarily pose a major problem as some researchers have suggested. The tactile sensing ability used in this study is well equipped to handle complicated manipulation tasks. In addition, a robotic system can compensate for response variations by recording temporal history of manipulator motion. Since increasing or decreasing force on an object is directly attributable to robot motion, it is possible to select an appropriate half of the hysteresis curve in order to translate the sensor output into force.

## CHAPTER FIVE

### Experiments and Applications for Optimization Grasping Force

Numerous research studies and experiments have been conducted in an attempt to attain firm and active object manipulation. [Bicchi, 2000] presented an overview of grasping and mentioned that one of the most needed advances in robotic prehension was to estimate object compliance. [Coelho et al. 2001] developed models of grasp policies and controls which were then verified through simulation. Combining tactile sensing with vision, [Hosada et al. 2002] invented a system that learned to detect slip from tactile sensor information. Using information from an intrinsic sensor, [Bicchi, 2000] developed a method to reduce the risk of slippage by controlling the normal force. [Laschi et al. 2002] presented an anthropomorphic robotic grasping platform developed for evaluation of neurophysiological and other physiologically inspired theories such as biologically-inspired grasping coordination. As one of the most refined robotic hands to date, the DLR dextrous hand has been used with respect to both mechanics and control, in studies using the neural approach to software development. [Borst et al. 2003] demonstrated that the DLR hand was able to catch a ball, play the piano, and to do other tasks. They have also implemented impedance control essential to more autonomous tasks.

Despite their variety in object manipulation and manipulation force control, these methods share the same principles. Robotic manipulation is sensitive to both object characteristics and contact conditions between the robot grippers and the prehended object. Consequently, any changes in contact conditions resulting from the environment will play a significant part on any prehension strategy. This factor needs to be investigated in order that an appropriate response to maintaining a firm grip can be achieved. Although impactive parallel jaw robot grippers are usually capable of prehending only simple object shapes such as cuboids or cylinders, much demands may be placed on force control ability should minimum prehension force be a requirement. To derive force control efficiency, two experiments have been conducted in this study: optimization of grasping force and contact identification which will be separately discussed in chapter 6.

## 5.1 Introduction to Optimization Grasping Force

There is a great deal of previous research in the field of grasp analysis and synthesis. [Pollard 1994] developed a parallel system capable of computing high quality grasps using prototype grasps as input data. [Fischer and Hirzinger 1997] created a system that used a heuristic approach to repeatedly choose 3 contact points on an object and to check whether these points could be realized by the robot hand. Given the goal of minimizing the sum magnitude of contact forces, [Kirkpatrick et al. 1990] proposed a general measure of quality for an  $n$ -contact grasp, defining it as the radius of the largest wrench space ball just fitting within the unit grasp wrench space. [Ferrari and Canny 1992] developed this measure further and proposed another measure minimizing the maximum contact force. [Li and Sastry 1988] noted that these measures were not invariant to the choice of torque origin and proposed using the volume of the grasp wrench space as an invariant quality measure. Li and Sastry also developed a quality measurement using task ellipsoids to better model the space of wrenches required for a specific task.

Robot gripper control has been employed widely in industry. One important aspect of this is simultaneous position and force control ([Raibert and Craig 1981], [Yoshikawa et al. 1988]) as the robot must interact with complex environments during its operation. However, most presently used robots control only position because a simultaneous control of both is complicated in practice. A major problem is that dynamic characteristics of the environment affecting the system are unknown. Moreover, although some features may be known, they usually have variable properties. Consequently, unless such characteristics are exactly known or pre-determined, robot control must be able to adapt itself in accordance with dynamic characteristics of the environment.

The stability in object prehension depends on two factors. The first factor is the adequacy of the grasping force. The second factor is the correct contact location. Numerous researchers have investigated robot gripper manipulation control. [Mason 1981], and [Mason and Salisbury 1985], for example, explained that the main

problem concerning prehension force was involved with a change in the contact location during pre-contact and post-contact.

In grasping and manipulating objects firmly, it knowledge of only the normal force is usually not enough: a more precise measurement of force is required. In addition to the normal force, shear forces are also important in many situations. Shear forces also play an important role in predicting object slippage which may be detected by specific algorithms [Cuttino et al. 1988].

Piezoelectric thick-film sensors are a primary transducer for a slip detection sensor. These sensors produce electrical charge across their surfaces when mechanically deformed. This is known as the direct piezoelectric effect. They have typical sensitivity of up to 130 pC/ Newton [Torah 2004] compared with a PVDF sensor of only 20–30 pC/ Newton [Yamada et al. 2001, Canepa et al. 1998]. Thick-film piezoelectric sensors have proved their ability to detect vibrations caused by slip [Cranny et al. 2005a, 2005b]. However, the sensors ability has not previously been quantified in terms of the initiation of object slip.

The piezoresistors can measure a force in the range of 0.1–8 Newtons with a maximum spatial resolution of 1-mm, which is the maximum resolution that a human fingertip can differentiate between two different objects [Howe and Cutkosky 1989]. Piezoresistors have been successfully used to detect normal forces on an object, as well as movements of the object associated with slippage. Howe and Cutkosky presented an experimental confirmation of the ability to detect the onset of slip. However, their slip sensing capabilities cannot be characterized directly because they depend on an accelerometer which is attached to the inner surface of the sensor skin. Large local accelerations can be measured when areas of the skin stick and slip while the sensor moves against the surface.

When compared with previously available slip sensors, the electrically resistive foam types used in this research have proved more sensitive. According to Figure 4.8, a maximum sensitivity of 700  $\Omega$ /Newton is available with indentation depths of up to 0.1-mm. Moreover, such systems are inexpensive and can be easily tailored to the

desired application.

The proposed tactile sensor will be applied in grasp experimentation by identifying the least force required for prehension - the method appropriately called pre-slip detections. The subjects used for the experiments consist of objects with different sizes and weights.

This dissertation introduces a new way to detect pre-slip using a resistive tactile sensor without additional sensors. The concept is based on principles of shear strain distribution. The tactile sensor detects the partial incipient slip of a tactile surface by sensing micro vibrations which are caused by an expansion of the slip regions within the contact area during variations in tangential forces. The micro vibrations are detected by an array of electrodes under the tactile surface. The location of the local slip is not specified but the occurrence of the local slip can be predicted immediately following occurrence of the micro vibrations.

## **5.2 Experiment Overview for Optimization of Grasping Force**

Many different slip sensor solutions have been investigated by a number of researchers with limited success. Although today there are still no real slip sensors included in any commercially available robot hand [Cotton et al. 2007], the idea of including them into a design can be tracked back to 1960s [Childress 1985].

However, in many practical cases, it is unacceptable to wait until total slip occurs. It has become apparent that there is a great need to detect the pre-slip and predict the imminence of total slip in order to prevent premature release. A more detailed review of many different slip detection techniques can be found in [Ibrahim and Abdel-Malak 2005].

Various factors, including environmental influences, must be considered in order to manipulate an object and prevent it from slipping when external loads exceed the frictional prehension forces. When an object is retained in the human hand, gripping forces are adjusted according to the object weight and surface friction

(e.g. [Johansson and Westling 1984], [Westling and Johansson 1984a], [Cadoret and Smith 1996]).

[Johansson and Westling 1984] explained the role of tactile signals need to achieve a precise grip during human manipulation. However, the task selected for their series of studies was relatively simple. An object was grasped between the thumb and index finger, lifted vertically off the table, and subsequently replaced on the table. This task is divided into Grasp-Lift-Replace phases where a transition from one phase to the next is triggered by one or more events signaled from tactile units on the fingertips such as slip or touch signals.

Nevertheless, Johansson and Westling's studies are interesting because the relationship between the prehension and load forces could be determined. In a typical lifting task the ratio between these forces remains constant after initial contact with the object. However, to perform the manipulation task smoothly, it is necessary to sense the coefficient of friction at the point of contact. It can be seen that the series of experiments conducted by Johansson and Westling contribute much to an understanding of how tactile sensors in the hands can contribute to control in fine manipulation tasks.

To determine whether similar mechanisms would be of help in the control of robot manipulation tasks, [Howe and Cutkosky 1989, 1996] applied hypotheses from human studies to robotic systems. Their robotic Grasp-Lift-Replace task involved five phases, i.e. approach, loading, manipulation, unloading, and release, linked together by four contact events. A change in the contact events marked the transition from one phase to another. Robotic tactile sensors described in [Howe and Cutkosky 1989, 1993], detect the contact events and trigger the transitions through the phases of the Grasp-Lift-Replace task. The specialized sensors detect slip during finger or object contact as well as information concerning vibration to identify the remote contact events.

The human hand is unrivaled in its ability to grasp and manipulate objects, but all its complexities are not yet understood. However, one benefit the robot fingers in

this study have over traditional robot hands is the fact that they conform to a grasped object's shape, giving rise to larger contact areas and the ability to apply larger frictional forces. Furthermore, a new contact optimization method which provides a better account of deformation is proposed.

In this research, the grasp experiments which account for the ability of a deformed finger to apply normal forces over an area larger than a point is introduced. In addition, the way in which simple methods, such as determination of contact area geometries together with frictional forces and moments, can be used for analysis and optimization of soft contact characteristics is described.

Specifically, the proposed tactile sensor is applied in grasp experimentation by identifying the least force required for prehension. The objects used consist of four different sized solid cylinders. Two experiments are conducted. In the first experiments, each of the four objects, placed on a surface, are prehended by a robot and the minimum prehension force determined by active force variation. Thus, the minimum grasping force is determined. This experiment is divided into phases. In each phase, the signals sensed by the tactile sensors and the techniques used in controlling it are presented.

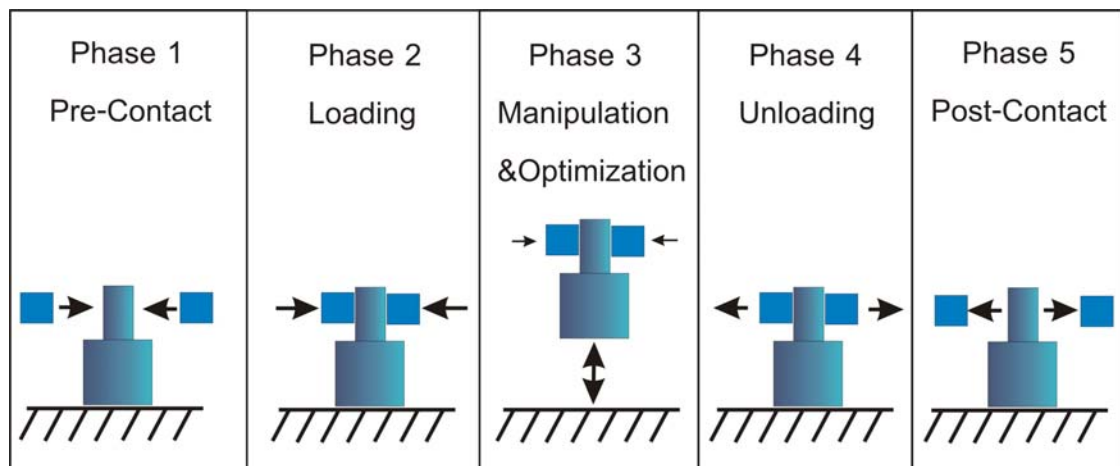


Figure 5.1: Grasp-Lift-Replace Experiments (GLR)

In the second experiments, each of the objects is prehended between the robot fingers above the surface. Prehension forces are then reduced until the first

occurrence of pre-slip is detected and the applied force noted as the minimum retention force.

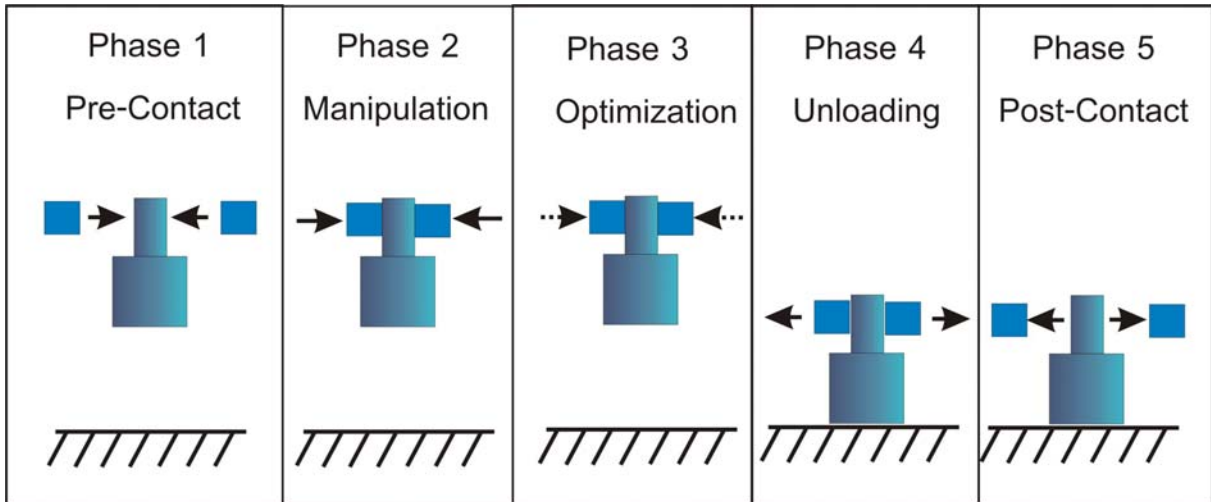


Figure 5.2: Grasp-Optimize-Replace Experiments (GOR)

The experiments also presented the results on grasp-span weights. The robot was subjected to picking objects of different weights and sizes as shown in Figure 5.3 and then was determined for the minimum grasped force.

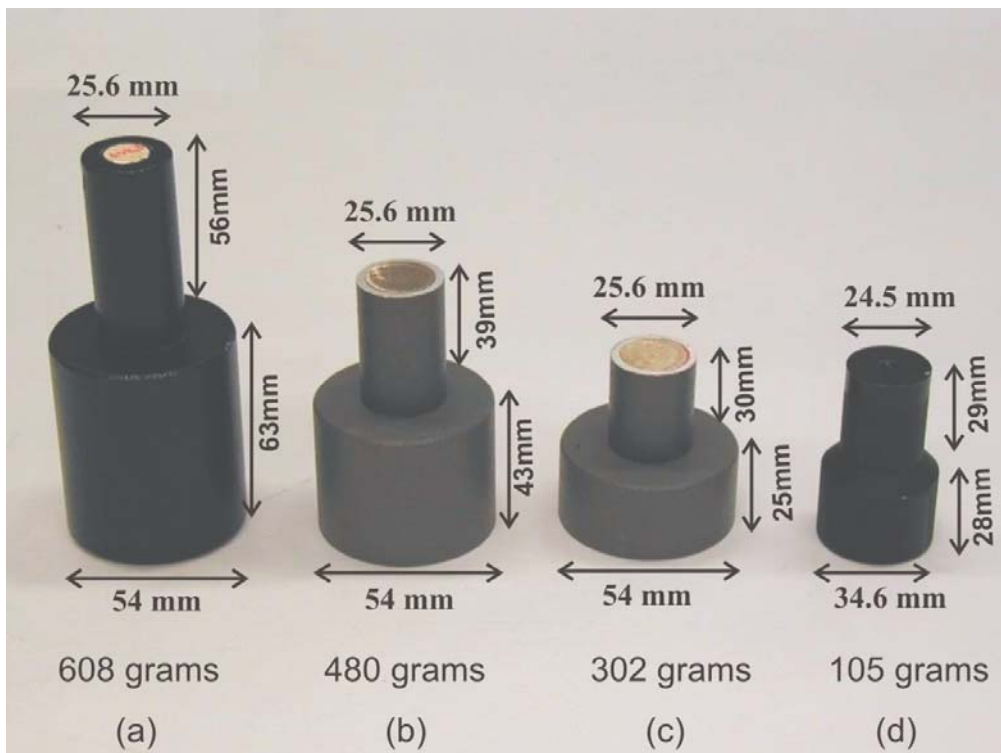


Figure 5.3: A set of test objects



The grasped objects were cylinders, and they were grasped across the narrow part (24.5 or 25.6 mm) of the objects, i.e. the neck of cylinders. The robot would apply the grasped force, which was enough to lift or hold the test weights selected in this order: 608 grams, 480 grams, 302 grams and 105 grams.

A standard lifting platform was used for the experiment. The gripper was in a fixed initial opening distance of 4.5 cm. The opening distance was able to be fixed according to the maximum stroke of the robot-gripper and the grasped position, and the problem of gripper's threshold, which shall be described in Chapter 7, was able to be avoided. The necks of objects were guided to be grasped in the middle of robot-fingers. The same instructions were given as to how to lift the weight, but all objects were observed to be lifted by about 10 cm over the platform and were held momentarily. Then grasped force was decreased, and those objects were placed down again depending on the test cases.

## 5.3 Experiment Setup for Optimized Grasping Force

### 5.3.1 Process

Grasp analysis methods use a variety of contact models to describe the possible forces and torques transmitted from one object to another through an interface. When two rigid objects come into contact at a point, there is always some amount of friction on the tangent contact plane. Static friction tangential to the plane of contact always exists in a single point contact situation. If one object is deformable, then the contact will not only occur at a single point but will spread over a contact area that increases with increasing normal force. Moreover, it is possible for the contact area to support larger frictional moments than in simple single point contact scenarios. The ability to resist friction depends on the magnitude of tangential friction not existent when the contact is just a point. This being applied to the present experiment, contacts on the robot fingers will be able to resist some disturbance moments within the contact tangent plane, leading to further deformation of the fingers and thus larger resistive moments in different directions.

Several theories and experimental results have presented the analysis of deformation contact models. [Goyal et al. 1991] presented the concept of limit surface, characterizing the relationship between relative motion and frictional forces as well as moments for planar contacts. [Howe and Cutkosky 1996] discussed the shape of the limit surface for different contact pressure distributions and developed practical methods for constructing the limit surface using experimental results.

Deformation contact is considered as an efficient object gripping method as it can be applied to intrinsic contact commonly found in practical manipulation such as that in humans. For example, when humans use their thumb and index finger to grasp a pen, the cylinder-shape curvature of the pen will replace the retracted space between the two fingers, which is called soft finger contact. Theoretically, soft finger contact occurs between the real body of the two objects in contact, causing a force distribution of the mass of one object into the other along the contact surface.

However, where the sensor is covered by a soft material, force distribution is a complicated continuum-mechanical science. While the retracted space is not symmetrically replaced by the mass of the other object, the nature of the force distribution requires a complete contact and is interrelated with the surface of the retractable object. These complexities cause difficulties in implementing the proposed sensor strategy: real-time sensory robotic manipulation is complicated and difficult to apply and places enormous computational demands on the control system.

One widely used solution, which will be followed in this study, uses electrodes arranged in an array to measure the shape and characteristics of force distribution. The limitation to this method is that it can only measure or sense normal-force components. Nonetheless, it is able to reduce the amount of information to process and is applicable to force-control devices. The information processed in the experiment is in the form of sets of points with electrodes functioning as tactile elements. This enables tracking of the shape and movement of the object being grasped and calculation of the centroid relative to the localized contacts.

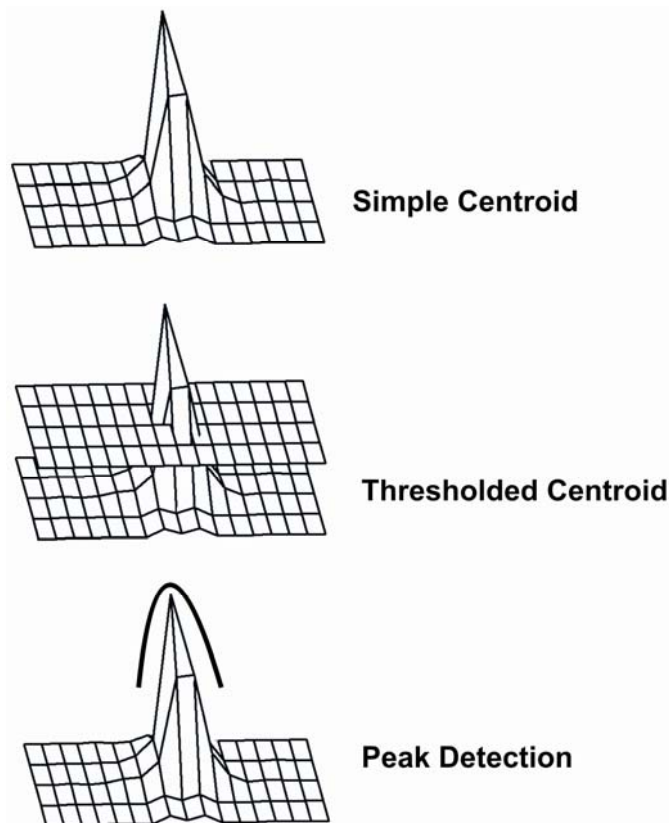


Figure 5.4: Tracking the localized contacts by centroid determination

A number of studies have been conducted on tracking localized contacts (cf. [Nakamura et al. 1986], [Maekawa et al. 1992]) and on the changing positions of centroid. There are three main methods used: simple centroid, threshold centroid, and peak centroid.

The simple centroid is a method that uses the center of force from every tactile element on the side of surface contact for calculating the centroid. The threshold centroid uses only tactile elements with more than 50% force from the maximum force of a certain localized contact for calculating the centroid, thus reducing the sensitivity to threshold noises in tactile elements not close to the contact point. The peak centroid (or peak detection) employs quadratic equations to fit the approximate point with the highest force of localized contact, and the maximum force regardless of its degree is used. Besides, this method interpolates information of the tactile elements close to the point with the highest force in order to track the position with the highest degree of strain at a localized contact point.

The peak centroid has been applied in a number of studies. For example, [Fearing 1990] used sinusoidal curves to fit localized contact information, and applied gradient methodology to find the highest degree of strain for contact localization. This enabled identification of contact points with a resolution of up to one-hundredth of the tactile element width and is thus considered to be an efficient method. [Son et al. 1994] used similar methods except that a quadratic equation was used to fit information around localized contacts to find the point with the highest strain representing the contact point. The resolution resulting from this method was also finer than that from simple tactile element distance (sensor resolution).

However, the amount of time consumed for CPU processing in both studies above is very high, which is inappropriate for real-time tasks. Moreover, the peak centroid is relatively unstable compared with other methods. For example, when there is no single force maximum, i.e., several local force maxima, the calculation will yield results outside the actual location of the tactile sensors.

In this study, the method chosen for tracking localized contacts is that of “threshold centroid” for three reasons. First, this method enables a better estimation of contact localization than do the other two methods. Although threshold centroid is limited in terms of noise from the normal and shear force, this problem exists for all three methods as they follow the principles of solid mechanical models. The model postulates that the surface of the tactile sensors acts as a linear elastic half-space and that the value for each tactile element results from both normal and tangent force components to the surface of the tactile sensors. Nevertheless, as for threshold centroid, if the signal resulting from shear force does not reach the threshold, it can be assumed that the shear force signal does not occur. This enables a better estimation of contact localization. Second, sensitivity to threshold noise is reduced. Finally, the time required for CPU processing is relatively low.

Since the shear force at the contact point is a variable causing slip, and noise is random, predicting the movement caused by the tangent force component to the tactile sensors is relatively inaccurate. Tracking speed in relation to the changing pattern of localized contacts is another important variable. The conditions that correspond with the behavior of the tactile sensors in measuring the changing signals whilst maintaining low micro-controller energy consumption seem to be the best option.

In this study, both sides of the tactile sensors in contact with the object are updated 100 times per second. Thus, the time required for information processing and tracking the pattern of localized contacts depends on the speed of the PC and the processing algorithm. The image data of localized contacts are kept in the database and processed on the computer. The frequency measurement, the amplitude, center of force and average value of the signals resulting from contacts on both sides are processed by the micro-controller in the tactile module.

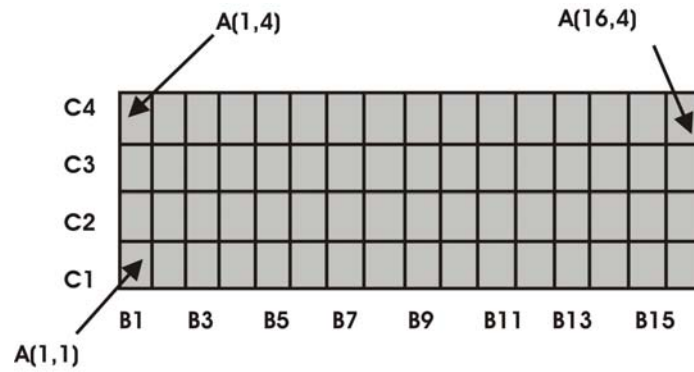


Figure 5.5: The center of force

$$B_n = \sum_{i=1}^4 A(n,i), \quad C_m = \sum_{i=1}^{16} A(i,m) \quad (9)$$

$$M_x = \sum_{n=1}^{16} B_n * i, \quad M_y = \sum_{i=1}^4 C_i * i \quad (10)$$

$$\bar{X} = \frac{M_x}{\sum_{n=1}^{16} B_n}, \quad \bar{Y} = \frac{M_y}{\sum_{m=1}^4 C_m} \quad (11)$$

The method for calculating the center of force on the tactile sensor surface is as follows: First, the vertical and horizontal axes of the tactile sensor plane are determined. The array elements  $B_1, B_2, \dots, B_n$  show summation of the data in columns 1, 2, ...,  $n$ . Similarly, the array elements  $C_1, C_2, \dots, C_m$  show summation of the data in rows 1, 2, ...,  $m$ . The bottom left corner of the Figure when compared with the Cartesian coordinate system is the coordinate (0,0). From this coordinate, an upward direction corresponds to an increasing y-coordinate. Likewise, a rightward direction corresponds to an increasing x-coordinate.

The symbol  $A(x,y)$  shows the data of the sensor element at the horizontal  $x$ -coordinate and the vertical  $y$ -coordinate. The summation of data can be done by totaling the value of each tactile element in the respective column or row. Then the moment on the  $x$ -axis and  $y$ -axis is calculated. Finally, the center of force of both the horizontal and the vertical axes will be represented by  $\bar{x}$  and  $\bar{y}$  respectively, as represented in formulas 9, 10 and 11.

## Slip Detection

For slip detection on the contact surface, frequencies of vibration must be determined by analyzing the tactile data.

Figure 5.6 graphically shows the sensor data of each tactile element at the time the robot grasps the ball while an external force is applied on it. The shape of the graph indicates that it is difficult to express this data by simple mathematical functions. The reason is that the graph consists of a convolution of various mathematical functions. As a consequence, the micro-controller is not able to identify the frequency of slip occurring between the tactile sensor surface and the object surface with complicated mathematics even when using information from all tactile elements in the array. Consequently, it is proposed that signals from only one tactile element be used for describing how frequency from the grasp data are measured, as shown in Figure 5.7.

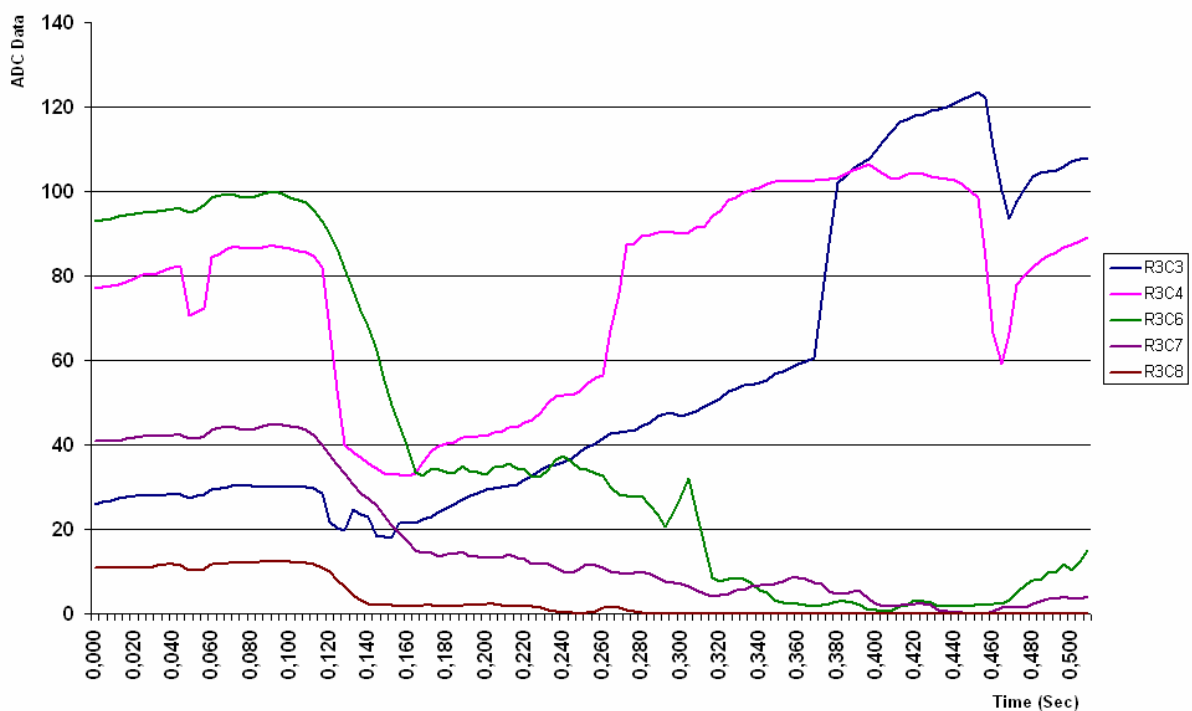


Figure 5.6: Ball Grasping



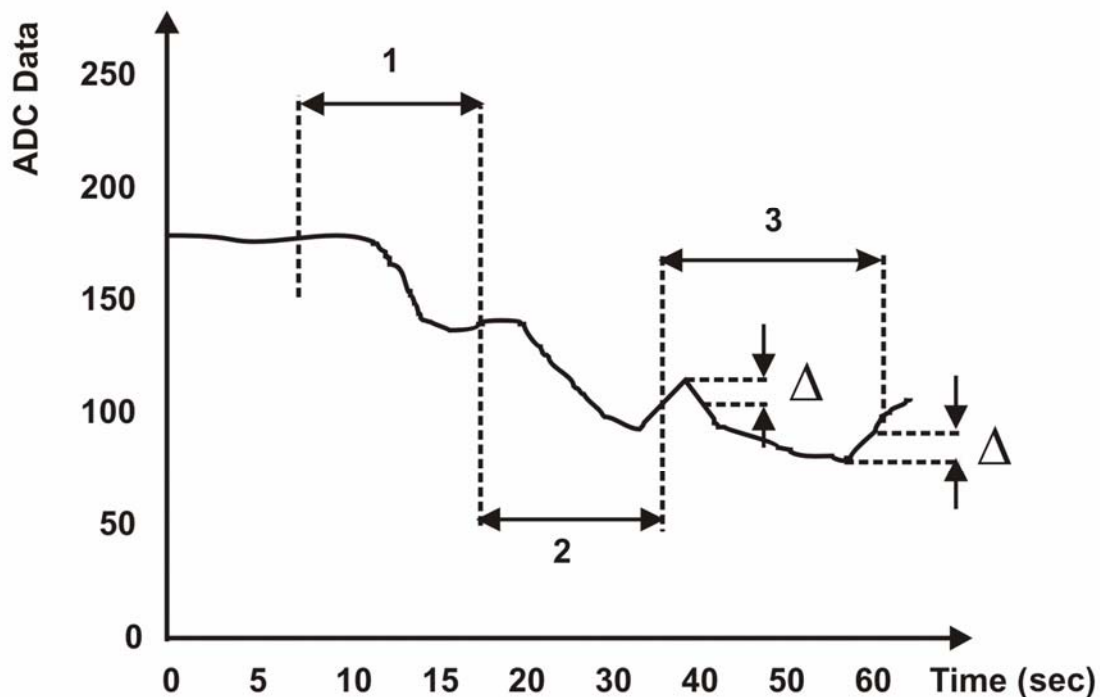


Figure 5.7: Algorithm to find cycle of signal

As discussed above, the signal cycle at each tactile element is not a pure sine-function, but a combination of various mathematical functions. Calculating the number of signal cycles is a simple procedure. Half a signal cycle is the period between a local maximum and the next local minimum. In Figure 5.7 above, there are three cycles. To calculate the local maximum or local minimum in a short duration of time, the threshold  $\Delta$ , must be determined. These are the actual operations of the computer programs running on the micro-controller for control of tactile sensor operations. From figure 5.7, it can be seen that the micro-controller operates on only the signals from one sensor element. Both sides of the tactile surface consist of 64 elements making 128 simultaneous micro-controller operations necessary.

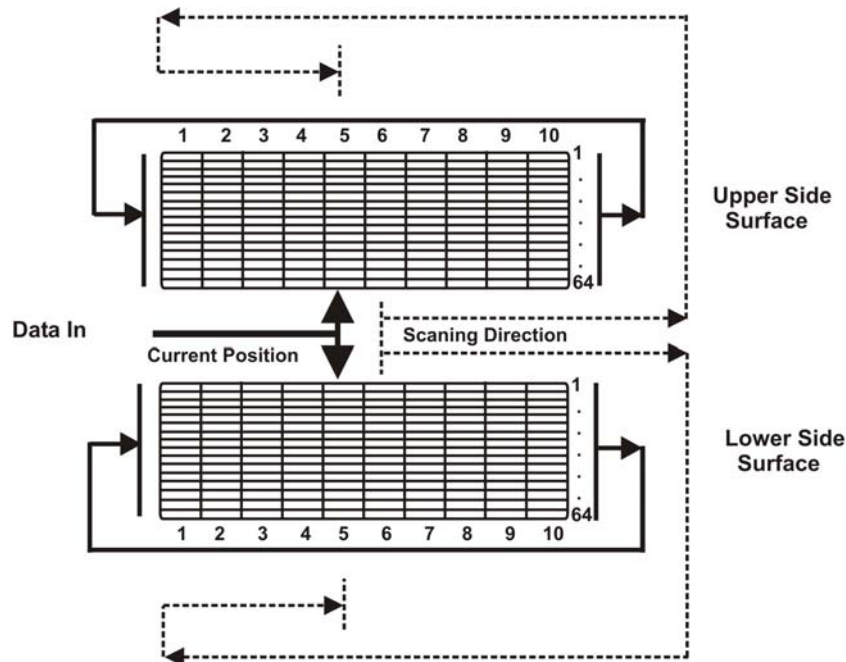


Figure 5.8: Memory queue for the routine to find cycle

Calculation methods consuming low CPU time should be used. In addition, they should be suitable for the speed of the micro-controller that has to keep time for other tasks. As shown in Figure 5.8, data from the two sensor arrays are queued in micro-controller memory as two tables consisting of two sets of 64 rows and a history stack of 10 columns, each of which represents the operations of one contact side. The numbers 1 to 64 represent the data in the 64 tactile elements on each side of the tactile surface which are simultaneously stored in corresponding micro-controller memory. The duration of time ( $\Delta t$ ) to keep the stored data will be programmed in the micro-controller. This is changeable when receiving commands from the BrainThread program in the PC2.

The time duration ( $\Delta t$ ) during which the data is retained is determined by the program. As the data in each column are from different times, filling data into the tables requires a data pointer which gives the present time ( $t$ ) indicating the most recent data. The data in the immediate left column are represented by the time at  $t - \Delta t$ , and those in the next by the time at  $t - 2\Delta t$ , respectively. The data is arranged as a circular queue which means when the data pointer points to a location above 10, the data pointer will be relocated to location number one.

Then the value in the first column will be more current than the value in the tenth column. Scanning (shown on dotted lines) is carried out from the oldest to the most recent of the 128 entries.

### 5.3.2 Experiment Model

Friction plays a central role in a variety of physical systems and thus has been a topic of focused research for more than 500 years. The fundamental experiments of Coulomb in 1785 have evolved into sophisticated surface and interface characterization techniques seen today. Paralleling these experimental efforts, friction models, both phenomenological and empirical, have emerged to provide predictive capabilities and design tools. Friction modeling is an important tool across a variety of engineering disciplines such as contact mechanics, system dynamics and controls. It can help describe and guide the algorithm for applying a tactile sensor in robot applications. The required degree of sophistication for friction models varies widely across application areas, depending on the nature of problems under investigation. Some of these problems, central to the present study, will be explored.

#### Point Contact with Friction

An understanding of the nature of physical contacts will aid in analyzing robotic prehension. When two objects come into contact, they will exert force on the contact point. The contact model of this study together with important variables will be described as follows. A contact coordinate frame is defined as an origin of strain, called a pressure weighted center, of the contact area. The z-axis is the axis parallel to the normal contact point  $n$  and normal forces are represented by  $F_n$ . Contact friction forces perpendicular to the normal force are represented by  $F_t$ . Contact friction forces on the x and y axes are represented by  $F_x$  and  $F_y$ , respectively. The frictional moment is represented by  $M_z$ . The contact point shared by two objects is called a point contact with friction. The tangential frictional force that does not result in movement can be explained by Coulomb's model, in which case there is no frictional moment, i.e.  $M_z = 0$ .

$$F_x^2 + F_y^2 \leq \mu^2 F_n^2 \quad (12)$$

### Deformation Contact with Friction

This case is more complicated in that the contact is not a point but an area whose dimensions are dynamically changing during the prehension process. Although the contact begins as a point, it rapidly conforms to the shape of the object [Ciocarlie et al. 2005]. Consequently, a new contact model must be developed.

Hertzian or uniform pressure methods can be used to find the frictional moment resulting from pressure distributions around a contact point. Although it is applicable only to certain types of problem, [Howe and Cutkosky 1989] demonstrate that the pressure distribution can be estimated by an ellipsoid model. The maximum tangential frictional force and the frictional moment are shown to be related. When the tangential frictional force increases, the frictional moment around the normal contact will reduce. When the frictional moment at the contact point is equal to zero, the friction force around the contact will be equal to the multiplication of friction coefficient and the normal force [Ciocarlie et al. 2005].

From its basic shape principles, the ellipsoid model may be considered as a circular equation with the radius equal to  $\mu(x, y)F_n$ . Therefore, it can be represented by the equation:

$$F_x^2 + F_y^2 + \frac{M_z^2}{e_z^2} \leq \mu^2(x, y)F_n^2, \quad (13)$$

whereby the variable  $e_z^2$  represents the eccentricity parameter that is related to the maximum  $M_z$  to the friction coefficient  $\mu(x, y)$  and the normal force  $F_n$ . Thus, the equation for the maximum frictional moment value is  $\max(M_z) = e_z \mu(x, y)F_n$  [Ciocarlie et al. 2005]. This equation can be applied in analyzing contact surface when the tangential frictional force is considered to be zero, and the variable  $e_z^2$  thus changes

according to the characteristics of contact area such as shape, size, and pressure distribution [Ciocarlie et al. 2005].

Considered in a differential form, the pressure at the contact area can be represented by the equation  $dF_n = p(x, y)dA$ , where  $p(x, y)$  is represented by the pressure distribution function, and  $dA$  is represented by any small areas of  $(x, y)$ . Thus, the tangential frictional force vector at those contact points is  $dF_f = \mu(x, y)p(x, y)dA$ , where  $\mu(x, y)$  represents the coefficient of friction. If the direction of such frictional force is represented by  $U(x, y)$ , the subsection of the local frictional force vector can be represented by  $dF_f = -\mu(x, y)p(x, y)U(x, y)dA$ . Therefore, the total friction force can be calculated by integrating the previously described equations across the whole contact area:

$$F_t = \begin{bmatrix} F_x \\ F_y \end{bmatrix} = -\int_S \mu(x, y)p(x, y)U(x, y)dA, \quad (14)$$

where  $S$  stands for contact area.

The frictional moment is equal to the cross product of the vector  $R$  (the vector from the contact area ( $dA$ ) to the center of rotation, which may be called velocity vector) and the direction of the frictional force acting on the area. Thus, the total moment  $M_z$  can be calculated by integrating the following equation.

$$M_z = -\int_S [R(x, y) \times U(x, y)] \mu(x, y)p(x, y)dA \quad (15)$$

As the velocity and vector  $R$  are always on the same plane, the frictional moment will thus be normal to the area.

From these two equations, the size of force and moment corresponding with the movement at a contact area can be identified.

The known pressure distribution  $p(x, y)$  and coefficient of friction  $\mu(x, y)$  can be used as parameters for finding solutions using optimization methods. However,

these can only be formulated without any guarantee of a unique solution. Furthermore, it is difficult to find the frictional forces in actual applications because of the wide variety of surface combinations and lubrication possibilities; the non-linear relationship between the contact pressure  $p(x, y)$ , the sliding speed, and the coefficient of friction; the effect of temperature rise due to frictional heating on the coefficient of friction.

In classical friction, Amontons (1663-1705) rediscovered Leonardo da Vinci's two laws of friction: the frictional force is directly proportional to the normal load, and the size of object does not affect the friction [Bowden and Tabor 1950, 1974].

In this study, however, the coefficient of friction  $\mu(x, y)$  is a function of the coordinate system, which is different from Amontons' theory. The surface contact between two objects results in deformation, whose degree depends on the size of the applied force, i.e. the coefficient of friction  $\mu(x, y)$ . The type of deformation can be classified into a temporary shape change and a permanent shape change. The temporary shape change is reversible on removal of the force, so that the object returns to its original shape. This type of deformation is called elastic deformation, which refers to a change in material shape at low strains which is recoverable after the strain is removed. It involves the stretching of atomic bonds without slip. On the other hand, permanent shape change occurs when there is breaking of a number of atomic bonds by the dislocations. This type of deformation is called plastic deformation.

When the contact area is small, the frictional forces on the surface are high, expanding the contact area due to its deformability. If the local plastic pressure  $\sigma_v$  is set as a constant, the area receiving the pressure  $N_i$  will be equal to  $A_i = \frac{N_i}{\sigma_v}$ . Thus, the total area receiving the pressure will be:

$$A_T = A_1 + A_2 + \dots + A_i = \frac{N_1}{\sigma_v} + \frac{N_2}{\sigma_v} \dots + \frac{N_i}{\sigma_v} = \frac{N}{\sigma} \quad (16)$$

where  $N$  represents the vector sum of all the normal forces. For hard objects, the actual contact area will be proportional to the magnitude of the force.

However, the situation becomes more complicated with less rigid, compliant viscoelastic surfaces such as the polymer foams found in tactile arrays.

However, in the case of contact with polymeric materials, deformation is viscoelastic and so the frictional forces cannot be calculated using the above formulas. In addition, the deformation does not only depend on the size of the normal force  $N$  but also on its direction and length, which in turn depends on the shape of the object in contact. If the deformation and the degree of force are held constant, then the contact area can be represented by the formula  $N^\beta$ , where  $\frac{2}{3} \leq \beta \leq 1$ . As an illustration, for an elastic solid like rubber,  $\beta = \frac{2}{3}$  [Lincoln 1952], which is a general characteristic of most polymers. The effective coefficient of friction will reduce as the size of the exerted force increases. In other words, the compressive area, as shown in Figure 5.10c, has a lower coefficient of friction than the tensile area.

Due to the viscoelastic properties of polymers, when a polymer is in contact with another surface for a period of time, the asperities start to creep under the normal load. This increases the actual area of contact, thereby increasing the frictional limit. This creep explains why there is a greater difference between static and dynamic coefficients of contact friction between polymeric materials than with contact between two rigid objects.

Howell's equation [Howell and Mazur 1953] of friction force can be reorganized as  $F = (KN^{\beta-1})N$ , where  $(KN^{\beta-1})$  is supposed to be equal to the coefficient of friction. This equation shows the complexity of the relationship between the normal force and the coefficient of friction, which consists of two variables. The first variable is force. The second variable is hysteresis loss at the point of contact

resulting from the surface characteristics of polymeric materials such as roughness or strength of molecular bonds.

The generation of roughness induced dynamic grasping at a deformable contact may be viewed most simply in the context of the model shown in Figure 5.9. The Maxwell model predicts that a material will act as if it were composed of an elastic spring in series with a dashpot. The Kelvin-Voigt Model places the ideal spring in parallel with a dashpot. We introduce qualitative models to describe the behaviour of a typical polymer. The Kelvin-Voigt model gives retarded elastic behaviour, and represents a crosslinked polymer. The Maxwell model gives steady state creep, and would represent an uncrosslinked polymer. With the composition model as shown, it can describe both types of behaviour. The models are simple and suitable for experimental representation of any polymer over an extended period of time.

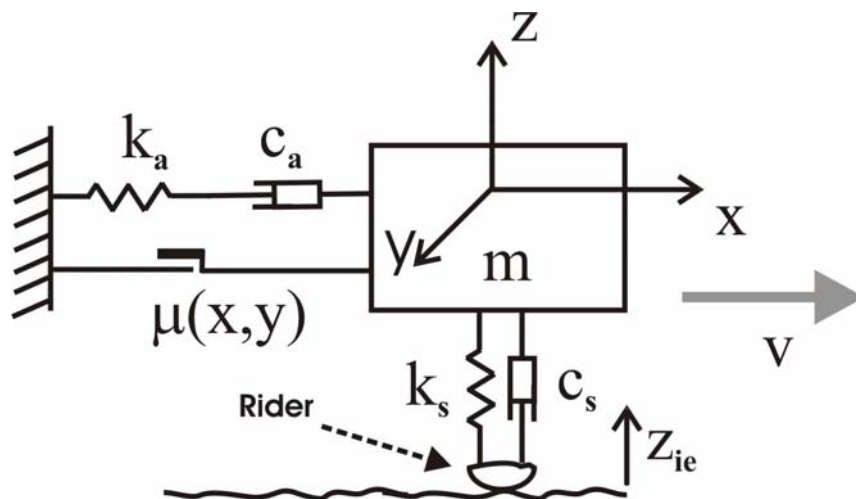


Figure 5.9: Dynamic model [Petchartee and Monkman 2007a, 2008a]

The smooth rider sits in contact with a rough surface moving at a constant velocity  $V$ . The rider is connected to a frame through a suspension characterized by a spring stiffness  $k_a$ , a damping constant  $c_a$  and a degree of static friction  $\mu(x, y)$ . The normal contact stiffness  $k_s$  and any associated damping  $c_s$  are lumped between the mass and the moving surface. The normal stiffness, linearized about the mean rider position, can be computed from Hertzian theory.



The normal motion of a rough surface when the rider moves along the direction  $V$  depends on an excitation  $z_{ie}(t)$  and the object mass, resulting from the roughness of the surface, the deformation of the normal contact point and the relative velocity of the rider,  $V - x$ . Normal motion is governed by the differential equation:

$$m\ddot{z} + c_s(\dot{z} - \dot{z}_{ie}) + k_s(z - z_{ie}) = 0 \quad (17)$$

Newton's 2<sup>nd</sup> law of motion states that mass multiplied by acceleration is equal to force. The  $-c_s\dot{z}$  term represents shock forces resulting from velocity and the  $-k_s z$  term is spring force. If the frictional coefficient is constant throughout the rider motion, the normal force will have a vibration characteristic, which can be estimated by multiplying the frictional coefficient with the normal load resulting from the object weight and gravity. However, in reality the situation is often more complicated.

In this experiment, the force exerted on the contact surface is assumed to result from the weight of the object, thus the normal motion force will be a function of the normal acceleration  $\ddot{z}$  and object weight  $m$ , according to the equation:

$$F(t) = -m\ddot{z} \quad (18)$$

If the frictional coefficient is held constant throughout the rider motion, the normal force will have a vibrational characteristic, which can be estimated by multiplying the frictional coefficient with the normal load resulting from the object weight and gravity. However, this is a simplified formula and real relationships can be more complicated.

With regard to constant friction, the argument is that in order for friction to change, the real contact area, and thus the mean normal separation, of the surface must change [Ibrahim 1994]. Efforts to verify this were made by [Godfrey 1967] who demonstrated a reduction in friction due to normal vibration. With the measured frictional shear force being a function of real contact area, an apparent reduction in friction in the presence of normal vibrations can be expected. The idea was that

normal vibrations could influence the mean surface separation and hence the real area of contact.

The two models in Figure 5.9 can be applied to explain the operation of robot gripper fingers covered by such tactile sensors, as shown in Figure 5.10.

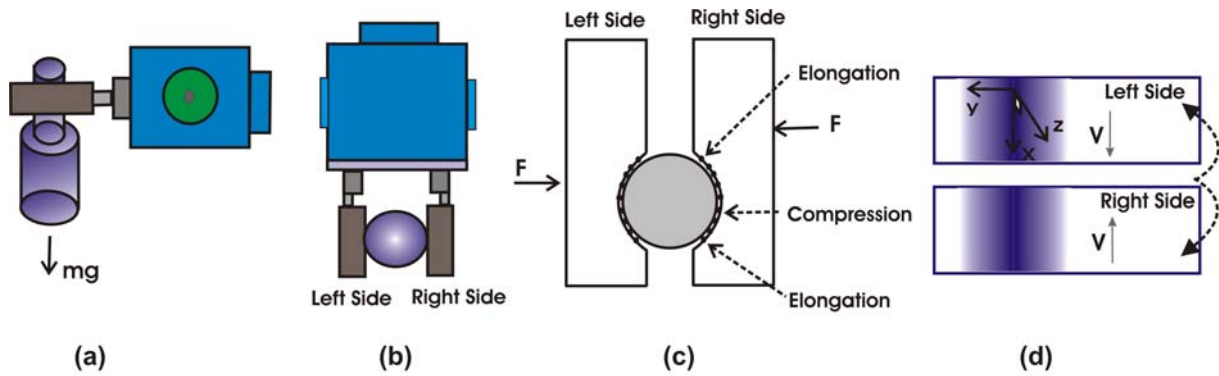


Figure 5.10: (a), (b) Object prehension, (c), (d) area of contact deformation and pressure distribution.

From Figure 5.10, (a) side and (b) plan views of the prehension operation can be seen. Figure 5.10c shows the maximum deformation of the tactile sensor surface when the object is normal to the motion of the gripper jaws. Both compression and elongation strains are apparent and shown as internal pressure distributions in Figure 5.10 d.

Also shown in this picture is the direction of object movement  $V$ . The coordinate system  $(x, y)$  in Figure 5.10 is consistent with that in figure 5.9. When this model is applied, equation 17 is no longer zero as shown in expression 19:

$$m\ddot{z} + c_s(\dot{z} - \dot{z}_{ie}) + k_s(z - z_{ie}) = F_N(t) \quad (19)$$

The normal and frictional force at the contact area are each composed of average components,  $F$  and  $M_G$  respectively and fluctuating components  $F_N(t)$  and  $F_G(t)$ .  $M_G$  is the object weight and  $F$  the prehension force.  $F_N(t)$  is the fluctuating force normal to the tactile surface while  $F_G(t)$  is the fluctuating friction

force. The average kinetic coefficient of friction is usually measured as  $\mu_k = \frac{F}{M_G}$ , but the actual friction, occurring during oscillation is dynamic and denoted by  $\mu(x, y)$ . The fluctuating part of the frictional force becomes  $F_N(t) = \mu(x, y)F_G(t)$ .  $\mu(x, y)$  will change according the object surface: the middle part of Figure 5.10c results from an area with a high pressure, as described in the coefficient of friction for polymeric materials. The equation of the object surface will be estimated by the parabolic cylinder equation  $y^2 - 2pz = 0$ .

From this relation, the instantaneous coefficient of friction becomes  $\mu_i = (F + F_N(t))/(M_G + F_G(t))$ . Tangential oscillations are governed by equations 20:

$$m\ddot{x} + c_a\dot{x} + k_a x = F_G(t) \quad (20)$$

whereby  $k_a$  is the tactile surface hardness, defined as the stress/strain ratio  $\frac{\sigma}{\varepsilon}$  and  $c_a$  is the damping constant;

### Mathematical proof of experimental results

Pre-sliding refers to the movement of an object that occurs when the relative displacement between two points on contacting surfaces is microscopic. There are also points of unbroken contact between the two contacting surfaces resulting in displacement hysteresis which denotes frictional behaviour. Above the force threshold, the system will be critically stable. Displacement will not remain constant for a constant applied force: the object will suddenly accelerate; all contact points are broken, and sliding takes place. Sliding refers to the movement of an object that occurs when the relative displacement is macroscopic. This phenomenon is associated with the stick-slip behaviour (sometimes called "sticktion"). This is the term first used by Bowden and Tabor [Bowden and Tabor 1964], when describing the relative motion of two surfaces in contact. They noted that the motion is governed by

a kinematic friction law while the surfaces are "slipping" and by a static law when there is no relative motion, "sticking".

From a mathematical point of view, understanding pre-sliding friction is important for high precision position control applications. The friction force usually relates to the resistance to motion during sliding. It usually has its maximum value at the commencement of motion (static friction) and then decreases with increasing relative velocity (dynamic or kinetic friction).

To develop a friction law that is fairly well suitable for modelling self-excited vibrations, it is thus necessary to review static and kinematic models and bring them to a point where synthesis is possible. In the "stick" phase, the applied tangential force  $F_t$  is exactly balanced by the friction force  $F$ . That is, the greater the applied force, the greater the force due to static friction becomes. However, there is a limiting value which is given by:

$$|F_t| \leq F_{\max} = \mu mg . \quad (21)$$

It is only when the applied force exceeds this value that slippage can take place.

To simplify the analysis as much as possible, but to retain the essential features to be investigated, the vibration considered at a contact point is a finite-cubic block attached to a rigid wall by a simple spring and dashpot. The system is controlled by the frictional forces between the finite-cubic block and the moving belt upon which it is resting. This results in a simple one-degree-of-freedom structure with a non-linear excitation term. A similar analysis including a many-degrees-of-freedom model for the wheel vibration, yet using only simple models for the friction, has been performed by Heckl and Abrahams [Heckl and Abrahams, 1996]. The governing second order equation for this system is

$$m\ddot{x} + r\dot{x} + sx = F(\dot{x}, \ddot{x}) \quad (22)$$

where  $m$  is the mass of the finite-cubic block,  $s$  is the spring constant, and  $r$  is the damping coefficient. The friction force is given by  $F(\dot{x}, \ddot{x})$ , although it may be more natural to think of it as varying with time.

### First Case: Grasp-Optimize-Replace

The governing equations for the contact surface, obtained by summing forces on the rider mass are

$$\begin{aligned} m\ddot{x} + c_a(\dot{x} - \dot{x}_{ie}) + k_a(x - x_{ie}) &= F_G(t) \\ m\ddot{z} + c_s(\dot{z} - \dot{z}_{ie}) + k_s(z - z_{ie}) &= F_N(t) \\ F_G(t) &= \mu(x, y)F_N(t) \end{aligned} \quad (23)$$

$F_N(t)$  is the fluctuating force normal to the tactile surface while  $F_G(t)$  is the fluctuating friction force. [Anand and Soom 1984] equates  $F_N(t)$  to  $F_G(t)$  using the reciprocal of  $\mu(x, y)$  as shown in (24). It is important to note that the deformation has a  $z$  component because some material passes underneath the contact which means that sliding speed in  $x$  and strain rate  $\dot{z}$ , normal to the surface, are directly coupled [Vellinga and Hendricks 2001].

$$m\ddot{z} + c_s(\dot{z} - \dot{z}_{ie}) + k_s(z - z_{ie}) = \frac{1}{\mu_D} (m\ddot{x} + c_a(\dot{x} - \dot{x}_{ie}) + k_a(x - x_{ie})) \quad (24)$$

When one of the contact points slips, the relation between displacement and time will be approximated to a linear function; i.e. [Howe and Cutkosky 1989].

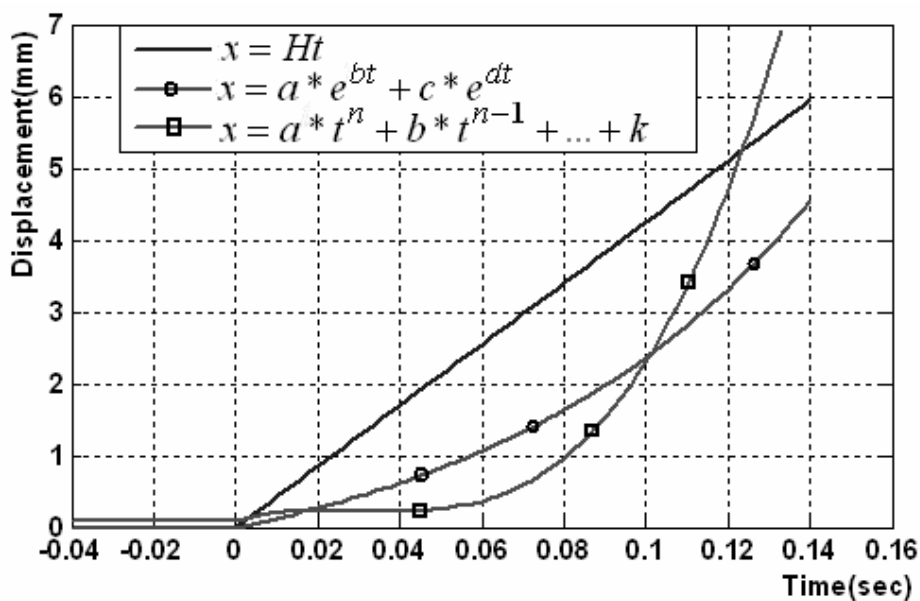


Figure 5.11: Slip displacement functions.

In linear cases as mention by [Howe and Cutkosky 1989], the slip displacement can be described as:

$$x = Ht, \quad (25)$$

where  $H$  is slope of figure 5.11.

Substituting  $x$  in equation (25) into the right hand side of equation (24) gives:

$$m\ddot{z} + c_s(\dot{z} - \dot{z}_{ie}) + k_s(z - z_{ie}) = \frac{1}{\mu(x, y)}(c_a H + k_a Ht).$$

The deformation surface between the object and tactile surfaces can be presented by

$$y^2 - 2pz = 0,$$

and from Howell's definition [Howell and Mazur 1953]  $\mu(x, y) = KN^{\beta-1}$ , with  $\beta = \frac{2}{3}$

and  $K = 1$ .

Then, the minimized form is

$$\begin{aligned} m\ddot{z} + c_s(\dot{z} - \dot{z}_{ie}) + k_s(z - z_{ie}) &= y^{2/3}(c_a H + k_a Ht), \text{ and} \\ m\ddot{z} + c_s(\dot{z} - \dot{z}_{ie}) + k_s(z - z_{ie}) &= A + Bt, \end{aligned} \quad (26)$$

where  $A = y^{2/3}c_a H$  and  $B = y^{2/3}k_a H$ .

The solution to the differential equation  $\ddot{z} + \dot{z} + z = 0$  will be in the form:

$$z(t) = z_c(t) + z_p(t)$$

$$z_c(t) = C_1 e^{-\frac{t}{2}} \cos\left(\frac{\sqrt{3}}{2}t\right) + C_2 e^{-\frac{t}{2}} \sin\left(\frac{\sqrt{3}}{2}t\right)$$

$$z_p(t) = -z_1 \int \frac{z_2 g(t)}{W(z_1, z_2)} dt + z_2 \int \frac{z_1 g(t)}{W(z_1, z_2)} dt$$

where  $z_1 = C_1 e^{-\frac{t}{2}} \cos\left(\frac{\sqrt{3}}{2}t\right)$ ,  $z_2 = C_2 e^{-\frac{t}{2}} \sin\left(\frac{\sqrt{3}}{2}t\right)$ ,  $g(t) = A + Bt$ .

The dominator,  $W(z_1, z_2)$ , is called the Wronskian parameter [Arterburn 1984] denoted as

$$W(z_1, z_2) = \begin{vmatrix} z_1(t) & z_2(t) \\ \dot{z}_1(t) & \dot{z}_2(t) \end{vmatrix}.$$

Following substitution,  $W(z_1, z_2)$  equals  $\frac{\sqrt{3}}{2} C_1 C_2 e^{-\frac{t}{2}}$ .

Solving the integral equation gives the solution of  $z_p(t)$  which becomes

$$z_p(t) = C_a H y^{\frac{2}{3}} (t-1) + k_a H y^{\frac{2}{3}}.$$

In the case of a nonlinear or polynomial function, such as:  $x = ae^{bt} + ce^{dt}$  or  $x = at^n + bt^{n-1} + \dots + p$  then nevertheless the model yields a single frequency solution.

Then, the completed solution to the differential equation is:

$$z(t) = C_1 e^{-\frac{t}{2}} \cos\left(\frac{\sqrt{3}}{2}t\right) + C_2 e^{-\frac{t}{2}} \sin\left(\frac{\sqrt{3}}{2}t\right) + c_a H y^{\frac{2}{3}} (t-1) + k_a H y^{\frac{2}{3}}. \quad (27)$$

The slip on some contact points (local slip) will appear before total slip occurs. This slip can be detected by checking the oscillation frequency (fluctuation signal) and is identified as a pre-slip condition for the whole object. In the experiment of Grasp-Optimize-Replace, the object was held between the robot gripper fingers. The robot would then decrease the prehension force until it could detect slipping at some contact points which in turn would be indicative of complete slippage. The rule sets can be adapted by checking the oscillation frequency (fluctuation signal) in the tactile array. If there exist some tactile elements having the same frequency of vibration, then whole slippage can be recognized.



## Second Case: Grape-Lift-Replace

In the second experiment, the equation  $y^2 - 2pz = 0$  or  $z = \frac{y^2}{2p}$  would not be correct any more because there exists additional deformation of the contact surface when the robot tries to lift the object.

[Dundurs and Comninou 1983] presented the solution for the shear tractions,  $S(x)$  with dislocation distribution on an elastic material. He introduced geometry of the problem for elastic contact as depicted in Figure 5.12. The two components of force, shear force- $P(t)$  and normal force- $Q(t)$ , can vary independently and introduced as shear traction. The contact between objects is separated into three zones corresponding to point locations along the  $x$ -axis. He described the shear traction based on the locations of points in the slip zone ( $a$ ) and stick zone ( $b$ ) when they are dislocated.

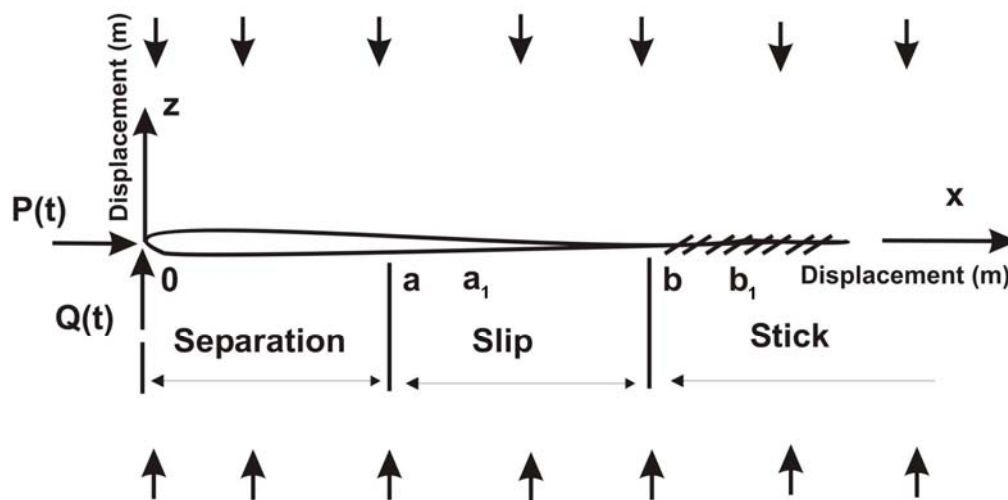


Figure 5.12: Geometry of the problem [Dundurs and Comninou 1983]

Point locations  $a$  and  $b$  along the  $x$ -axis at initial distributions will be moved to location  $a_1$  and  $b_1$  when variation of  $P(t)$  and  $Q(t)$  along the  $x$ -axis occurs. Then shear traction along the  $x$ -axis will be a function of  $x$ . By defining a set of regime (rules), Dundurs presented the existence of shear traction fluctuations as shown in Figure 5.13.

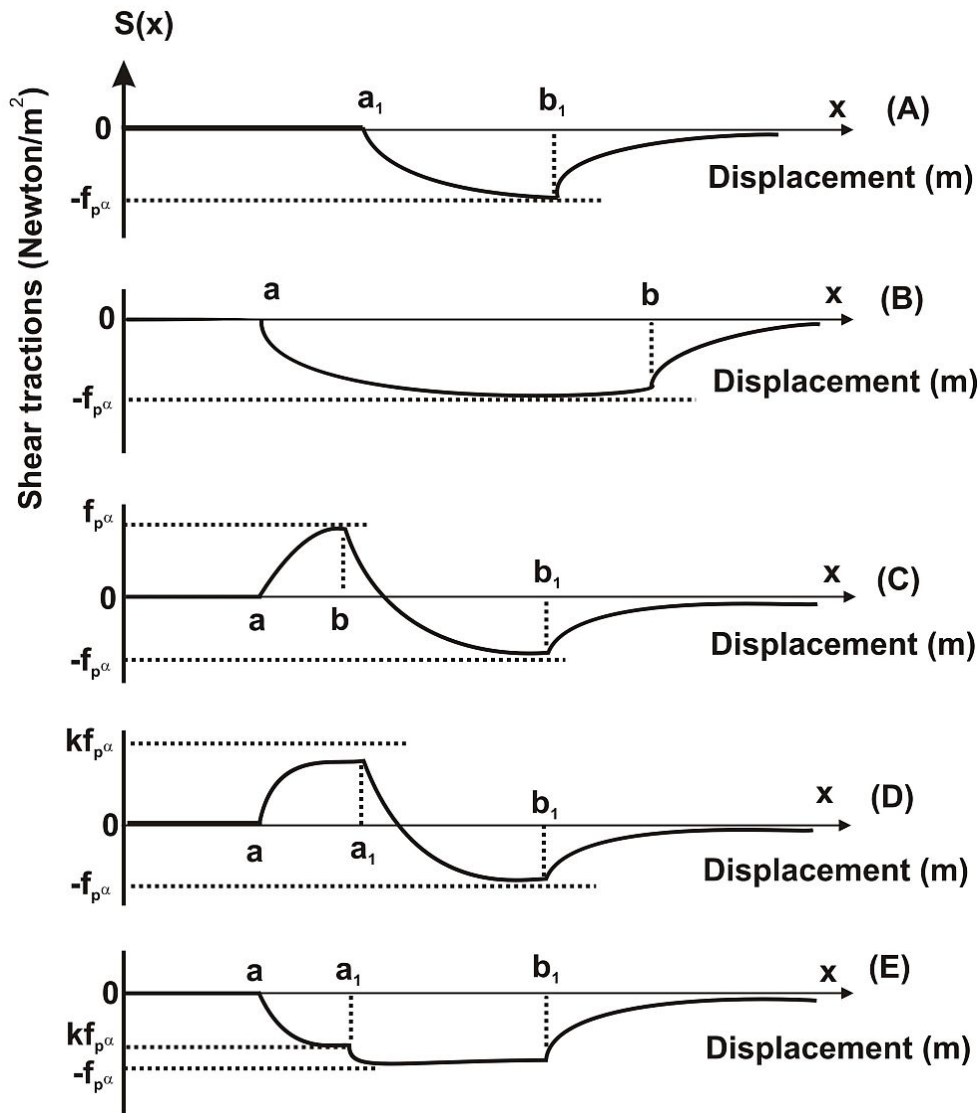


Figure 5.13: Distributions of shear tractions for loading from (P1, Q1): (A)-Initial distribution; (B)-regime I; (C)-regime II; (D)-regime III with  $k > 0$ ; (E)-regime III with  $k < 0$  [Dundurs and Comninou 1983].

From the conclusions made by Dundurs, this means there exists an extra term varying with time in the equations pertaining to surface deformation, i.e.  $\sin(at)$ . Then

the equation of surface deformation will be  $z = \frac{y^2}{2p} + \sin(at)$ .

With Howell's definition [Howell and Mazur 1953], the friction coefficient will

be  $\mu(x, y) = K \left( \frac{y^2}{2p} + \sin(at) \right)^{\frac{1}{3}}$  or  $\mu(x, y) = (C + D \sin at)^{\frac{1}{3}}$ , where  $C = K^{-3} \frac{y^2}{2p}$  and

$D = K^{-3}$ .

Equation (24) will be  $m\ddot{z} + c_s(\dot{z} - \dot{z}_{ie}) + k_s(z - z_{ie}) = (C + D \sin at)^{\frac{1}{3}}(c_a H + k_a Ht)$ , and

$$g(t) = (C + D \sin(at))^{\frac{1}{3}}(c_a H + k_a Ht).$$

The same method can be used to find the solution to the differential equations, but  $z_p(t)$  will be different. The Wronskian's method [Arterburn 1984] denoted as

$$z_p(t) = -z_1 \int \frac{z_2 g(t)}{W(z_1, z_2)} dt + z_2 \int \frac{z_1 g(t)}{W(z_1, z_2)} dt$$

By substitution  $z_1 = C_1 e^{-\frac{t}{2}} \cos(\frac{\sqrt{3}}{2}t)$ ,  $z_2 = C_2 e^{-\frac{t}{2}} \sin(\frac{\sqrt{3}}{2}t)$ , and the dominator

$W(z_1, z_2) = \frac{\sqrt{3}}{2} C_1 C_2 e^{-\frac{t}{2}}$ , the completed solution to the differential equation is:

$$\begin{aligned} z_p(t) = & -\frac{2}{\sqrt{3}} e^{-\frac{t}{2}} \cos(\frac{\sqrt{3}}{2}t) \int e^{\frac{t}{2}} \sin(\frac{\sqrt{3}}{2}t) (C + D \sin(at))^{\frac{1}{3}} (A + Bt) dt \\ & + \frac{2}{\sqrt{3}} e^{-\frac{t}{2}} \sin(\frac{\sqrt{3}}{2}t) \int e^{\frac{t}{2}} \cos(\frac{\sqrt{3}}{2}t) (C + D \sin(at))^{\frac{1}{3}} (A + Bt) dt \end{aligned} \quad (28)$$

It may not be necessary to find the integral solution because somehow the solution,  $z_p(t)$ , will always contain the term "sin(at)". That means in this case, there is more than one of oscillation frequency (different numbers of fluctuation cycles) in the tactile array. One frequency comes from the solution of  $z_c(t)$ , another one comes from the solution of  $z_p(t)$ .

In this experiment, the rule sets can be expressed: if there are more tactile elements that have different frequencies of oscillation (different numbers of fluctuation cycles), then the commencement of pre-slip can be assumed.

On the contact surface, there exists stress. A fluctuation in tactile element data is an interval of time during which a sequence of stresses is cyclically applied to the specimen at the contact point. The stress waves used in experiment are generally triangular, square, or sinusoidal, and the typical cycles of stress are reverse stresses, fluctuating stress, and irregular or random stress [Dieter 1981].

### 5.3.3 Real Experiment

#### 5.3.3.1 Grasp-Lift-Replace Experiments

In this experiment, after the robot grippers successfully approach the object, the robot will use test lift the object using minimum prehension force. Then it will examine the information from the tactile sensors in an attempt to identify slip. If slip is detected the robot will place the object down and recommence object prehension with a larger force. It will repeat the process until at a certain force, lifting is possible without slip, upon which the robot will notify acoustically.

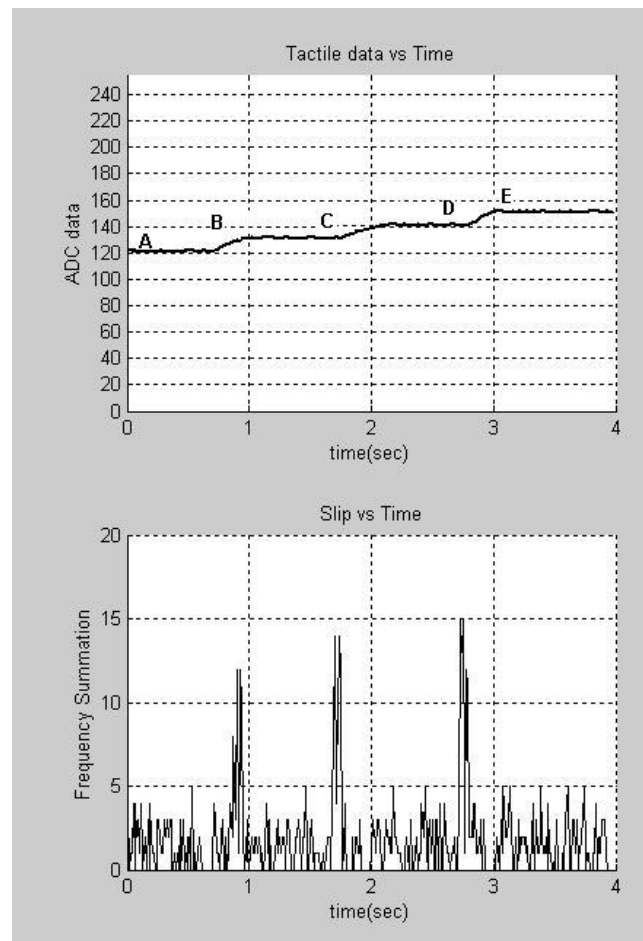


Figure 5.14: Minimum prehension force determinate by increasing the applied force.

Point B of Figure 5.14 is when the robot first senses slip. Force is then increased until the tactile data increases to point C. If slip frequency is not sensed, the robot will prolong that degree of force while examining the response.

At point D when the frequency at the tactile sensor surface meets the slip conditions, the robot will increase the force until the sensed tactile data reaches point E. The lower graph of Figure 5.14 exhibits the results of frequency response sensed from all 64 tactile elements. The final decision as to whether slip has occurred or not depends on analysis of the complete data. Points B, C, and D in Figure 5.14 are found to have slip, and the least possible force needed to lift the object shown by the tactile sensors is approximately 150 (dimensionless ADC data).

### **5.3.3.2 Grasp-Optimize-Replace Experiments**

The experiment starts with the manual stage in which the object to be grasped is placed between the robot fingers. Then the robot commences gentle prehension of the object. As the gripper fingers close, the robot will analyze the information from the tactile sensors to determine the least force needed to retain the object and then notify acoustically when this force has been identified.

The second experimental results are illustrated in the upper part of Figure 5.15, which shows the basic control of the robot grippers, to whose fingers the tactile sensors are attached. At the outset, the robot will use a predetermined force to grasp the object. When the inner surface of the grippers make contact with the object and the tactile data are approximately 90 (dimensionless ADC data) at point A, the robot will decrease the prehension force, i.e. by incrementally increasing the distance between the fingers. The tactile data will gradually decrease to point B, upon which the frequency response will be sensed and follow the conditions described in the lower graph of Figure 5.15.

The lower graph of Figure 5.15 exhibits the results of frequency response sensed from all 64 tactile elements. To reach a decision as to whether a slip condition has been reached or not requires another account as the sensed signals do not all result from slip (see the analysis in section 5.4). For instance, they may result from the nature of the material used to develop the surface of the tactile sensors (which is in this study foam). Many tactile arrays are made from polymeric materials and in many types of foam.

These have physical characteristic which differ enormously from those of rigid materials such as metals. Slow shape restoration results in unstable foam mass, causing the frequency response to fluctuate. Hence, the response does not result from slip, but from the characteristics of the tactile sensor surface material.

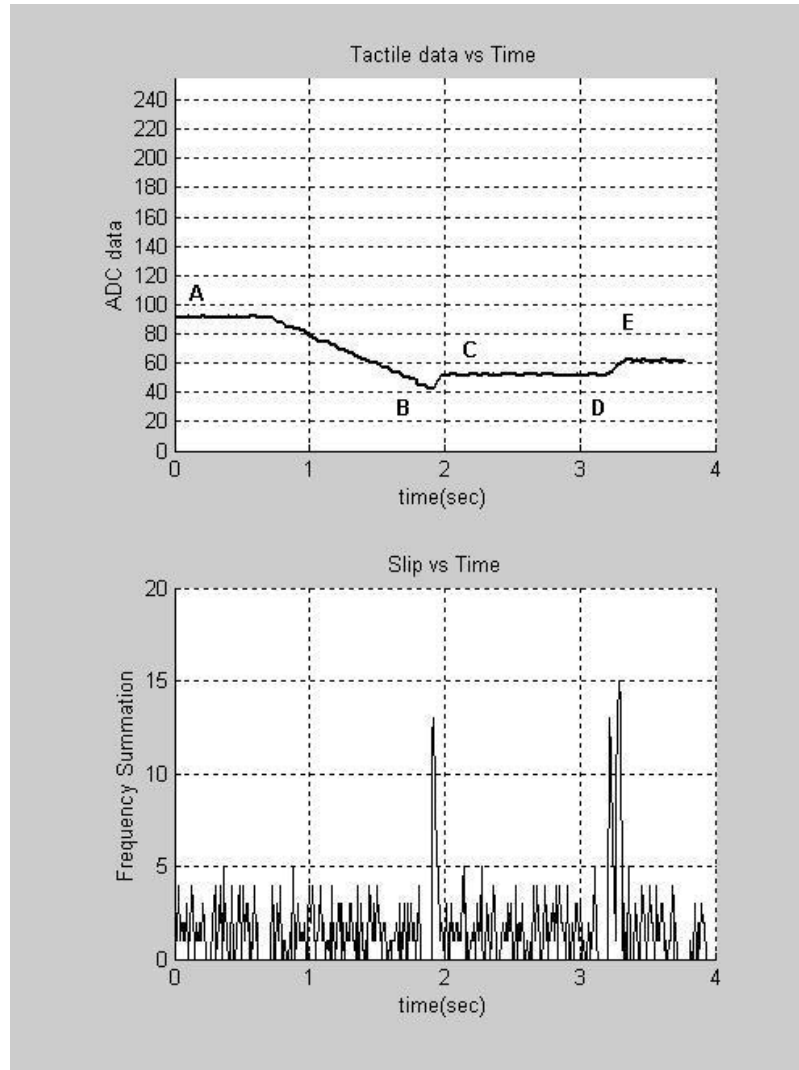


Figure 5.15: Minimum prehension force determined by decreasing the applied force.

From the behavior of the localized contacts between tactile sensor and object surfaces, the minimum force cannot be determined by a unidirectional increase or decrease in applied force. This means the same degree of force exerted at different times will result in different prehension stabilities. To exemplify, at a certain point in time the force at point E lies between that at point A and C and is adequate for object

prehension without slip. The force required to grip the object now must be equal to or greater than that at point E.

## 5.4 Analysis of result

### Slip detection during operation for Grasp-Lift-Replace experiments

Active vibration techniques are used in this study to examine slip during robotic manipulation with no other equipment added. The slip signal is the frequency superimposed on the signal measured from the response to the force at the time of object manipulation. The superimposed signal is caused by the force on the object needed for horizontal motion along the surface of the tactile sensors. In other words, the normal force component to the surface of the tactile sensors produce a direct current signal, but the slip signal is in the form of an alternating signal.

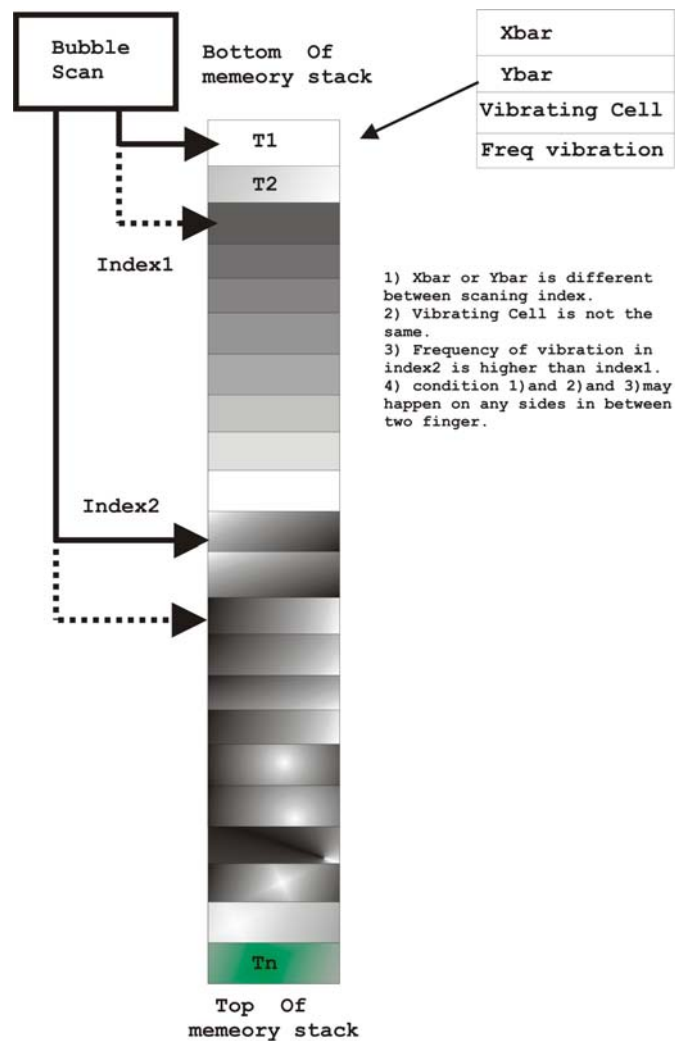


Figure 5.16 Explanation of algorithm used to measure slip



The alternating currents will disperse in numerous tactile elements. When slip occurs, some of the elements will be considered. When the robot is gripping an object, the tactile sensor surface will retract in accordance with the shape of the prehended object. The tangential force component causing slip will affect only some elements under the surface in contact with the object. On commencement of movement, the object will cause signal fluctuation in these tactile elements. Analysis of slip actually requires a high-bandwidth and fast-response system.

The alternating currents disperse throughout numerous tactile elements. When slip occurs, some of the elements give rise to signal changes. During prehension, the tactile sensor surface retracts in accordance with the shape of the object. Slip causing tangential force components affects only certain tactile elements. To rapidly measure the slip signal during prehension the computer memory may be organized in stacks. The locations  $T_1, T_2, \dots, T_n$  hold information from tactile sensors in the form of  $\bar{x}$  (average x-axis coordinate of force) and  $\bar{y}$  (average y-axis coordinate of force), vibrating cell (position of x, y with signal presence), and vibration frequency (number of sensed vibrating waves). The subscript to  $T$  is the time of data collection - the number with the highest value in the stack being the most recent one.

To compare stack data index (pointers) called 'index 1' and 'index 2' are used to scan the data. Index 1 locates the starting point of the scan or the oldest stored data, whereas index 2 locates the finishing point of the scan or the data next to those located by index 1. The data located by index 1 is compared with those located by index 2. Index 2 values are continually compared with Index 1 figures and increased until the latest data is located. The location of index 1 is repeatedly scanned until index 2 locates the most recent data which means that the process is complete.

From Figure 5.16, index called 'index 1' and 'index 2' will be used to scan the data in the memory stack. Index 1 will locate the starting location of the scan or the oldest data stored, whereas index 2 locates the finishing location of the scan or the data next to those located by index 1. The data located by index 1 will be compared with those located by index 2.

Index 2 figures will be continually compared with Index 1 figures and increased until the latest data located by it is shown in the memory stack. The location of index1 is repeatedly scanned until index 2 locates the oldest data which means that the process is complete.

There will be four conditions which if true indicate slip. The first one is unequal  $x$ -bar and  $y$ -bar coordinates determined by index 1 and 2. The second one is unequal vibrating cells determined by index 1 and index 2. The third one is the frequency of vibration determined by index 2 - which must be larger than index 1. The final condition is that the first three conditions are simultaneously true on any of the fingers. To check these slip conditions, two simultaneous sets of these procedures, each responsible for each side of the tactile sensors contacting the prehended object, will be conducted.

### **Slip detection during operation for Grasp-Optimize-Replace experiments**

Parallel jaw robotic manipulators have been used in a variety of settings. To optimize their applications, controlling the force to avoid damage from slip and over-force is very important. Various techniques compiled by [Dubey et al. 1997] have been employed. However, some of these are not applicable to real-time tasks, particularly when adjustments to an additional force need to be accounted for. For example, during robotic prehension, movement of the object into any direction depends on the weight of the object and the end-effector acceleration which causes additional external forces. Therefore, these two factors must be known.

Surface curvature is also a factor in determining the minimum slipless prehension force. It significantly affects the prehension stability [Jenmalm et al. 1997]. Moreover, different curvatures on each side of the object result in different force distributions on the gripper surfaces causing the slippage on the side with the lowest force distribution to occur first [Turrell et al. 2001]. Alternatively, should each side of the robot gripper fingers have the same of force distribution then the responsibility will be equally shared.

Hence, [Jones and Hunter 1992] suggest that the shear force element between the robot gripper and the object changes in accordance with the direction of the force from the object surface onto the surface of the robot gripper.

From Figure 5.17, there are three conditions which successfully indicate slippage. The first one is different vibrating cells determined by index 1 and index 2. The second one is equal frequency of vibration determined by index 1 and index 2. The last condition is that the first two conditions must both be simultaneously true for both sides of gripper to conclude that slip occurs. To check these conditions, two sets of these procedures, each responsible for each side of the tactile sensors contacting the gripped object, have been done simultaneously.

In conclusion, the measurement method to attain the least prehension force is similar to that used in measuring slip in order to find an appropriate degree of force. Slight differences are the measurement conditions which will be analyzed for both sides of the tactile sensors contacting the object. True conditions on both sides suggest that the present force is less than that required and more force should be exerted. A detailed explanation of this procedure has been presented here and the successful results can be used to confirm the proposed model.

- 1) Vibrating Cell is not the same cell.
- 2) Frequency of vibration in index2 is equal to index1.
- 3) condition 1) and 2) have to happen on both sides of finger at the same time.

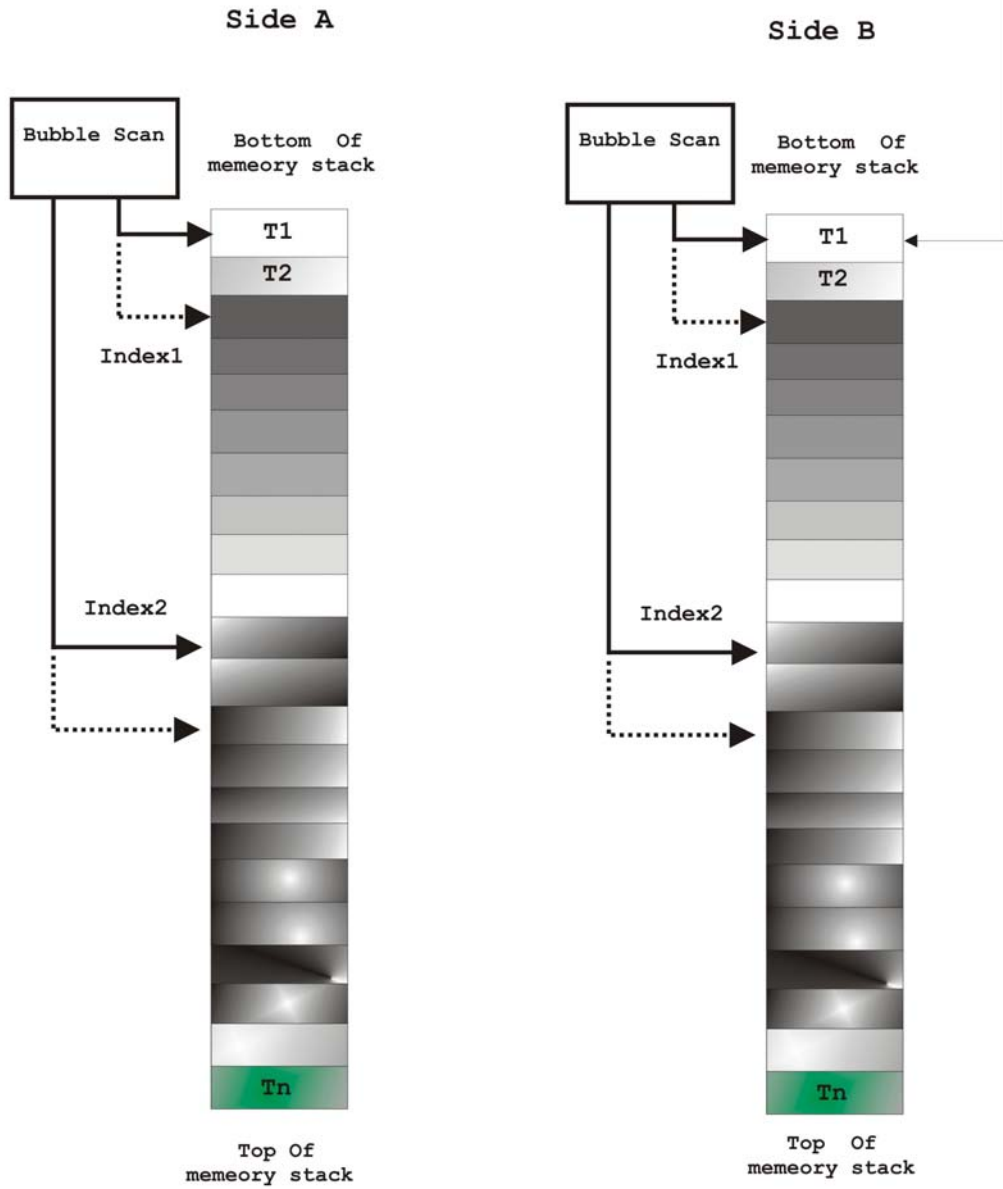
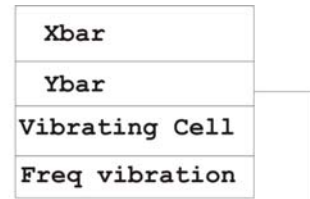


Figure 5.17: Explanation of algorithm using the least force in object manipulation.

## **5.5 Statistic Tested Results**

### **5.5.1 With dead weight**

A statistical experiment was designed in order to obtain appropriate results, which can be analyzed by using statistical methods, and to reach valid and objective conclusions. It is also important to properly indicate the precision with which each measurement is made. Variation of the measured values corresponds to the measurement precision, and accuracy of the measured values shall be expressed in terms of standard errors. The knowledge that any individual measurement made in the laboratory lacks perfect precision often leads to taking multiple measurements at some independent variable level. This group of values will cluster about the true value that we are trying to measure. The mean value of the data, the standard deviation, and the standard error are used to represent the overall distribution of the data.

Experiments that cannot be reliably reproduced are generally not considered to provide useful scientific evidence. Alternatively, results that prove to be highly reproducible are typically given more credence by scientists. This is based on an intuitive application of the principle of induction, rather than on the application of the principles of falsifiability.

When selecting the dependent response or variables, the experimenter must be certain that the response that will be measured actually provides useful information about the process under study. In designing the experiment, the average of the measured characteristic is usually the response variable; therefore, replicates should be made [Box et al. 1978].

In these experiments it was necessary to use metal balls to weight the grasped object in order to evaluate the minimum grasping force before the object was forcibly released from the robot gripper. Each metal ball weighed 3.5 gram and the experiments were repeated thirty times for both Grasp-Lift-Replace and Grasp-Optimize-Replace and the number of balls recorded every time for statistical evaluation.

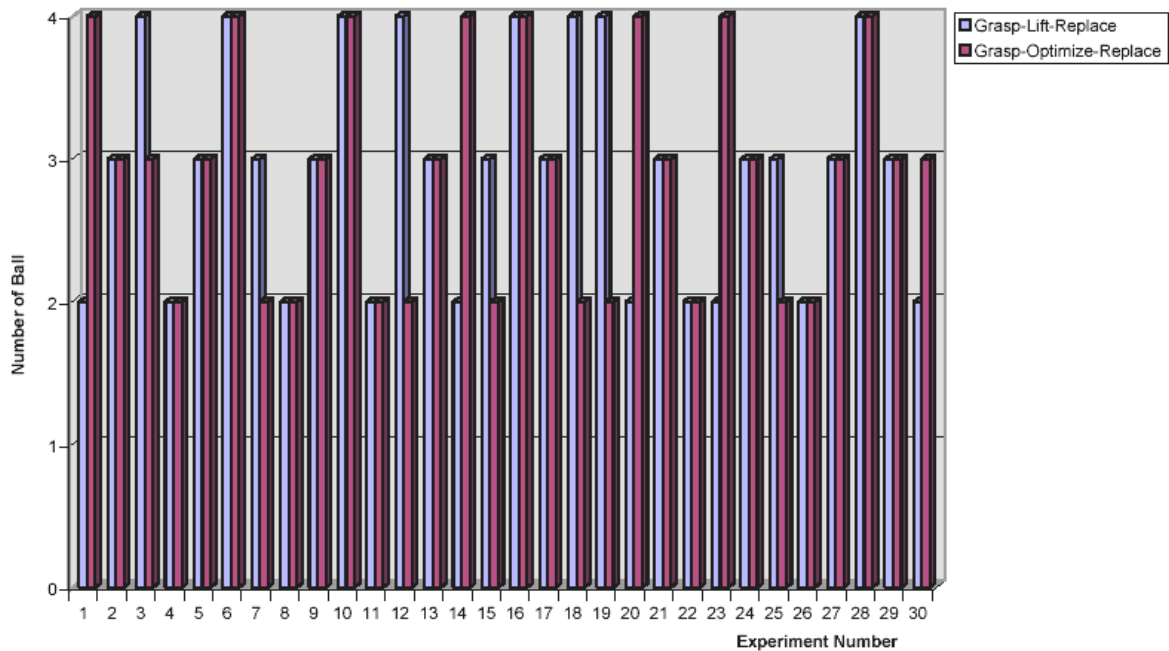


Figure 5.18: Statistical experiments

In this case, the types of experiment are independent variables being manipulated, and the numbers of balls are dependent variables being recorded. For clarity, the data for the dependent variables (numbers of balls) were plotted on the scatter plot in different colours and symbols for two types of experiments. Notice that the numbers of balls recorded for each of the experiments. For Grasp-Lift-Replace and Grasp-Optimize-Replace experiments (shown in Figure 5.18 in blue and red respectively), the numbers of balls all hover around 3. On the other hand, at both 2 and 4 balls, the values are spread over a larger range. In fact, the means calculated for both experiments are close to each other, and the values approximately correspond to three balls showing that there is little difference in the numbers of balls resulting from both Grasp-Lift-Replace and Grasp-Optimize-Replace experiments.

To find the measurements uncertainties, the standard deviation  $\sigma$ , of the measured values must be calculated. Standard deviation is a measure of variation of at least thirty data points  $(X_1, \dots, X_N)$  about an average value,  $\bar{x}$ , and is typically called the uncertainty in a measurement. The average or mean value,  $\bar{x}$ , of a set of thirty or more measurements is calculated as:

$$\bar{x} = \frac{1}{N} \sum_{i=1}^N x_i$$

Once the mean value of the measurements is determined, it is helpful to define how much the individual measurements scatter around about the mean. The deviation,  $d_i$ , of any measurement,  $x_i$ , from the mean is given by

$$d_i = x_i - \bar{x}$$

Since the deviation may be either positive or negative, it is often more useful to use the mean deviation, or  $\bar{d}$ , to determine the uncertainty of the measurement. This is found by averaging the absolute deviations,  $|d_i| = |x_i - \bar{x}|$ ; that is,

$$\bar{d} = \frac{1}{N} \sum_{i=1}^N |d_i|$$

The standard deviation  $\sigma$ , (sometimes called the root-mean square) is given by

$$\sigma = \sqrt{\frac{1}{N} \sum_{i=1}^N d_i^2}$$

Finally, the experimental result  $E_v$ , can then be written as

$$E_v = \bar{x} \pm \sigma$$

where  $\sigma$  gives the measure of the precision of the measurement. We use the value of the standard deviation to serve as a data error. In Figure 5.19, the vertical bars located before and after the mean value (indicated by the 68% range) are the minus-one standard error and the plus-one standard error data ranges, respectively.

The standard deviation under repeatability conditions is often used as a measure of precision, although it should be noted that "precision" is most often used qualitatively. Reproducibility is one of the main principles of scientific methods and refers to the ability of a test or experiment to be accurately reproduced or replicated.

The term is very closely related to the concept of testability and may require the test or experiment to be falsifiable.

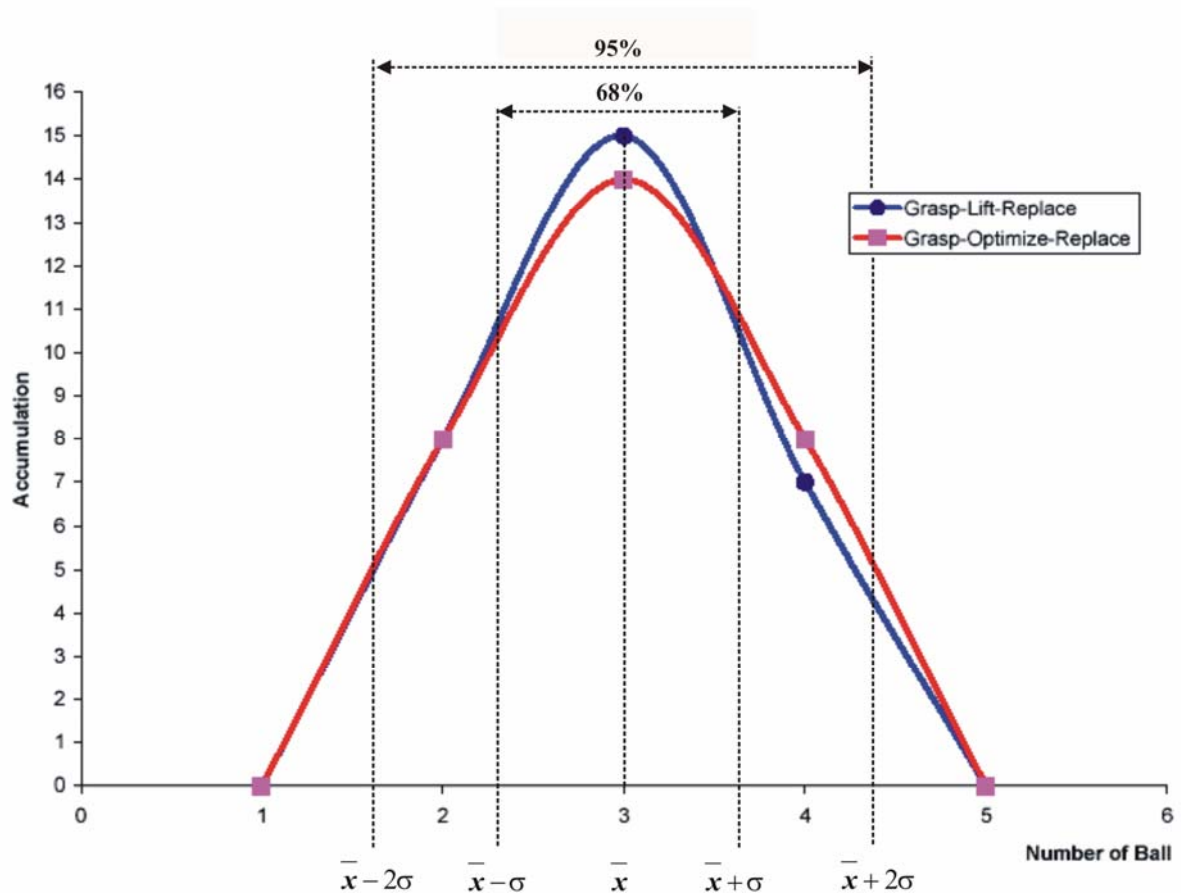


Figure 5.19: Standard deviation of experimental results

It can be shown that there is a 68% likelihood that an individual measurement will fall within one standard deviation ( $\pm\sigma$ ) of the true value. Furthermore, it can be shown that there also exists a 95% likelihood that an individual measurement will fall within two standard deviations ( $\pm 2\sigma$ ) of the true value.

We can include additional information to indicate how closely the means are likely to reflect the true values. We can do this using standard errors - the commonest way to statistically describe uncertainty in measurements. Since what we are representing is the means in the graph, the standard error is an appropriate measure to be used to calculate errors.



Test Number	Grasp-Lift-Replace	Grasp-Optimize-Replace
1	3	4
2	3	3
3	4	3
4	2	2
5	3	3
6	4	4
7	3	2
8	2	2
9	3	3
10	4	4
11	2	3
12	4	2
13	3	3
14	2	4
15	3	3
16	4	4
17	3	3
18	4	2
19	3	2
20	2	4
21	3	3
22	3	2
23	2	4
24	3	3
25	3	3
26	2	2
27	3	3
28	4	4
29	3	3
30	2	3
Mean	2.966	3
Standard Error	0.128	0.133
Standard Deviation	0.706	0.730

Table 3: Experiment 1 Results

The standard error is calculated by dividing the standard deviation by the square root of the number of measurements that make up the mean (often represented by  $N$ ). In this case, 30 measurements were made. So, the standard deviation is divided by the square root of 30. By dividing the standard deviation by the square root of  $N$ , the standard error grows smaller as the number of

measurements (N) grows larger. This reflects the greater confidence in the mean value as more measurements are made. It can be stated that, based on 30 measurements, the impact ball at Grasp-Lift-Replace is  $2.96 \pm 0.128$  balls and at Grasp-Lift-Replace is  $3 \pm 0.133$  balls.

The  $\pm$  values are the standard errors and express a level of confidence that the mean values (which are 2.96 and 3) represent the true values of the balls.

### 5.5.2 With acceleration sensor

The GOR experiment (see 5.2) has been verified by the accelerometer chip to confirm the sensitivity of proposed algorithm. As shown in figure 5.20, the accelerometer is attached on the surface of a grasped object. Whenever the grasped object slipped or moved away from the gripper finger, the acceleration sensor would notify. The output vibrations produced by an acceleration sensor and the display were then recorded while the robot decreased its grasping force. Overall, the response of the system was adequate for the purpose of testing the effectiveness of proposed algorithm. The system is capable of logging the acceleration and it does this with a sample frequency of 200 Hz. The acceleration signal is also sampled with a frequency of 200 Hz. The acceleration sensor is shown in figure 5.20 where the accelerometer is the small chip on the printed circuit board. The acceleration sensor, SCA3000 chip, is a three-axis accelerometer consisting of a 3D-MEMS sensing element. The sensor offers acceleration information via the SPI interface, and the measurement resolution is  $0.75 \text{ mm/s}^2$ . The measured response amplitude was flat within  $\pm 2 \text{ m/s}^2$  across. There appeared to be severe mechanical vibrations or acceleration when the grasped object slipped from the finger gripper.

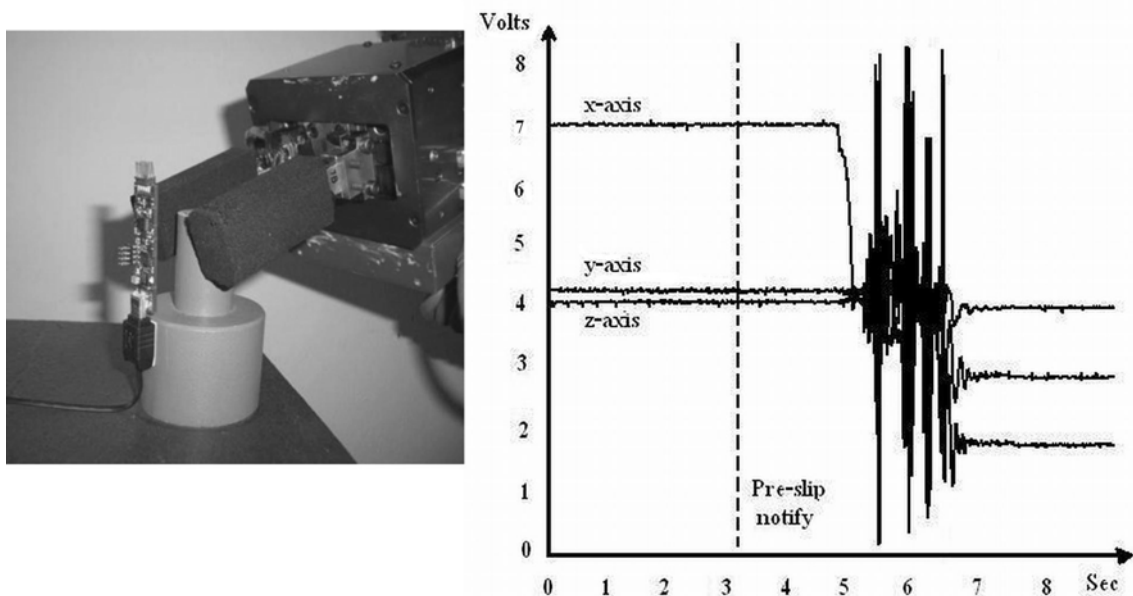


Figure 5.20: The GOR experiment evaluated with the acceleration sensor

In observing ten trials of experimental results, it can be confirmed that proposed algorithm is faster and more sensitive than the detectability of the acceleration sensor. The ranges of the warning of a slip are three to six decreasing steps before the grasped objects begins slipping and falls down from the gripper finger. The robot will vocally warn “I found pre-slip signal” when it finds the pre-slip and then keeps decreasing the grasping force until the grasped object falls down. The impressive results are even when the robot are warning the pre-slip, acceleration sensor does not yet notify any vibrating status. Until the massive slips are happening, then the vibrating status can be captured by acceleration sensor.

To verify the GLR experiment with the acceleration sensor, there exist additional steps in-between when the robot senses the pre-slip signal from its finger. As shown in flowchart of figure 20, the robot will decrease the grasping force while another monitor program is executing the read data from the acceleration sensor. The numbers of decreasing steps are statistically analyzed after ten identical experiments have been conducted.

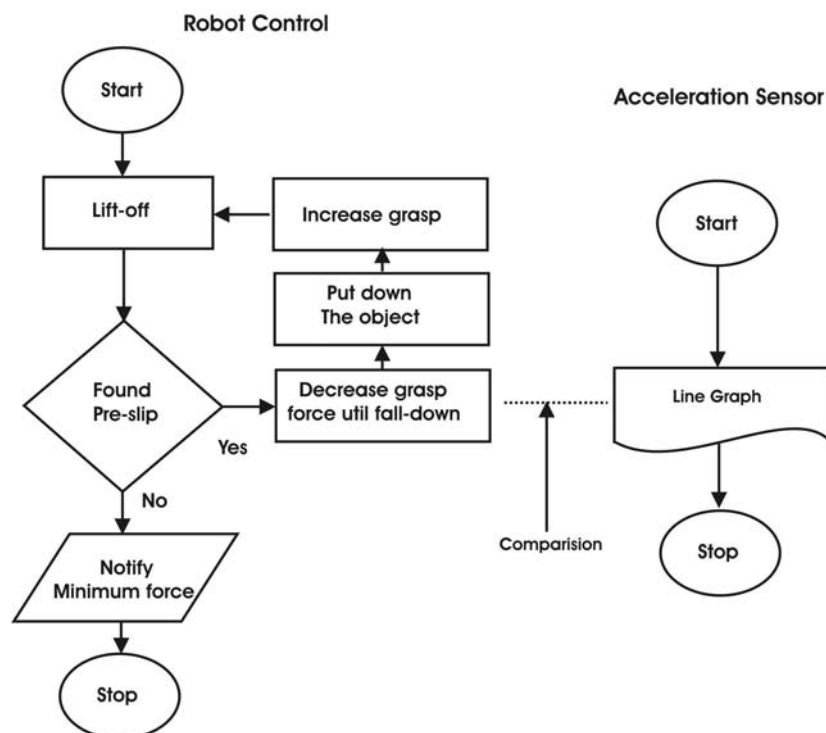


Figure 5.21: Flowchart of the GLR experiment evaluated with the acceleration sensor

In the GLR experiments, pre-slip detection will apply while the grasped objects are being lifted up. The grasped object will slip relatively to the gripper finger, but not to the earth, and hence two acceleration sensors are needed in this case. One accelerometer attached to the grasped object is used to indicate the acceleration of the grasped object relative to the earth. Another accelerometer is also attached to the tip of the robot finger, which indicates the acceleration of the robot finger relative to the earth as well. To notify the slip between the grasped object and the robot finger while lifting up the object, the transformation between two different frames of those sensor's coordination are needed before the slip status can be found in their comparisons.

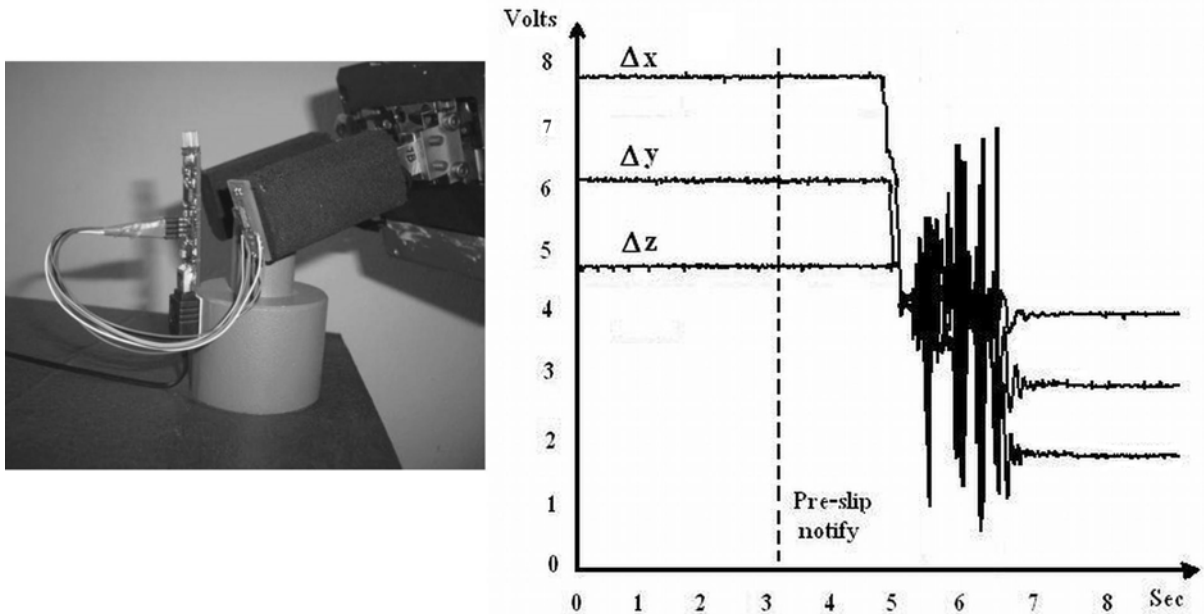


Figure 5.22: The GLR experiments evaluated with the acceleration sensor

The GLR experiment has been repeated ten times and yielded the same results as the GOR experiment. Every time the robot finds the pre-slip signal, it will verify that signal by decreasing the grasping force until the grasped object falls down. The interval of the decreasing steps is perfectly in range of three and six.

The experiments showed some of the limitations of the acceleration sensor to indicate the pre-slip in both experiments. It is for instance quite limit to integrate those acceleration sensors to the robot to get a measurement of pre-slips over time. When it comes to using an accelerometer for a real-time control, it is disturbing to see how many vibrations in the floor and the surroundings affecting the measurements of the accelerometer. It is also obvious from the experiments that much better equipment is needed to make a thorough examination of the tactile sensor. The tactile is capable of measuring near static acceleration which is interesting to investigate. A proposed method for calibrating the tactile data to the measured pre-slip is useful.

## 5.6 Conclusions

The fact that two fingers of the gripper enclose the prehended object, the combination of force and compliance provides a firm grasp. However, if the grasped objects are different in shape from the ones used in these experiments, the grasp with global minimum forces might not always be obtained. A single incident of prehension does not always provide global solutions for the all possible grasped points. The contact points, in turn, provided additional minor rules that resulted in global minimum forces. Placements of the grasped points on the object boundary may affect the prehension quality. The grasping forces depend on the selection of the contact points and grasping forces must be minimized in order to ensure stability without damage to the object. This criterion may be violated in a poor selection of contact points [Abu-Zitar and Al-Fahed Nuseirat 2001].

Optimal contact points and minimum forces must be considered together. A large amount of literature has been published regarding the problem of firm prehension of rigid bodies [Bicchi 1992, Montana 1992, Stavrulakis et al. 1996, Al-Fahed Nuseirat et al. 1999]. The ultimate goal was to end up with minimum forces applied by the finger to the grasped object. Linear programming techniques as well as heuristic search methods were used in finding the best solutions [Liu 1999, Abu-Zitar and Al-Fahed Nuseirat 2000]. Those techniques and methods consume much computation time and power, and their corresponding algorithms have only been simulated and have not been realized on real robot grippers.

Most techniques available only focus on formulating a cost function and then minimizing this cost or energy function in order to satisfy some constraints. In contrast, the techniques proposed in this research use less computing power, even when applied to multiple-finger hands.

A predictive model has been proposed which uses a basic method adapted for real application in grasp optimization. Prevention of premature release with minimum prehension force is addressed without measuring the coefficient of friction between object and robot gripper. Predictive models have been used to develop a set of rules

which predict the presliding based on fluctuations in tactile signal data. This predictive model represents a significant step forward in developing useful applications to which no known analytical or parametric models have been identified.

The robot encountered some difficulties using its gripper at the time of the experiments. The robot-gripper did not always move linearly with the controlled commands. It could miss a control step while running the experiments. These were the effect of gripper's threshold which will be concluded in Chapter 7, section 7.4. While the robot kept decreasing the grasped force, the friction on movements in the gripper-finger also exerted effort on holding the objects. For example, with 302 grams or 105 grams objects, the grasped objects sometimes might be held with the zero grasped force applied by the gripper. This kind of situation depended on how much the contact areas were consumed between the gripper and grasped objects and orientations of the gripper were with respected to the earth.

Moreover, the experiments revealed that the weight of the grasped objects was related with the decision time loop--the times spent for the robot to read and to process the tactile data until it was able to determine the slip. At 608 grams, the grasped object sometimes had fell down before the robot announced the slip-state. This was the problem of communication bottleneck in the test system. There existed much time delay in the test system. For example, after the previous step of decreasing the grasped force, the tactile controller had to re-scan the tactile arrays and wait for the polling messages in the CANBUS from C40 networks which were commanded from PC1.

Then, whenever PC1 received the data, it would store that data in the database inside PC2. There were still negotiation messages between both PCs. PC2 would decide the grasping states by processing the tactile data and tactile events inside the database. Referring to section 3.1 of Chapter 3, the hardware architectures of the test system did not encourage a real-time system. However, with the 480 grams object, it seemed to be perfectly avoiding both problems.



## CHAPTER SIX

### Experiments and Applications for Touch identification

#### 6.1 Introduction to touch identification

The 3-D recognition process is an integral part of computer and robot vision systems and still presents itself as a topic of high interest in both fields. The importance of this type of registration system comes generally from the fact that it is found in different applications including surface matching in [Zhang 1994], 3-D medical imaging in [Thirion 1994], pose estimation in [Lavallee and Szeliski 1995], object recognition in [Dorai and Jain 1997], [Chua and Jarvis 1996], [Johnson and Helbert 1998] and data fusion in [Bergevin et al. 1995], [Soucy and Laurendeau 1998]. Tactile sensing systems of robot for object recognition should essentially emulate biological haptic perception mechanisms ([Lederman et al. 1992], [Tzafestas 2003]).

A number of approaches have been put forward to process the output of tactile sensors in order to yield useful characterizations of contact surfaces for applications such as characterizing the surface textures for different manipulations as well as object identification. For example, the output of a single-point sensor sliding over different textures has been used to identify surfaces based on the frequency power spectrum of the sensor response [Baglio et al. 2002].

Pattern recognition, a kind of object recognition, is a more complicated task in tactile perception than in visual perception. This is because there are a number of additional factors which affect the quality of tactile images such as complex strain-stress relationships in elastic overlays, amount of force, and contact angle during the tactile perception process. Due to these limitations, tactile sensing is used mostly as an aid to vision only in object recognition applications (e.g. [Allen 1988]).

The experiment in this study proposes a surface recognition algorithm that determines the types of contact surface by fusing information collected by the tactile sensor system. Due to the relatively long slow tactile sensor time constants, a simple and speedy method of shape representation, where accumulated data can be

analysed and used to predict the shape and identity, is required. This algorithm can recognize and localize 3-D objects using a 2-fingered robot hand, on which tactile sensors are mounted. The sensors are capable of measuring the position and normal vector of the test object at the contact point.

## **6.2 Experimental Overview for touch identification**

The shape recognition by tactile sensing arises when we try to manipulate an object with the aid of a robotic hand [Famularo and Muraca 1995]. Many papers have been written about this problem but we can split them into three classes: the first one describes the contact problem between an object and the tactile sensor in terms of relations obtained with the aid of linear elasticity [Fearing and Hollerbach 1985, Hayes, et al. 1972, Zhang and Chen 2000, Iwata and Sugano 2003]; the second one discusses implementation rules and different types of transducers [Nicholls and Lee 1989, Maekawa et al. 1993, Shinoda and Ando 1994, Nagata et al. 1999, Yuji and Shida 2002]; the third one considers and examines inversion techniques in detail [Pati et al. 1988, Fearing et al. 1986, Worth and Spencer 1992, Kinoshita et al. 2001].

Hitherto, there have also existed techniques for contact identification based a tactile sensing. For examples, [Ibrayev and Jai 2004, 2005] proposed the recognition of low-degree polynomial curves based on minimal tactile data. In their application, Euclidean differential and semi-differential invariants were derived for quadratic and special cubic curves. Those invariants, independent of translation and rotation, were evaluated over the differential geometry at up to three points on a curve. The contact locations were then found on the curve, thereby localizing them to a specific contact sensor. Unfortunately, no implementation methods or experiment results were presented.

[Kim et al. 2005] classified surface textures by using a polymer-based microelectromechanical systems (MEMS) tactile sensor array using a statistical approach. Five simple textures were distinguished using a  $4 \times 4$  strain gauge sensor array serving as a transduction element. Five of the texture arrays were diagonal, enlarged diagonal, check pattern, four corner pixels, and perimeter pixels only.

Texture classification was achieved by using a maximum likelihood decision rule that optimally classified patterns in the presence of random noise and noise produced by texture variation. Their final results were analyzed by using cross validation to yield an acceptable overall performance of 68% correct classification. Their research strategies can be distinguished from those presented this dissertation: 1) sample textures are bound to only 4 x 4 tactile elements, 2) the experiments cannot cope with neither rotation nor translation invariants.

There exist some research works on tactile shape recognition based on planar shapes using neural networks. The neural network for classification generally requires that planar shapes be presented in a fixed position, orientation and dimension. To avoid this problem, a pre-processing stage is required to normalise the shape of the input data after all of prehended object data are obtained. Examples using the radius vector method of shape representation have shown good results with neural network classifiers [Lynch and Rayner 1989, Ng 1989, Yan 1990]. Another example [Ng et al. 1991] uses angles and lengths of planar polygons to represent the differences among the grasped objects. The objects data is acquired by robotic tactile sensors, and a neural network is then used to recognise the shape. Ng's method is straight-forward and seems to work well on simple shapes. It is also rotation, translation, and scale invariant, but he uses only fixed-size shapes presented in his experiments. [Ohka et al. 2006] presented research work in tactile sensing using both a neural network model based on human tactile sensation and a tactile-oriented associative memory model to enable a robot to recognize object contours. In their model, the direction vectors belonging to segments of the object contour were quantized by the chain-symbolizing method and stored in a memory matrix that accumulates matrix-products between the vector and its transposition. In the recalling process, complete vectors could be remembered even if some input vector elements had disappeared. In their experiments, a tactile sensor was installed into a robotic manipulator. Introduced into the experiments were five types of contour: a circle, a square, a triangle, a star, and a hexagon. After the robot had memorized a complete contour, it could then recognize the same contour by touching some part of it. In using planar shapes for shape recognition, the apparent problem is how to distinguish between objects having the same planar shape but differences in surface

curvature. The neural network is unable to recognise partial angle and length sequences of planar shapes.

In this study, an algorithm that can discriminate between types of contact surfaces and recognize objects at the contact stage is proposed. A tactile sensor array is used because it provides several types of meaningful information unavailable or difficult to acquire by a single sensor. Tactile arrays can recognize surface types on contact, making it possible for a tactile system to recognize translation, rotation, and scaling an object independently. The type of contact surfaces obtained by the tactile system will be determined from the shape of the object image which can then be characterized using the mathematical properties of quadric surface (see details in 6.3.2).

To identify the properties of the quadric surface, the eigenvalues of the contact surface will be calculated. The term *eigen* is a German word first used by Hilbert in 1904. It can be translated as 'own', 'characteristic' or 'individual', emphasizing the importance of eigenvalues in defining the unique nature of a specific transformation. Eigenvalue problems occur in stability problems, dynamics and vibrations, and several other application areas. They appear whenever a problem has a valid solution for only certain specific values. Such special values are called characteristic values or eigenvalues. Specifically in this study, the eigenvalue represents the matrix properties of the quadric surface of object prototypes calculable from the eigenvalue trajectory of the object types. The types of contact surface can be classified, for instance, into: elliptic, plane, cylindrical and spherical surfaces.

However, the proposed method does not consider the variation of the image of the contact surface obtained by the tactile sensor on the imposed force, which is the same problem as that in the study of IAN and James; [IAN and James 1984]. IAN and James experimented on surface recognition by characterizing the lengths of long and short axes, using the ratio of the long and short axes of the image that could be calculated by finding its eigenvector. The problem for his recognition method was an unstable recognition rate. Following the research of IAN and James, [Dong-Hwan and Hahn 1996] proposed the fuzzy data fusion algorithm that was less influenced by

the variation of contact surface area on the magnitude of the imposed force than that of IAN and James. However, Dong-Hwan and Hahn developed only formulas and theories with no experimental results.

By the method proposed in this study, when an object is pressed with either increasing or decreasing force, the trajectory of eigenvalues will not vary according to the position of contact, rotation or translation. Therefore, other criteria as well as the ratio of axes for the identification of the types of contact surfaces need not be considered, which is different from the experiments of IAN, James, Dong-Hwan and Hahn.

Four shapes of object have been used to test the robot's ability in recognizing object types. The robot makes contact with these objects, and the data from the tactile sensor is stored and analyzed. Later, one of the four objects is grasped again but with different magnitudes of force and in different positions and rotations. The ability to distinguish between object types is calculated. To determine the contact similarity between an object and the original object, their shape must be three dimensionally compared. However, in this study, surface shape comparison will be conducted using the parameters of surface shapes instead of the actual surface shapes. This will be explained further in 6.3.3.

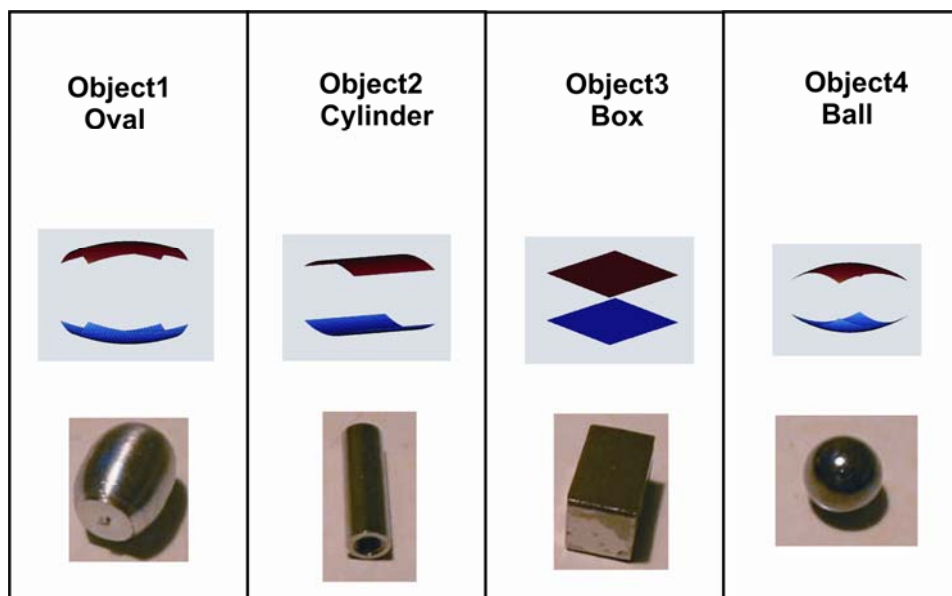


Figure 6.1: Quadric Surface in the experiments of Object Identifications.

The tested objects are an oval object with two major axes of 14 mm and 11.7 mm, a cylindrical object with 6.0 mm in diameter and 20 mm in length, a cube with dimensions 10 x 15.9 x 10 mm and a ball with a diameter of 9.5 mm respectively.

## 6.3 Experimental Arrangement for touch identification

### 6.3.1 Process

Regarding the algorithm identifying the similarity or difference between contact surfaces, this experiment uses mathematical calculation of 3-D shapes for which indices are established to enable model matching. The basic principles in constructing the 3-D shapes are fast calculation, low data storage requirement, ease of indexing, and independence from transformations made on the shapes such as translation, rotation, and scaling.

Previous research on 3-D model matching can be classified according to their approach into three types. The first types are statistically based methods where an object is presented in the form of a feature vector in multidimensional space. The vector in the space will be coded to contain the object shape. For example, [Ankerst et al. 1999] proposed a 3-D image recognition system using a histogram that divides an object into its components around the model's centroid. [Osada et al. 2002] used probability distributions of geometric properties for their image modeling method, in which points of the object surface were randomly selected for calculation. However, statistically based methods do not yield adequately fine object discrimination.

The second type of approach is the topology-based method. [Hilaga et al. 2001] compared the similarity of 3-D shapes by constructing multiresolutional graphs (MRGs) having different coding structures according to each shape resolution. The MRG method performs continuous functions on the 3-D shapes, particularly those involving geometric distance of a curved shape. However, this technique is unable to actually discriminate between types of object.

The final type of approach is a geometry-based method. For example, [Novotni and Klein 2001] proposed a mathematical calculation drawing on differences in the volumes of the original object surfaces and of a sequence of offset hulls belonging to the 3-D images to be tested. [Tangelder and Veltkamp 2002] reconstructed a 3-D shape with a weighted point set. Identification of the similarity between two objects would be done by weighted transportation. [Funkhouser et al.

2003] developed an algorithm that matched 3-D shapes using spherical harmonics in recognizing object similarities or differences. Kazhdan [Kazhdan et al. 2003] used the method called reflective symmetry descriptor in measuring the symmetry of various model shapes on every plane through the model's center of mass. The geometry-based method mainly takes into account geometric shapes, and the shape models are described by mathematical functions. However, it is inconvenient to search for a specific model for the object being compared in case there are several models. In addition, the method has only limited abilities in object classification.



### 6.3.2 Experimental Model

The 3-D shape classification method used in this experiment makes use of 3-D object with geometric features independent of the resolution of the tactile sensor. Nonetheless, the method must prove that it has good surface classification properties. In the experiments, the eigenvalue based method is found to be stable as a result of single eigenvalues and sensitivity to outliers. The proved results will be discussed in 6.4. Here, the way in which 3-D surface from the tactile data can be presented is discussed.

The shape representation designed for this study is both rotation and translation invariant. The quadric surface seems to be a simple, yet adequate, method for the proposed tactile sensor as the dimension of the tactile array (16x4) cannot represent a complex object surface. The basic way of creating quadric surfaces uses least squares interpolation. Considering a general 3-D surface expressed in the contact point as

$$f(x, y, z) = 0 \quad (29)$$

the general surface function can be approximated locally at the contact point as the following second order polynomial equation [Bangert and Prautzsch 1999]:

$$ax^2 + by^2 + cz^2 + 2dxy + 2eyz + 2fxz + 2gx + 2hy + 2jz + k = 0 \quad (30)$$

Equation (30) can be rewritten in a quadratic form of matrix equation:

$$P^T \cdot Q \cdot P = 0 \quad (31)$$

$$Q = \begin{pmatrix} a & d & f & g \\ d & b & e & h \\ f & e & c & j \\ g & h & j & k \end{pmatrix} \text{ and } P = \begin{pmatrix} x \\ y \\ z \\ 1 \end{pmatrix}$$

The properties of surfaces represented by  $Q$  can be easily translated, rotated and scaled. Given a 4 x 4 transformation matrix  $M$  of the form developed, the transformed quadric surface [Dai and Newman 1998]  $Q^*$  is:

$$Q^* = (M^{-1})^T \cdot Q \cdot M^{-1} \quad (32)$$

The general transformation matrices ( $M$ ) are of the Denavit-Hartenberg type combining both translation and rotation. Examples of the transformation matrices  $M$  that contain translation, rotation and scale are shown below.

$$\begin{pmatrix} 1 & 0 & 0 & 0 \\ 0 & \cos \phi & -\sin \phi & 0 \\ 0 & \sin \phi & \cos \phi & 0 \\ 0 & 0 & 0 & 1 \end{pmatrix}$$

Rotate around  $x$  axis

$$\begin{pmatrix} \cos \phi & 0 & \sin \phi & 0 \\ 0 & 1 & 0 & 0 \\ -\sin \phi & 0 & \cos \phi & 0 \\ 0 & 0 & 0 & 1 \end{pmatrix}$$

Rotate around  $y$  axis

$$\begin{pmatrix} \cos \phi & -\sin \phi & 0 & 0 \\ \sin \phi & \cos \phi & 0 & 0 \\ 0 & 0 & 1 & 0 \\ 0 & 0 & 0 & 1 \end{pmatrix}$$

Rotate around  $z$  axis

$$\begin{pmatrix} 1 & 0 & 0 & t_x \\ 0 & 1 & 0 & t_y \\ 0 & 0 & 1 & t_z \\ 0 & 0 & 0 & 1 \end{pmatrix}$$

Translation

$$\begin{pmatrix} s_x & 0 & 0 & 0 \\ 0 & s_y & 0 & 0 \\ 0 & 0 & s_z & 0 \\ 0 & 0 & 0 & 1 \end{pmatrix}$$

Scale

### Basic operations on the surface matrix

Some of the operations required for later adaptation are demonstrated below. (Further details on their proofs can be found in [Beyer 1987], [Hilbert and Cohn-Vossen 1999] and [Mollin 1995].

1. Addition and/or subtraction:

The surface  $Q$  as a result of the addition and/or subtraction of two surfaces  $Q_1$  and  $Q_2$  is  $Q = Q_1 \pm Q_2$ .

This property implies that a complicated surface can be represented as the sum or difference of some simple primitive surfaces.

2. Frame transformation:

The surface  $Q$  as a result of the coordinate transformation from the primitive surface  $Q_0$  can be represented as  $Q = (T^{-1})^T Q_0 (T^{-1})$ .

This transformation will preserve all the properties and operations of surface matrix.

3. Surface normal:

The surface normal  $n = (n_x, n_y, n_z)$  at the point  $x = (x_0, y_0, z_0)$  is given by  $N = 2 * Q * X(x_0, y_0, z_0)$ .

**3D Surface Interpolation**

The least-square problem arises when the polynomial is being fit [Dai and Newman 1998]

$$ax^2 + by^2 + cz^2 + 2dxy + 2eyz + 2fxz + 2gx + 2hy + 2jz + k = 0$$

at some data points  $\{(x_i, y_i)\}$ ,  $i = 1, . . . , m$ , where  $m$  is greater than or equal to the number of unknown variables. A further generalization of the linear least-square problem is to take a linear combination of basic functions  $\{f(x_1, y_1), f(x_2, y_2), \dots, f(x_m, y_m)\}$ . Firstly, the  $c$ ,  $e$  and  $f$  variables of  $Q$  are set to zero to get an explicit form as shown below:

$$z = f(x, y) = ax^2 + by^2 + 2dxy + 2gx + 2hy + k \tag{33}$$

$z$  or  $f(x, y)$  represents the tactile data of the tactile elements at the location  $(x, y)$ .

The problem of fitting this polynomial can be written as:

$$\begin{aligned} z_1 &= ax_1^2 + by_1^2 + 2dx_1y_1 + 2gx_1 + 2hy_1 + k \\ z_2 &= ax_2^2 + by_2^2 + 2dx_2y_2 + 2gx_2 + 2hy_2 + k \\ z_3 &= ax_3^2 + by_3^2 + 2dx_3y_3 + 2gx_3 + 2hy_3 + k \\ &\dots\dots\dots \\ z_m &= ax_m^2 + by_m^2 + 2dx_my_m + 2gx_m + 2hy_m + k \end{aligned}$$

which denotes a system of linear equations. Also, recall that the  $x$ ,  $y$  and  $z$  are given and that the  $a, b, d, g, h$  and  $k$  are the unknowns.

In the matrix form  $Ac \approx Z$ ,  $A$  is a square matrix, the unknown  $c$  is a column vector, and  $Z$  is also a column vector:

$$z = \begin{pmatrix} z_1 \\ z_2 \\ z_3 \\ z_4 \\ z_5 \\ z_6 \end{pmatrix}, A = \begin{pmatrix} x_1^2 & y_1^2 & x_1 y_1 & x_1 & y_1 & 1 \\ x_2^2 & y_2^2 & x_2 y_2 & x_2 & y_2 & 1 \\ \cdot & \cdot & \cdot & \cdot & \cdot & \cdot \\ \cdot & \cdot & \cdot & \cdot & \cdot & \cdot \\ x_m^2 & y_m^2 & x_m y_m & x_m & y_m & 1 \end{pmatrix}, c = \begin{pmatrix} a \\ b \\ 2d \\ 2g \\ 2h \\ k \end{pmatrix}$$

The residual vector is:  $r = z - Ac$ .

The least-squares problem becomes:

$$\min \|z - Ac\|^2. \quad (34)$$

A solution of the least-squares problem is the solution  $c$  to the linear system:

$$A^T Ac = A^T z,$$

that is known as a *normal equation*. The solution of the least-squares problem is obtained by analyzing the singular value decomposition [Akritas and Kotsireas 2002] of  $A$  as shown below. As  $A = U^T SV$  and:

$$\|z - Ac\|^2 = \|z - U^T S V c\|^2 = \|U(z - U^T S V c)\|^2 = \|Uz - S V c\|^2$$

If  $Uz$  is substituted by  $d$  and  $Vc$  by  $r$ , then:

$$\|z - Ac\|^2 = \|d - Sr\|^2 = \begin{vmatrix} d_1 - \delta_1 r_1 \\ d_2 - \delta_2 r_2 \\ \cdot \\ \cdot \\ d_m - \delta_m r_m \end{vmatrix} = (d_1 - \delta_1 r_1)^2 + (d_2 - \delta_2 r_2)^2 + \dots + (d_m - \delta_m r_m)^2$$

where  $\|\cdot\|$  denotes the determinant of the matrix.

To minimize this problem, each term in this summation will be equated to zero. Then, the coefficients of the system equation are obtained by  $r_i = d_i / \delta_i$  respectively. The solution to the least-squares problem is then obtained from  $c = V^T r$ .

At this point, we do not aim to prove that the smallest eigenvalue can facilitate contact identification, but the proof can be obtained elsewhere [Petchartee and Monkman 2007b, 2007c, 2008b]. The conclusions of those proofs confirm that the smallest eigenvalue of the Quadric parameter is identical with the Quadric parameter itself. This means the smallest eigenvalue of the Quadric parameter yields identical characteristic to the Quadric shape. Consequently, it is reasonable to use the smallest eigenvalue to classify the contact surfaces. Every symmetric matrix has this property, including its covariance which is also a symmetrical matrix. In order to achieve better noise tolerance in real applications, using the covariance of  $Q$  in finding the smallest eigenvalue is reasonable. Everson and Roberts [Everson and Roberts 2000] also demonstrate a proof for the covariance matrix in terms of the effect of noise arising in all eigenvalues by variance  $\sigma^2$ , where  $\sigma$  is the standard deviation of random noise. Moreover, the variation in eigenvalues will coincide with  $\lambda_n + \sigma^2 b_- \leq \omega_n \leq \lambda_n + \sigma^2 b_+$ , where  $b_{\pm} = (1 \pm \sqrt{y})^2$ ,  $y = N/T$  and  $N$  is the dimension of the vector space for a number of samples  $T$ .

### 6.3.3 Real Experimental

#### Fitting Accuracy

We have been experimenting with quadric surfaces with an arbitrary set of data points. The fitting accuracy evaluation is to use a simple root-mean-squared (RMS) error function where each error value is the distance from a tactile data point to the point on the interpolation surface.

There may be many surfaces that fit the data with little RMS error, but some will have lower RMS values than others. For more noisy data, there may be a trade-off between the quality of the fitting and smoothness. We have sets of data points forming a surface in 3D-space, and we wish to fit a quadratic form to this surface. Specifically, we are trying to fit the surface

$$z = f(x, y) = ax^2 + by^2 + 2dxy + 2gx + 2hy + k,$$

where  $(x, y, z)$  are the coordinates of the data points in the coordinate frame. The  $z$  direction of a quadric surface is a function of second order equations in  $x$  and  $y$  which together represent a three dimensional space. We can use a simple mean square error to measure the fitting accuracy based on the distance between the surface and data points of the tactile element along the  $(x, y)$  coordinate.

To account for the spatial error under the surface, an RMS error was calculated for the average square of different errors with an interpolation period:

$$RMS = \sqrt{\frac{1}{N} \sum_{i=1}^I \sum_{j=1}^J (z_r(i, j) - z_o(i, j))^2} \quad (35)$$

where  $I$  is the total number of grid points in the  $x$  direction;  $i$  is the index of those points;  $J$  is the total number of points in the  $y$  direction;  $j$  is the index of those

points; and  $N$  is the total number of grid points. Also,  $z_o(i, j)$  is the data of tactile element at location  $(i, j)$ , and  $z_r(i, j)$  is the value of the interpolation on a surface at location  $(i, j)$ .

The bar graphs in figure 6.2 are grouped into four different types of object shapes. The random noise was simulated using the Matlab '*randn*' function. It generates normally distributed random numbers, whose values are in the range [1, 20] mixing with the tactile data sets. The best fit surface through all the data points still can be shown, and a close agreement between the data points and the fitted surface can be clearly seen.

Figure 6.2 shows the mean square distance deviation over 10 iterations of the experiments on different data sets. It was attempted to minimize this quantity in each interpolation period. The lower RMS error gives the minimum square distance deviation. The random noise inserted into the tactile data leads to a decrease in surface fitting accuracy. From the experiment, an RMS deviation of 2 to 27 is reached after 10 interpolation periods, and the maximum RMS deviation is dependent on object shape.

The random noise associated with the interpolation in a real application can generate variations in eigenvalues. This requires an investigation into the eigenvalue trajectory under random noise. Consequently, the variation in eigenvalue levels with different periods of interpolation under the influence of random noise must be presented.

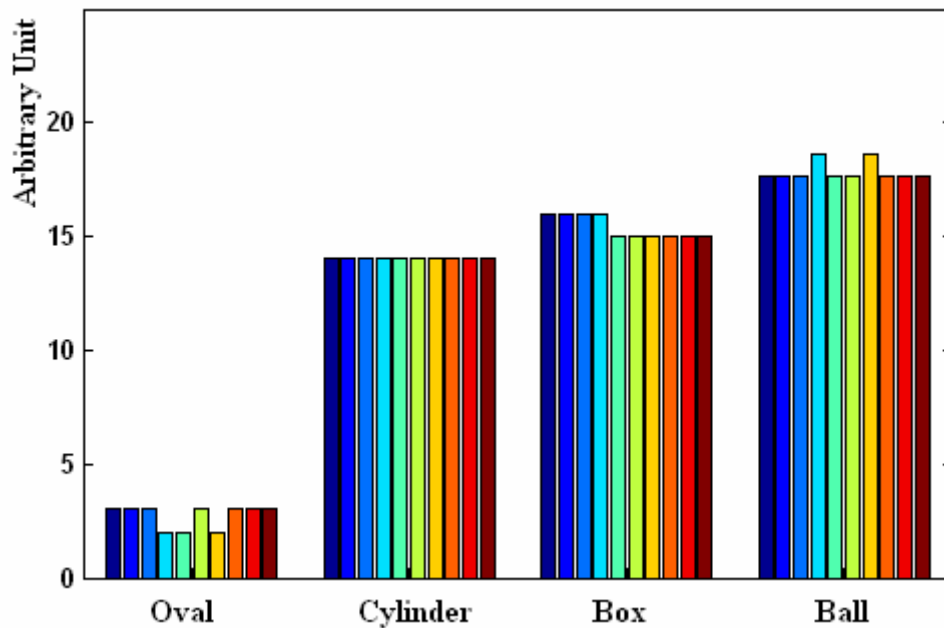


Figure 6.2: Fitting Accuracy

### The eigenvalue trajectory of covariance in the quadric-surface matrix ( $Q$ )

In the proposed method, the property of the quadric surface ( $Q$ ) will be used to calculate the eigenvalue but not in a direct way. Instead, the  $Q$  matrix will be multiplied with its transpose, to produce the covariance matrix. This covariance matrix is then used to find the eigenvalue trajectory.

$$Q = \begin{pmatrix} a & d & 0 & g \\ d & b & 0 & h \\ 0 & 0 & 0 & j \\ g & h & j & k \end{pmatrix}$$

The covariance matrix of the same data set is  $(X - \mu_x)(X - \mu_x)^T$ , where  $\mu_x$  is the mean value of  $X$ . However, for a simple covariance matrix, it can be presented as  $XX^T$ . Thus, the simple covariance matrix equation is:  $C_x = QQ^T$ .

The components of  $C_x$ , denoted by  $c_{ij}$ , represent the covariances between the random variable components  $q_i$  and  $q_j$ . The component  $c_{ij}$  is the variance of the component  $q_i$ . The variance of a component indicates the spread of the component



values around zero. If the two components  $q_i$  and  $q_j$  of the data are uncorrelated, their covariance is zero  $c_{ij} = c_{ji} = 0$ . The covariance matrix is, by definition, always symmetric.

The exact value is not as important as its sign (i.e. positive or negative). If the value is positive, as it is here, both dimensions ( $q_i$  and  $q_j$ ) increase together. That is, generally as the number in  $q_i$  increases, the number in  $q_j$  will also increase. When the value is negative, if one dimension ( $q_i$ ) increases, the other dimension ( $q_j$ ) will decrease. In the last case, if the covariance is zero, it indicates that the two dimensions are independent of each other.

Physical problem behaviour can sometimes be expressed as  $\bar{A}\bar{X} = \lambda\bar{X}$  or  $[\bar{A} - \lambda\bar{I}]\bar{X} = \bar{0}$  where  $\bar{A}$ ,  $\bar{X}$ ,  $\bar{I}$  and  $\bar{0}$  represent a known square matrix, a column vector of variables, a unit matrix, and a zero vector, respectively. The parameter  $\lambda$  is the eigenvalue for the matrix  $\bar{A}$ , while  $\bar{X}$  is the corresponding eigenvector. If  $\bar{A}$  is a  $n \times n$  matrix, then there will be  $n$  eigenvalues and  $n$  corresponding eigenvectors.

If  $[\bar{A} - \lambda\bar{I}]\bar{X} = \bar{0}$ , then the determinant  $\|\bar{A} - \lambda\bar{I}\|$  must vanish. The equation:

$$\|\bar{A} - \lambda\bar{I}\| = 0 \quad (36)$$

is a short form for the polynomial equation:

$$\lambda^n + \alpha_{n-1}\lambda^{n-1} + \alpha_{n-2}\lambda^{n-2} + \alpha_{n-3}\lambda^{n-3} + \dots + \alpha_1\lambda + \alpha_0 = 0$$

where,  $\alpha_i$  represent simple coefficients. In this study, the dimension of  $A$  is 4 by 4, then the value of  $n$  is 4. Any solution in terms of  $\lambda$  for the above polynomial gives valid eigenvalues. In this case, there exist four eigenvalues. If a valid eigenvalue is substituted in the equation  $[\bar{A} - \lambda\bar{I}]\bar{X} = 0$  and the vector  $\bar{X}$  is solved, the result will be the corresponding eigenvector associated with the particular eigenvalue. Eigenvalues are the roots of a characteristic polynomial with coefficients simply derived from the elements of the matrix.

In this experiment, the training procedure is done to check classification performance, as shown table 4. The quadric surface properties are modified by multiplying with transformation matrix for translation, rotation and scaling operations.






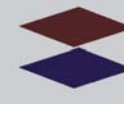


Object	Quadric Surface	Scale Ratio (time)	Translation in x-axis (mm.)	Translation in y-axis (mm.)	Rotation About x-axis (radian)	Rotation About y-axis (radian)	Rotation About z-axis (radian)
		0.1 to 4	-2 to 2	-4 to 4	0 to $2\pi$	0 to $2\pi$	0 to $2\pi$
		0.1 to 4	-2 to 2	-4 to 4	0 to $2\pi$	0 to $2\pi$	0 to $2\pi$
		0.1 to 4	-2 to 2	-4 to 4	0 to $2\pi$	0 to $2\pi$	0 to $2\pi$
		0.1 to 4	-2 to 2	-4 to 4	0 to $2\pi$	0 to $2\pi$	0 to $2\pi$

Table 4: Procedure for the evaluation of eigenvalue trajectories

By descending order of eigenvalues (largest first), an ordered orthogonal basis with the first eigenvector having the direction of largest data variance can be created. In this way, directions in which the data set has the most significant amount of energy can be found. To classify the type of contact, the smallest eigenvalue is used. From the experiment, there are four eigenvalues, the smallest one being in the range of  $10^{-3}$ , and the largest one in the range of  $10^2$ . Thus, the eigenvalues in the first three columns ordered ascendingly are not used while the one in the last column is utilised because it is the smallest eigenvalue.

This experiment applies several numerics, symbolic and graphical techniques to study the behavior of matrix eigenvalues after the matrix elements change. This change normally requires numerical analysis and perturbation theory, but the

technique called “eigenvalue trajectory analysis”, illustrated in Figure 6.3, is more widely applicable and will be adopted.

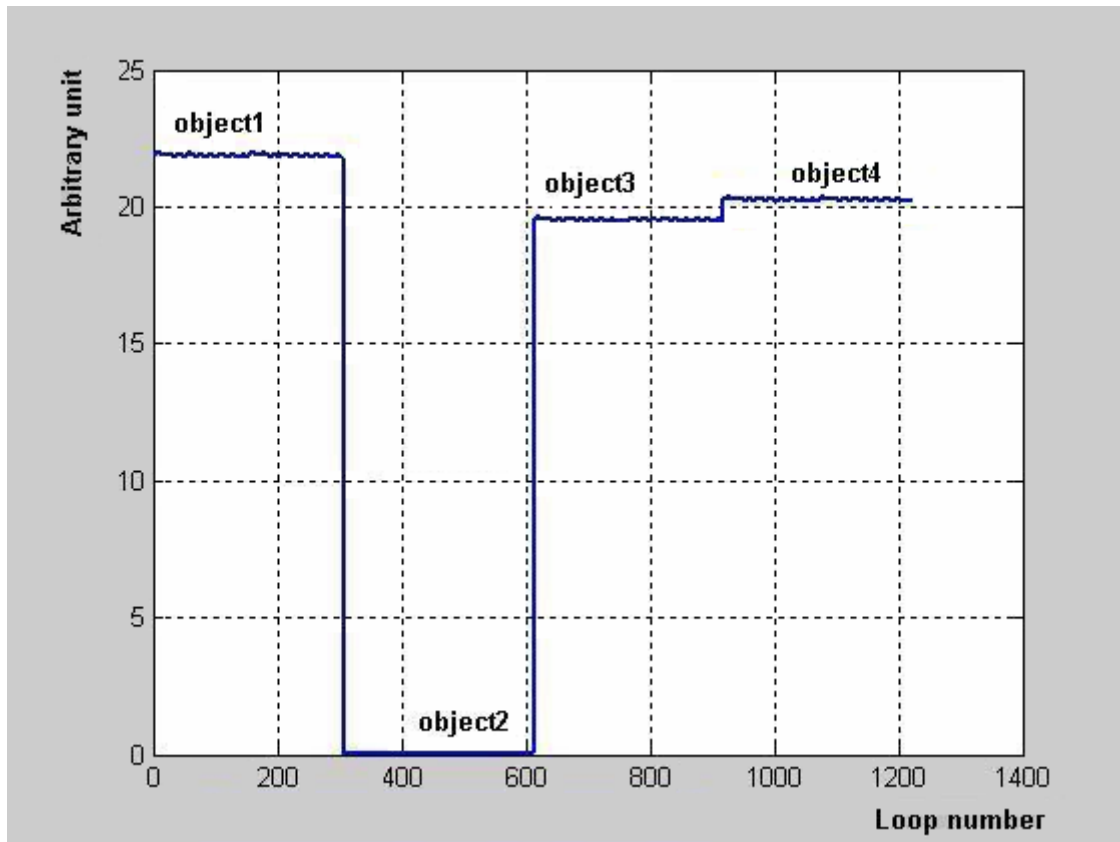


Figure 6.3: Eigenvalue trajectories of quadric parameters under different tested objects.

This graph shows the smallest eigenvalue of the covariance matrix of the quadric surface property independent of translations in all two axes (along x-axis, along y-axis), of rotations around any axis (around x-axis, around y-axis, around z-axis), and of scalable values. After the trajectory of the eigenvalue is derived, it can be used to classify to the contact surface of object by matching the level of eigenvalue of surface-property matrix belonging to the object prototype.

There are many different numerical methods for solving equation 36 for the eigenvalues  $\lambda$ . In summary, a relatively straightforward algorithm extracts the eigenvalues by solving a  $n$  degree polynomial, and then derives the eigenvector space for each eigenvalue. An important tool for describing the eigenvalues of square matrices is the characteristic polynomial. Conversely, this equation has exactly  $n$  roots.

In considering the machine hardware, each arithmetic operation is generally affected by round-off errors because the hardware can only represent a subset of real numbers (floating-point numbers). As an illustration, after an addition, subtraction, multiplication or division, the true value of an operation cannot be represented exactly as a floating-point number. Instead, it must be approximated by a nearby floating-point number before it can be stored in the memory. The difference between this approximation and its true value counterpart is denoted as a round-off error. Thus, an arithmetic operation is said to round correctly according to the machine precision.

In considering the software, the most common problems resulting from the round-off errors occur either when two quantities very close to each other are subtracted, or when a number is divided by another number which is close to zero. Other sorts of round-off errors can also occur when there exist operations attempting to convert a high-order number (64-bit number) to a low-order number (16-bit number) or when integers were converted to decimal numbers in C. This means that round-off errors in finding eigenvalues mainly depend on the arithmetic operation methods.

Eigenvalues of large matrices should not be computed using the characteristic polynomial: computing the polynomial becomes expensive in itself, and exact (symbolic) roots of a high-degree polynomial can be difficult to compute. For instance, the Abel–Ruffini theorem implies that the roots of high-degree polynomials cannot be expressed simply using  $n^{\text{th}}$  roots [Edgar 1930]. Moreover, although effective numerical algorithms for approximating the roots of polynomials exist, small errors in the eigenvalues can lead to large errors in the eigenvectors. Then, the eigenvalues using the characteristic polynomial give unexpected results in our tests. General algorithms for finding eigenvectors and eigenvalues are often iterative, but only a few iterative methods can provide round-off errors small enough to be useful for our purposes.

The easiest method is the power method in which a random vector  $\mathbf{v}$  is chosen and computed as  $A\mathbf{v}$ ,  $A^2\mathbf{v}$ ,  $A^3\mathbf{v}$ , ... The aim of the power method is to find only the largest eigenvalue  $\lambda_1$ . For example, if matrix  $A$  consists of several eigenvalues, ranging from  $\lambda_1 > \lambda_2 \geq \lambda_3 \geq \dots \geq \lambda_n$ ,  $\lambda_1$  will be the dominant value of the matrix. If matrix  $A_{n \times n}$  has  $n$  linearly independent eigenvectors, the vector  $X_0$  can be represented by  $X_0 = c_1V_1 + c_2V_2 + \dots + c_nV_n$ , whereby the vector set  $\{V_1, V_2, \dots, V_n\}$  is the set of linearly independent eigenvectors with  $n$  variables. Thus, the equations can be rewritten as:

$$AX_0 = c_1\lambda_1V_1 + c_2\lambda_2V_2 + \dots + c_n\lambda_nV_n$$

$$A^2X_0 = c_1\lambda_1^2V_1 + c_2\lambda_2^2V_2 + \dots + c_n\lambda_n^2V_n$$

$$A^mX_0 = c_1\lambda_1^mV_1 + c_2\lambda_2^mV_2 + \dots + c_n\lambda_n^mV_n$$

When the last equation is divided by  $\lambda_1^m$ , the following equation is derived:

$$\frac{1}{\lambda_1^m}A^mX_0 = c_1V_1 + c_2\left(\frac{\lambda_2}{\lambda_1}\right)^mV_2 + \dots + c_n\left(\frac{\lambda_n}{\lambda_1}\right)^mV_n$$

If  $m$  is larger, making the terms  $\left(\frac{\lambda_2}{\lambda_1}\right)^m, \dots, \left(\frac{\lambda_n}{\lambda_1}\right)^m$  approaching zero under the condition  $|\lambda_2 / \lambda_1| < 1, \dots, |\lambda_n / \lambda_1| < 1$ , then it can be concluded that for large  $m$ :

$$\frac{1}{\lambda_1^m}A^mX_0 \cong c_1V_1$$

From this equation, when  $c_1$  is not equal to zero,  $\lambda_1$  can be estimated when the number of interpolations ( $m$ ) is large. The problem with this method is that should matrix  $A$  not have a dominant eigenvalue, the time consumed for finding  $\lambda_1$  will tend to be longer.

Moreover, if the data in matrix  $A$  has errors, the square of  $A^m$  will exacerbate them leading to higher round-off errors. Although the modified method enables estimation of the smallest eigenvalue, these two limitations are inevitable.

This algorithm is easy to apply for the smallest eigenvalue, but not very useful due to round-off errors. Even though the level enabling classification of objects is only in the range of  $10^{-3}$ , the computing method to find an eigenvalue needs a very small round-off error. Moreover, there are some methods used in finding the roots of polynomials via eigen-functions like those in Matlab. The algorithms simply involve computing the eigenvalues of the companion matrix. Although it is possible to prove that the results produced are the exact eigenvalues of a matrix within given round-off errors of the given companion matrix, this does not mean that they are the exact roots of the polynomial with coefficients within the same round-off errors. And, it has been tested in our experiments yielding a useless result. So, these methods may not be used for our contact identification.

On the other hand, popular methods such as the QR algorithm used in the LAPACK library (Linear Algebra Software Package), have good classification ability since a precise resolution within the range of  $10^{-3}$  is possible with very small round-off errors. The QR algorithm can be used for either general matrix or non-symmetric matrix. According to the QR algorithm, matrix  $A$  will be transformed into a Hessenberg matrix using householder convergence. Then this matrix is used to calculate the eigenvalue. An important step is the factorization  $A_i = Q_i R_i$ , which undergoes the iteration process using the equation  $A_{i+1} = Q_i R_i = Q_i^T A_i Q_i$ . The pseudo code of the QR method is as follows:

- 1)  $i = 0$
- 2)  $A_i = A$
- 3) *Repeat*
- 4) *Factor*  $A_i = Q_i R_i$
- 5)  $A_{i+1} = Q_i R_i = Q_i^T A_i Q_i$
- 6)  $i = i + 1$
- 7) *until convergence.*

## 6.4 Analysis of results

### Effects of Random Noise on Eigenvalue Trajectory

This section investigates the sensitivity to noise of contact identification algorithms developed earlier. The effect of noise on the classification accuracy is considered when the incoming trajectories are corrupted with noisy data. Noise is simulated using a random function with a normal distribution with values in the range [1, 20]. Then, they are added to every tactile data element. The analysis of the simulation results shows varying abilities of the algorithms to cope with the noise perturbations. In most instances, high prediction robustness was achieved. Few of the simulations showed sensitivity to noise.

An emphasis should be placed on demonstrating the existence of noise and showing that small, as well as large, peaks can lead to significant errors in eigenvalue trajectory. The variation of noise peaks indicates that noise changes the magnitudes of eigenvalues of different object types and their surface transformations.

Figure 6.4 indicates that noise on the trajectory dampened some graph levels during the test experiments. Nonetheless, it did not reduce contact classification capability with respect to the overall error growth. Contact classification can still be achieved through level checking.

All of the eigenvalue trajectories were tested with noise levels ranging from 1 to 20, for 10 iterations. The noise levels for all tactile elements were randomly and simultaneously increased, yet only to the maximum values of 8% of ADC's maximum (255), and the performance of algorithms was demonstrated as shown in figures 6.4. This leads to the conclusions that if the noise level is kept below 8% it will not be statistically meaningful for, nor affect, classification.

By experimenting, it is also clear that classification capability reduces if the random noise peaks are greater than 8% of the ADC's maximum value. Invalid classification was tested by increasing noise to a level higher than 8%, and

consequentially, the crossing levels of eigenvalue trajectory appear. As a result in figure 6.6, contact classification cannot be achieved by simple level checking.

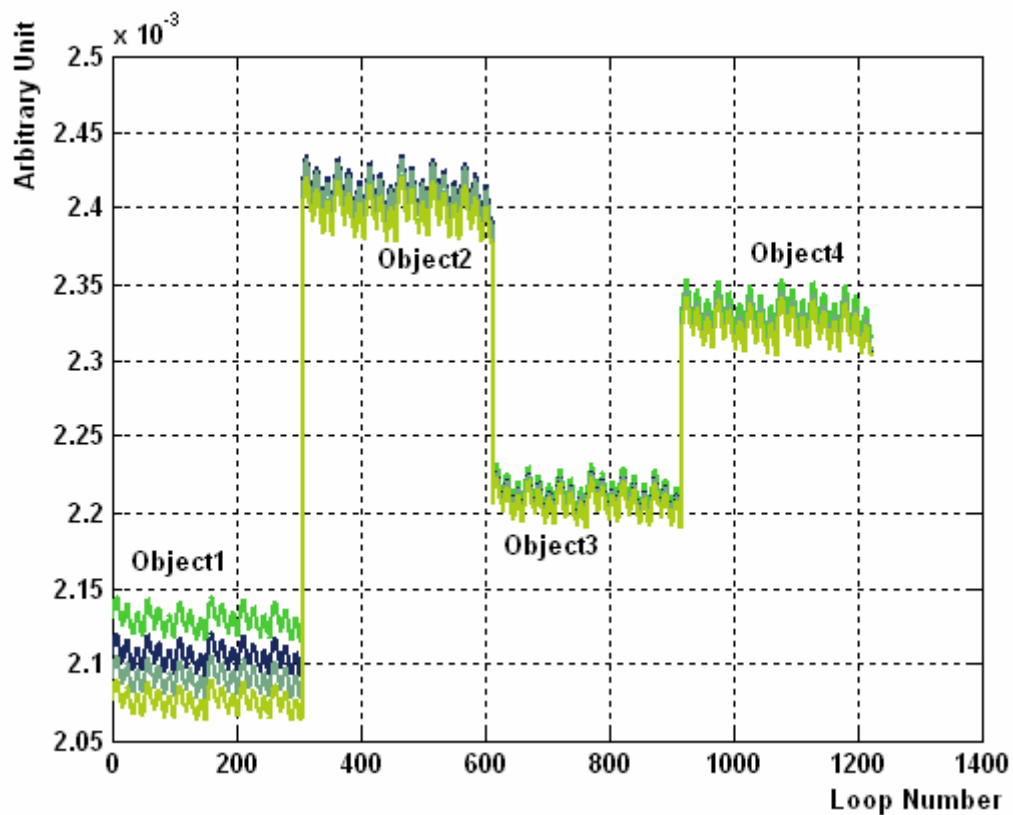


Figure 6.4: Noise Tolerances

By observation, the use of a noise filter on the tactile data reduces the effect of noise on the eigenvalue trajectory, and such a filtration must be performed before surface interpolation was applied.



## Margin of classification

The principal idea that is used to classify the contact is in the matched threshold of the eigenvalue trajectory. For example, in figure 6.5, the 'a' level can be used to distinguish between object A and object B; the 'b' level can be used to distinguish between object A and object C, and so on. As formerly mentioned, random noise has an effect on the eigenvalue trajectory. The windows of different sizes (A, B, C) have their uses on defining different thresholds for the eigenvalue trajectory, and classification by thresholds has to be adjusted dynamically.

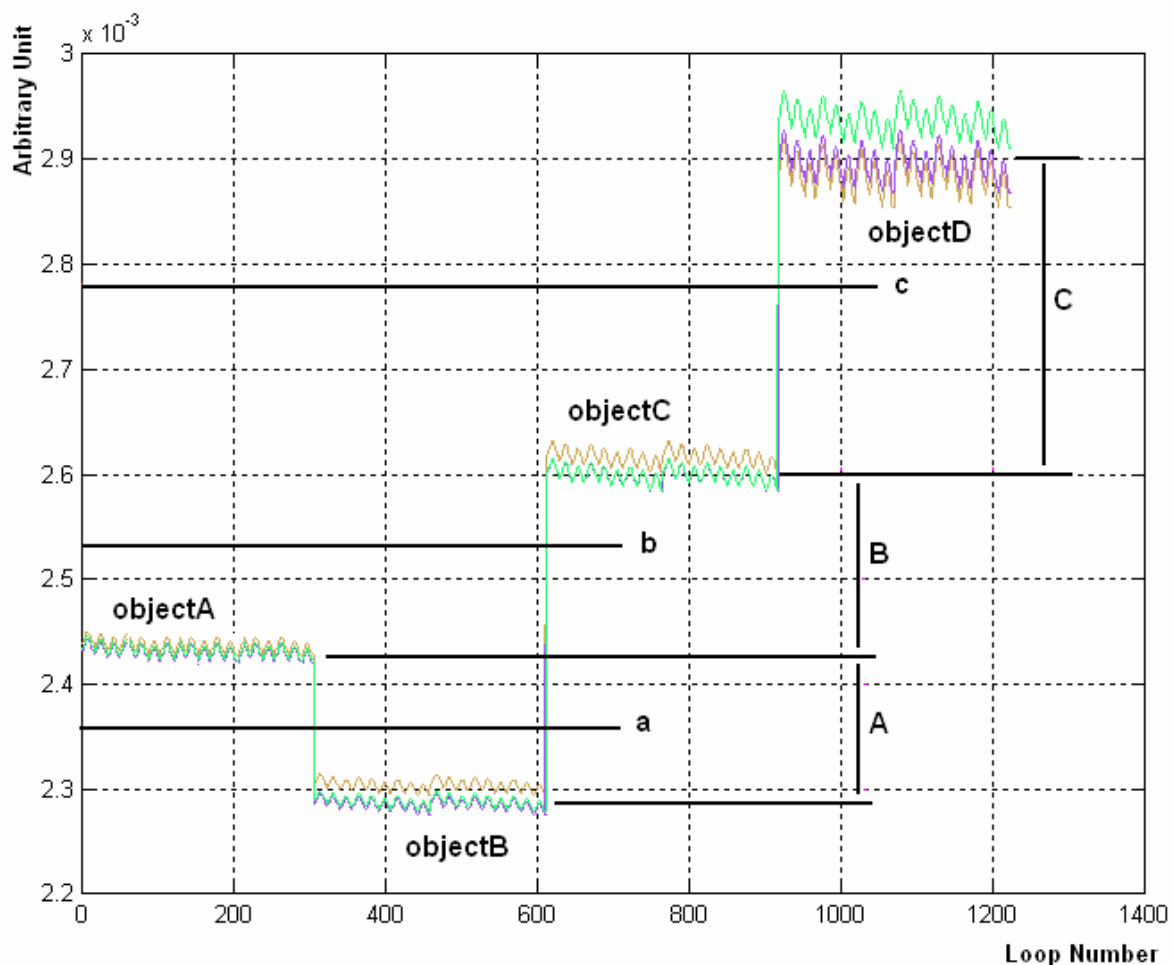


Figure 6.5: Windows of Margin

In cases where the noise amplitude falls outside the range [1, 20], this classification method cannot guarantee correct classification of object shapes. Experimental results are presented in figure 6.6. Another limitation of the algorithm is the differences of the object shapes and noise affected in surface interpolation. If the

shapes of the test objects are not much different, the classification will fail as random noise can reduce the window size to zero. Also, some object shapes are very sensitive to noise which leads to them being identified wrongly in the interpolation process. As displayed in figure 6.6, object A and object B yield little difference in terms of the smallest eigenvalues, which lead to a classification failure. In reality, the noise mixed with the tactile data also has an effect on the smallest eigenvalue. If the window size is too small, then the added noise will make the classification capability approach zero.

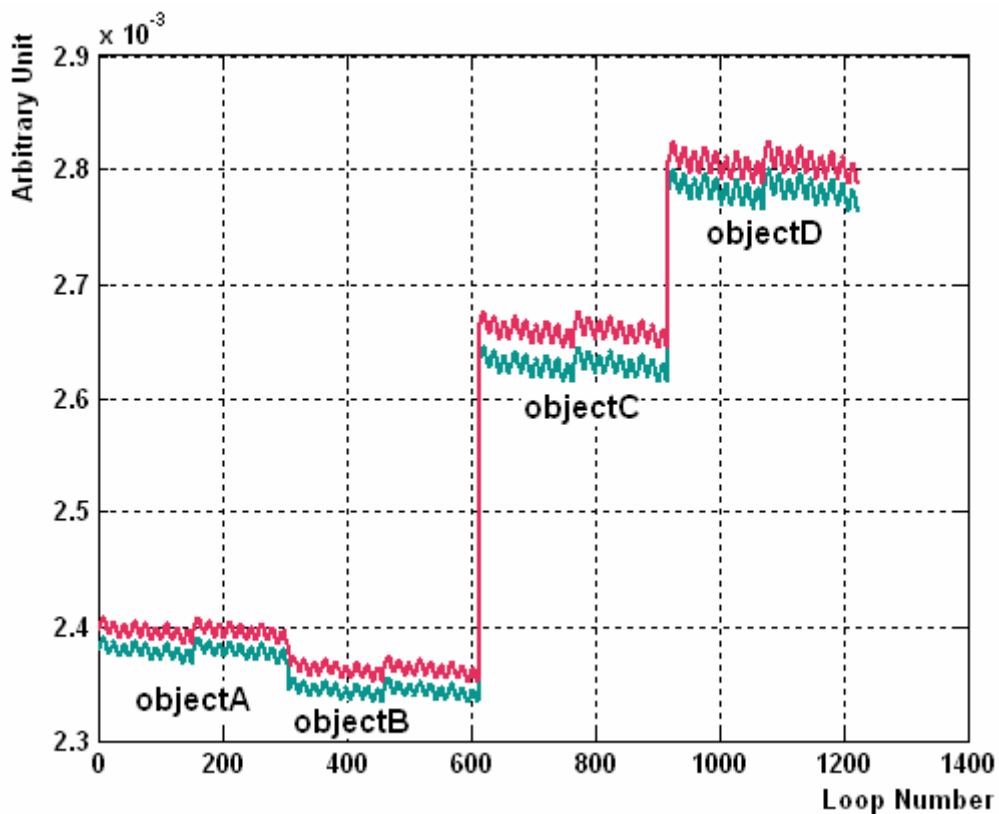


Figure 6.6: Mixed threshold

In terms of actual implementations using tactile sensors, the set of objects and other criteria also affect the optimal classification performance. It also seems reasonable to think that the degree of deviations or differences between any two object shapes should eventually entail classification performance between them, and our experiments appear to have uncovered such a case.

In the experiment, the training procedure is done as shown as Pseudo-code in Algorithm1. The inputs consist of  $N$  Quadric surfaces ( $D$ ) which are randomly selected by the number  $I$ .

The Quadric surfaces are transformed by translation, rotation and scaling matrices. The smallest eigenvalues are calculated and stored in the variable ( $traject$ ) from which the trajectory is generated. The threshold of classifications ( $\hat{a}, \hat{b}, \hat{c}, \hat{d}, \dots$ ) are then determined. The smallest eigenvalue of the selected surface  $I$  is compared to this threshold of classifications. The algorithm returns the output in the variable  $T$  as an index.

**Algorithm 1.** Contact-Classify( $T = (N, D_{N \times 4 \times 4}, I_{4 \times 4})$ )

1. Initialization:  $Objnum, i$
2. **while**  $Objnum \leq N$
3.   **for**  $scale = 1; step = 0.1; scale \leq 4$
4.     **for**  $tranXY = -2; step = 0.1; tranXY \leq 2$
5.       **for**  $rotXYZ = 0; step = \pi / 8; scale \leq 2\pi$
6.          $tmpMatrix = Transform(D(Objnum), scale, tranXY, rotXYZ)$
7.          $traject(i) = MinEigen(tmpMatrix)$
8.         Increase  $i$
9.       **end for**
10.     **end for**
11.   **end for**
12.   Increase  $Objnum$
13. **end while**
14.  $[\hat{a}, \hat{b}, \hat{c}, \hat{d}, \dots] = FindThreshold(traject)$
15.  $T = CheckLevel(\hat{a}, \hat{b}, \hat{c}, \hat{d}, \dots, MinEigen(I))$

According to figure 6.4, the thresholds of object 1, object 2, object 3, object 4 correspond with oval, cylindrical, cube and ball shapes, respectively. Each object has a different eigenvalue in the eigenvalue trajectory with no particular increasing or decreasing order in terms of their levels. This leads into misclassification in case of two very close threshold values. Table 5 demonstrates the test results, whose testing were performed ten times on each object shape. The classification results reveal correct recognition as well as misrecognition. These differences may indicate that there are indeed limitations on the ranges of classification due to the similarity of test objects, fitting performance, and random noise.

Object Features	Percent of misclassify in object class				Percent Error
	Oval	Cylinder	Box	Ball	
(1) Oval	0	0	10%	0	10%
(2) Cylinder	0	0	0	0	0%
(3) Box	10%	0	0	0	10%
(4) Ball	0	0	0	0	0%

Table 5: Statistic error of classification

For examples, the oval object can be misclassified as a box object by 10%. Yet, the oval may be less likely misclassified as a cylinder object, because their thresholds are not in neighbouring ranges.

## 6.5 Conclusions

A technique for recognizing objects using tactile sensor arrays, and a method based on the quadric surface parameter for classifying grasped objects is described. It has been shown that the covariance matrix from parameter of quadric surfaces by interpolation of tactile data may be formulated by eigenvalue decomposition and can reflect under all contact geometries. The smallest component of an eigenvalue can be used to estimate and identify object shape without using any other references, whereas classification is used as the principal indication of surface identity. The shape reflectance parameter pertaining to (unique to) each surface may be recovered and identified. It has been shown that the reliability of the surface classification method and the accuracy of transformation are independent of object shapes. The Authors also proposed methods to improve the classification performances using boundary alignment based multivariate regression [Petchartee and Monkman 2007b] and forth-order perturbation of SVD [Petchartee and Monkman 2007c].

## **CHAPTER SEVEN**

### **SUMMARY AND OUTLOOK**

This Chapter concludes the dissertation by providing a summary of the results obtained in the preceding chapters, a description of major contributions and conclusions drawn from those results, and suggestions of areas for future work.

#### **7.1 Summary of Results**

This dissertation has investigated the sensing capabilities of conductive foam tactile sensors for attachment to robot gripper fingers through sensory experiments. The analyses mainly concerned the ascertaining of minimum grasping forces, contact classification, and a neural network model for the inverse tactile problem. The optimized grasping force and manipulation of objects have been demonstrated. Subsequently, it has been shown that quadric surfaces can provide contact location information necessary for obtaining shear and moment force sensing. Estimation of shear and moment forces was shown to be more difficult to attain, especially during the grasp process. Nevertheless, this yields a better understanding of the capabilities of such sensors and how they should be used.

This research also recognizes the importance of contact surfaces. Contact identification can be utilized to determine unknown object properties, primarily the shape. Contact identification and prehension can be accomplished by any robotic hand and tactile sensors used to reposition or reorientate the object in order to access different areas of the objects surface.

One significant result emanating from this research is a method for detecting and identifying surfaces in the context of tactile prehension with robotic fingers. A wide variety of two-fingered robot grippers are commercially available and most rectangular-shaped fingers are adequate for prehension by effectively mimicking the geometry of human fingers and thumb.

By choosing the appropriate shape for the fingertips, in conjunction with a robot having the necessary articulation, the object may be firmly grasped. Based on the definition of certain features of quadric parameters, a set of algorithms have been developed for such contact identification.

It is also well-known that the coefficients of friction of the contact area play an important role in terms of prehension. Consequently, it is interesting to observe its importance in tactile sensing as has been shown in the first experiments, namely grasping force optimization. This may be achieved by allowing the robot to effectively modulate the frictional parameters between fingers and grasped object. To these ends, changes in the contact area (increasing the grasping force) corresponding with fluctuations in tactile signal, may be used as feedback to control the effective contact area.

In Chapter 3, the development of the resistive tactile sensor, its applications, and system configuration of the test robot are described. Here, the mechanism of the resistive tactile sensor was introduced and the signal processing method described. Measuring the resistive changes and the parameters of the tactile sensor in Chapter 4, the contact location and the slip detection conditions were obtained. Furthermore, the principal behavior of the tactile sensor under rotation and translation of the contact object were introduced. With NURBS interpolation, the contact surface in experiments which gave local curvature information at the contact point on the object, were presented.

As seen in Chapter 4, contact localization is also an important factor which a tactile sensor can provide. With this sensor, accuracy of point source localizations was very good, and grasp stability analysis became relatively simple to achieve.

Chapter 4 also revealed the importance of calibration techniques on the reliability of curvature estimates from tactile data. Although it was clear that data from all sensor elements fit the nonlinear elastic model (four parameter models), it implied that nonlinear elastic models can be used to describe the capabilities of tactile sensors and to predict responses from real sensors.

This approach was shown to almost halve the variance of the estimated curvatures. To predict responses, it is actually better to fit nonlinear mapping between the pressure distributions and the sampled strain values, but theoretically, we do not know the pressure distribution and stress value as only, strain sensing is obtained. Newer nonlinear techniques might produce better results, though at this point it can be said that the questions brought up in Chapter 4 have been adequately addressed. In this chapter shape sensing capabilities within the class of a sphere, a torous, a cylinder and a cuboid using a tactile array under 20 mm by 55 mm of the contact area were also investigated. With the current construction techniques, it was possible to make contact shapes with the existing tactile sensor array density.

In Chapter 5, the grasping force optimization problem was considered. The optimization problem becomes a set of rule-based problems. Using the tactile feedback information and contact kinematic equations, the local coordinates at the contact point could be updated in real-time. Hence, optimization of the robots grasping force could be achieved. Adopting memory queue computing techniques, a real-time algorithm based on tactile sensor feedback was implemented.

For touch identification in chapter 6, the algorithm in which object classification is theoretically possible given the current sensor noise was also investigated. It was shown that an eigenvalue of the property matrix of a quadric surface interpolated from the tactile data is identical to the contact object under the variation of any transformation.

## 7.2 Review of Contributions

Major contributions of this research are summarized here along with rationales based on the above summary of results. A procedure for combining manipulation and tactile information of an unknown object under prehension is the main contribution. A method for accomplishing this with a minimal grasping force for a two-finger gripper with different object weights and sizes has been developed. This procedure emphasizes the importance of the link between manipulation and tactile information. In addition, parallel surfaces created by the two-finger gripper can be used for contact identification. Thus, tactile sensor data is necessary for this purpose. Algorithms for performing contact identification on robotic fingers in three dimensions were successfully tested. A contact procedure was developed and tested so to enable gripper fingers to identify contact features. Algorithms employing surface parameters for tracking the trajectories of eigenvalues were also capable of discriminating between different levels of eigenvalues. The above results form a cohesive procedure for contact identification of objects under prehension. The general procedure and algorithms can be extended to many different types of robotic hands and objects.



### 7.3 Future Works

There are many intriguing avenues emanating from this research. Some possibilities are direct extensions of the work documented in this dissertation, while others suggest the application of some of the concepts developed here in other subject areas. Following directly from this dissertation, it is important to develop further sensing methods for tactile sensors. The parameter matrix of a quadric surface may be analyzed using a logical decomposition method that produces a series of smaller matrices. If there are other surface regions added to the original contact surface whose features modify the surface boundary, then it may be desirable to perform local interpretation on that surface region in order to generate a strain tensor as proposed by [Frederick and Chang 1965].

It may also be desirable to develop a global algorithm to prove that all strain tensor components of additional regions may be used to explain the characteristics of the shear and moment components on the tactile surface. Efficiency of various decomposition techniques can also be investigated. In performing the experiments for this dissertation, it became evident that, while the state of the tactile surface has certainly improved over the strain tensor fields, there is still no existing decomposition technique that is ideal for this purpose. While there exist many kinds of tactile sensors that have the same structure and characteristics to which this solution is applicable, it is the solution of a single sensor measuring signals in only one axis which can sense physical values in six axes or directions. Consequently, many other forms of tactile sensor could also be utilized. In addition, the application of tactile sensing and its evaluation as described here may eventually have an influence on robotic hand design.

Moving on to the broader extensions of this work, one particularly interesting topic is the development of a reality-based modeling system that can measure other types of object property. While this dissertation focuses on contact identifications, there are many other properties that can be explored, such as mass/inertia, friction, temperature, texture, and stiffness. While roughness has been characterized using fractal [Allison et al. 2000] and stochastic ([Donald and Salisbury 1997], [Juhani and Dinesh 1996]) methods, texture is still a nebulous concept and is therefore difficult to detect, identify, and model. Some other properties, such as friction [Christopher et al. 1999] and impact dynamics ([Eberman and Salisbury 1994], [Allison et al. 1998]), have been automatically identified.

The proposed control scheme only considers the robotic manipulation of an object in a fixed contact prehension scenario. How to design an event-based motion reference for a multi-fingered robotic hand under sliding contact is still an open problem which constitutes a future research area. Some tactile sensing-based schemes to produce coordinated gripper motions and to optimize grasping forces have been proposed. [Maekawa et al. 1995, 1997] considered manipulation and dynamic grasping of an unknown object by a multi-fingered hand with rolling contact.

[Bicchi et al. 1996, 1998 and 1999] presented some results on manipulating unknown objects. They discussed a method for building an approximation of the surface of an unknown object from data gathered by exploring the object through rolling motions. Generating coordinated motions and optimizing grasping forces by using tactile sensor feedback for an unknown object is another intriguing further research issue. However, improvements in tactile sensing and data interpretation are still needed to support general manipulation of unknown objects.

## 7.4 Problem Solution

Robot gripper control was found to be a problem during this research and is an issue which needs to be discussed further. The internal structure of the gripper used employs a 12-volt DC motor as prime mover. The gripper receives commands via a CAN-bus. To control the gripper the robot receives a set of 8-bit signed numbers, the PWM values.

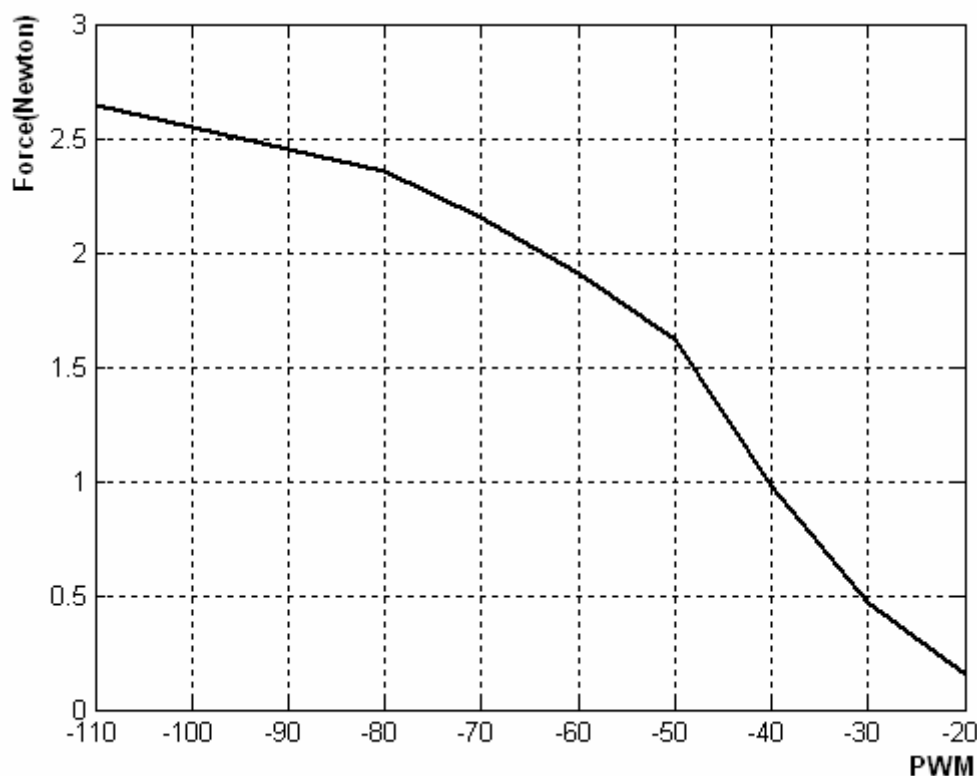


Figure 7.1: Graph showing the relationship between PWM values and resulting forces

To control the robot gripper for prehension or retention (close), negative numbers within the range from  $-300$  to  $-20$  must be sent to the robot. The larger the modulus of the negative numbers the greater the holding forces. On the other hand, positive numbers within the range from  $20$  to  $300$  must be sent in order to achieve object release (open). The greater the positive number, the lower the retention force on the object.

Figure 7.1 exhibits the graph showing the relationship between the PWM values sent to the robot gripper and the resulting retention forces which agree with the output from the FSR sensor. Normally, manufacturers of robot grippers provide design formulas or equations making the calculation of prehension forces simple. However, in the case of the gripper used in this research, the actual relationship is not so simple since the internal operational mechanism of the robot gripper relies on a wheel and axle. Over projected use, the wheel and axle can become loose causing imbalance in the two jaw forces. Consequently, their respective shear force components will increase or become unstable (hysteresis).

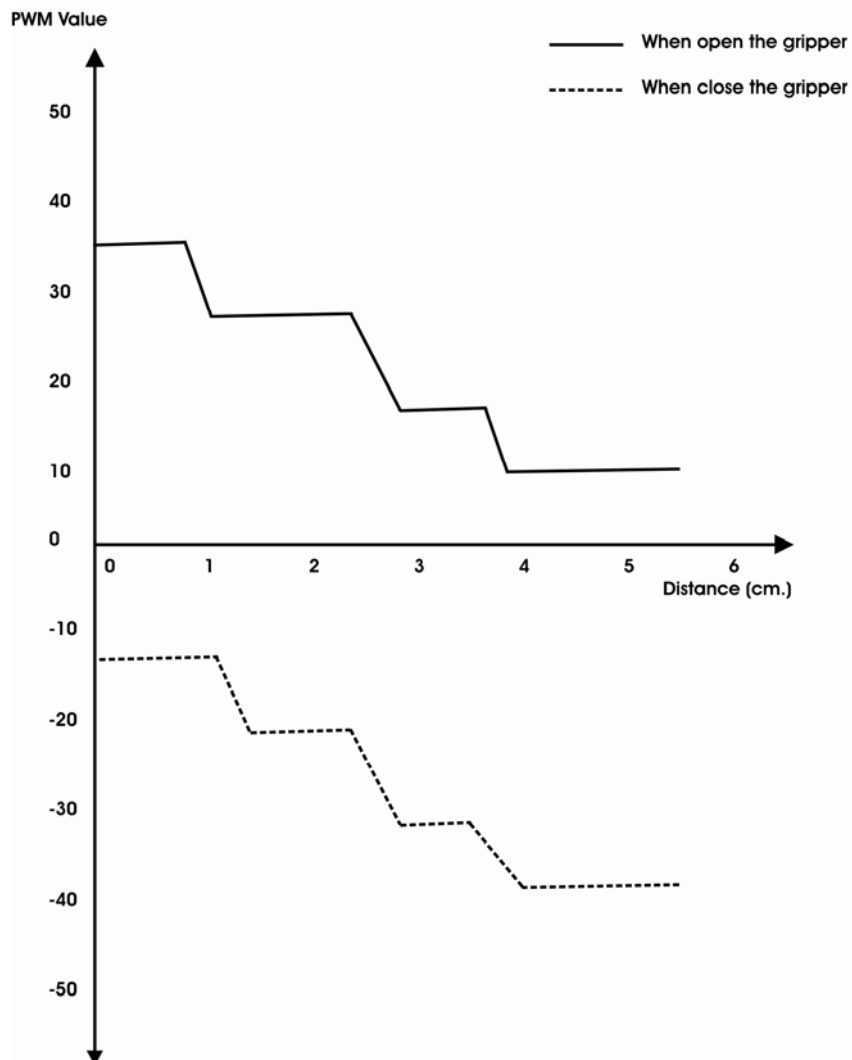


Figure 7.2: Graph showing the lowest PWM values for gripper movement

From Figure 7.2, it can be observed that the robot gripper has a maximum stroke of 5.5 cm. In case of maximum closing, the distance is zero. With different distances during opening and the closing, the minimum PWM values required for the gripper movement will vary. Put another way, a certain minimum threshold of PWM values is necessary to cause the gripper to open or close. Degree of closeness/openness is prior to the command to drive the grippers to open/close. A larger openness always requires the least PWM values which are lower than does a smaller openness. This result from the threshold values is to control the operation of the grippers. These values depend on the direction of finger movement.

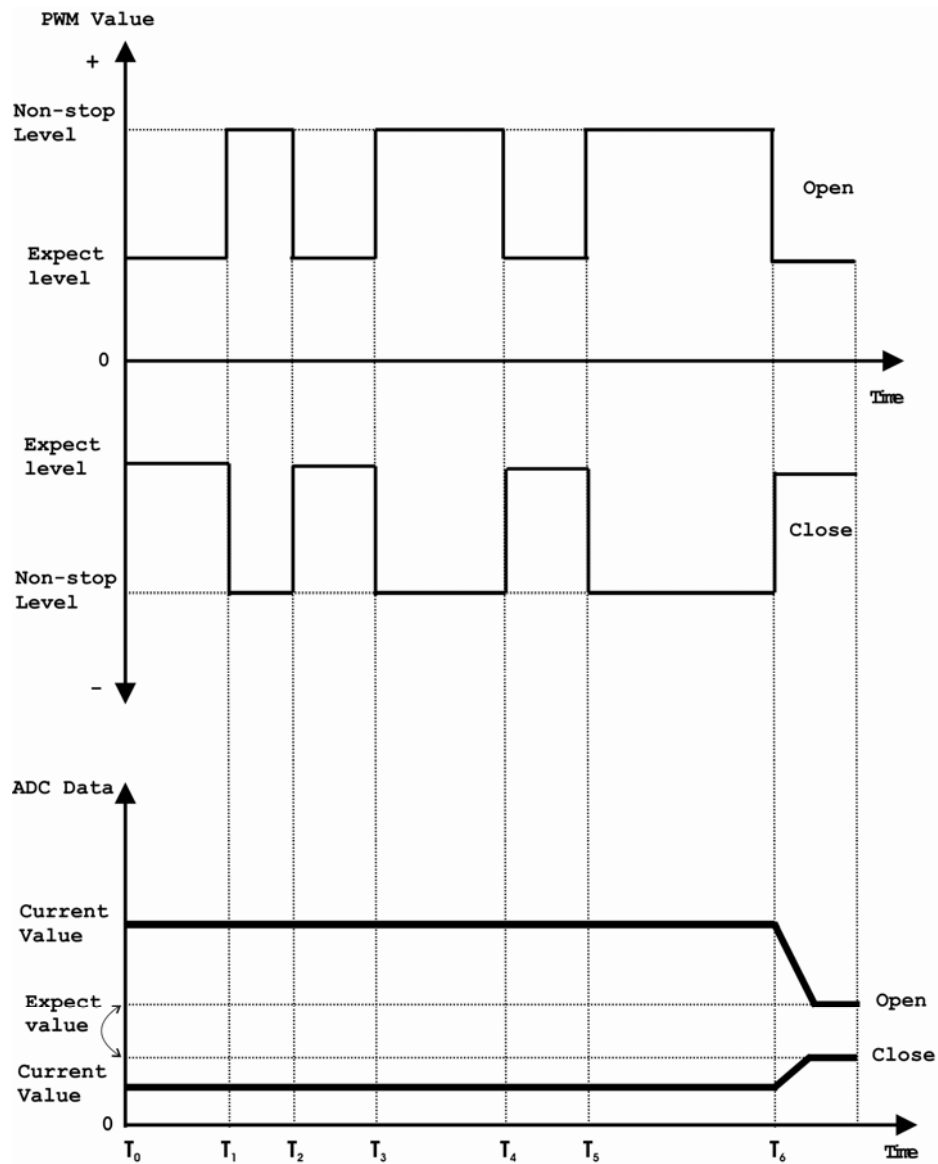


Figure 7.3: Solutions to gripper threshold

From the problem discussed above, a simple solution is proposed. That is, the difference in the threshold shown in Figure 7.3 should be compensated for. At the instigation of prehension movement at time  $T_0$ , a minus PWM value to create a desirable force will be sent to the gripper. However, from the lower part of the same Figure, the force shown by the tactile sensors is still stable from time  $T_0$  to  $T_1$ , implying that the PWM value sent to the gripper is not sufficient to move the gripper.

To solve this problem, a higher minus PWM value (to cause closure) will be sent to the gripper at time  $T_1$ . At the point where the value reaches the nonstop level, (i.e., the highest threshold), the gripper will certainly move, e.g. to close or to open depending on the plus or minus sign. When a high negative value is sent to the gripper for a short period of time during  $T_1$  and  $T_2$  and followed by the desired PWM value, the force from the tactile sensors will show if there is any change. In case there is no change in  $T_2$ , a higher negative PWM value must be sent again but with a prolonged duration from  $T_3$  to  $T_4$ . This is then followed by the desired PWM value, after which the force from the tactile sensors is read. These steps must be repeated over a prolonged duration with a high PWM value until a stable force is signaled by the tactile sensors.

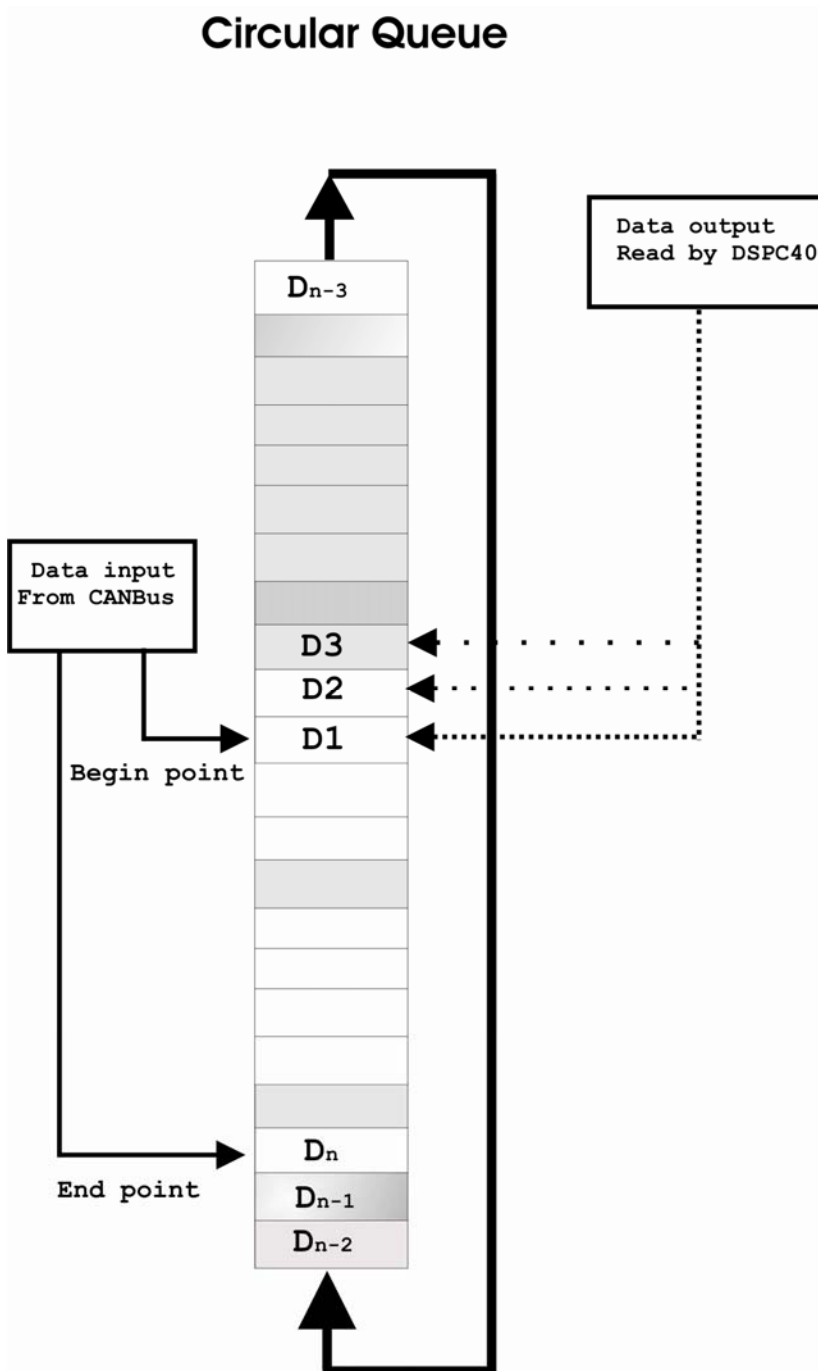


Figure 7.4: Speed of communication protocols and devices

Using CPU, micro-controllers, and digital-signal processors with different speeds and communication protocols to form a network or a robotic system as described in Chapter 3 causes several problems with respect to robotic manipulation based on force control. One problem is the asynchronous speed of operation. The tactile sensor micro-controllers operate at a speed of 20 MHz and transmit data via the CAN-bus to the CAN-master (which in this case is the IPackTIM module installed on the C40 module) at the rate of 250 Kbits/sec. Hence, data transmission using the CAN-protocol is carried out by hardware on the IPackTIM module controlled by the DSP Chip on the C40 module. A program to control this operation has also been developed.

However, there are several parallel operating programs on the C40 module. For instance, the program controlling the mobile platform operation shares the same DSP on the C40 module as the above for data transmission to and from the host PC. This process uses a hardware transputerlink which adjusts the signal to the RS485 system - a requirement for mobile-platform data transmission. Another program operating on the C40 module is used to transmit data between the C40 module and other processors connected to the DSP network.

A significant problem to this parallel processing is that the three programs used as examples above operate simultaneously. An overload in any of the programs will cause the DSP to slow down, resulting in slower operation for the other programs as they share the same processing unit. For example, when the tactile controller transmits data through the CAN-bus via the DSP network to the PC, and a point exists along the transmission line which cannot respond to the operation promptly, then the data from the tactile controller will encounter an overrun error. Thus, old data that have not yet been transmitted will be overwritten by new ones and the old data will be lost.



Programs interacting with the DSP do not have differing priorities because it is difficult to determine and set appropriate priorities. In transmitting data to other parts of the network, a program operating on the DSP will depend on other programs sharing the same DSP. However, this relationship is not one-to-one as the destination to (or from) which the data is transmitted can frequently be shared by a third program. For instance, despite their set priority in relation to the second program, the first and the third programs will encounter an overrun error during simultaneous transmission as one program will function faster than the other. Thus, setting priorities is not really helpful in solving this problem. The use of dynamic priorities may help in that priorities can be allocated dependant on computational workload.

One proposed solution to this problem is to employ secondary memory (a circular queue) to temporarily store the data. This mitigates problems in cases where the program at the data source happens to transmit data faster than it can receive it from the destination (or a problem in the transmission is encountered). The circular queue has an index to identify the location of the data already transmitted and the most recent data not transmitted. The circular queue can be tested to determine its current size. Figure 7.4 shows the circular queue used to connect the data from the CAN-bus to the program which reads and transmits the data to other DSP's on the DSP Network.

## 7.5 Conclusions

The tactile sensors used in this research are simple to construct and also not difficult to apply for the basic robot applications. However, it is important to note that the sensor can be used in a “nonlinear” manner during manipulation tasks. For example, when the finger first makes contact with an object the stress distribution under the finger skin varies rapidly. Similarly, small slips at the edge of the contact area just before a grasped object begins to slide produce rapid stress transients. In many cases a simple threshold technique will be sufficient for robotic applications. Since these phenomena represent important transitions in the mechanical state of the hand-object system, this sensor can be used to improve the robustness of robotic manipulation throughout a range of tasks. However, for advance applications (i.e. multiple-axis sensing), it seem to be unable to adapt for (based on its structure) because it can provide only a limited number of useful data.

Another improvement might be derived from using additional electrodes to better determine the actual deformation of the tactile surface during prehension. Improvements to this design include the introduction of floating electrodes to better measure the support reactions. One intriguing alternative boundary condition is mounting electrodes inside the tactile material to permit greater flexure of the tactile material during prehension. For ease of construction and improved sensing ability, the first of these orientations was selected so that the displacements between the floating electrodes are regularly spaced within the center of the tactile material.

Similarly, the design of tactile images can be improved by referring to research on the perception and cognition of tactile information. However, such an approach has not yet been applied to tactile cartography in a systematic way. Furthermore, this model represents a useful starting point for the development of high resolution surface tactile sensors. It provides physical insight into the sensor’s functioning, indicates improvements to the sensor design, and suggests further lines of investigation into tactile sensing of fine surface features.

The principal lesson we learned from this research effort was the importance of designing the sensor for the task. Better task specification and consideration of many transduction methods present many opportunities for improvements in tactile sensing.

## REFERENCES

- Abu-Zitar, R. and Al-Fahed Nuseirat, A. M. (2000):** *A neural network approach to the frictionless grasping problem.* Journal Intelligent and Robotic Systems Vol. 29, pp. 27–45.
- Abu-Zitar, R. and Al-Fahed Nuseirat, A. M. (2001):** *A Theoretical Approach of an Intelligent Robot Gripper to Grasp Polygon Shaped Objects.* Journal of Intelligent and Robotic Systems Vol.31, pp. 397–422.
- Akritas, A.G. and Kotsireas, I. S. (2002):** Applications of Singular Value Decomposition (SVD). the 8th International Conference on Applications of Computer Algebra, ACA 2002, University of Thessaly Press, pp. 50-51.
- Albus, J. S. (1981):** *Brains, Behavior, and Robotics,* Byte Publications, Inc. Peterborough, NH, pp. 143 - 179.
- Albus, J. S. (1983):** *Robot Sensing for a Hierarchical Control System.* International Symposium on Industrial Robots and Robots 7.
- Al-Fahed Nuseirat, A. M.; Hamdan, A.M.A. and Hamdan, H. M. A. (1999):** *Stability and modal control of an object grasped by a multifingered robot hand.* ZAMM, Z. Angew. Math. Mech, Vol. 79, No. 7, pp. 473–479.
- Allen, P. (1988):** *Integrating vision and touch for object recognition tasks.* International Journal Robotic Research, Vol. 7, No. 6, pp. 15–32.
- Allison, M. O.; Dennerlein, J. T. and Howe, R. D. (1998):** *Vibration feedback models for virtual environments.* In Proceedings of the IEEE International Conference on Robotics and Automation, Vol.1, pp. 674-679.
- Allison, M. O.; Michael A. C.; Michael, L. T.; Christopher, R. and Mark, R. C. (2000):** *Haptic exploration of surfaces.* Experimental Robotics VI, Lecture Notes in Control and Information Sciences, Springer-Verlag, Vol. 250, pp. 423-432.
- Anand, A. and Soom, A. (1984):** *Roughness-Induced Transient Loading at Sliding Contact During Start-Up.* Journal of Tribology, Vol. 106, pp. 49-53.
- Ando, S. and Shinoda, H. (1995):** *Ultrasonic emission tactile sensing.* IEEE Control Systems, Vol. 15, pp.61-69.
- Ankerst, M.; Kastenmuller, G.; Kriegel, H. P. and Seidl, T. (1999):** *3D shape histograms for similarity search and classification in spatial databases.* In Symposium on Large Spatial Databases, pp. 207–226.

- Ansoft Maxwell (1997):** Eminence User's Manual, Release. 5.0.
- Arterburn, D. R. (1984):** *Differential Equations Problem Solver*, Research & Education Association.
- ASTM Standard D 257-99**, Standard test methods for D-C resistance or conductance of insulating materials, 1999.
- Baglio, S.; Muscato, G. and Savalli, N. (2002):** *Tactile measuring systems for the recognition of unknown surfaces*, IEEE Transaction on Instrument Measurement, Vol. 51, pp. 522–31.
- Bajcsy, R.; Buttazzo, G. and Dario, P. (1986):** *Finger based explorations*. SPIE, Vol. 726, pp. 338-345.
- Bangert, C. and Prautzsch, H. (1999):** *Quadric Spline*. In: CAGD, Vol. 16, pp. 497-515.
- Beyer, W. H (1987):** *CRC Standard Mathematical Tables*, FL: CRC Press, 28<sup>th</sup> edition. Boca Raton, pp. 210-211.
- Bergevin, R.; Laurendeau D. and Poussart D. (1995):** *Registering range views of multipart objects*. Computer Vision and Image Understanding, Vol. 61, pp. 1-16.
- Bicchi, A.; Salisbury, J. K. and Dario, P. (1989):** *Augmentation of Grasp Robustness Using Intrinsic Tactile Sensing*. In Proceedings of the IEEE International Conference on Robotics and Automation, pp. 303-307.
- Bicchi, A. (1992):** *On the closure properties of robotic grasping*. International Journal Robotics Research, Vol. 14, pp. 319–334.
- Bicchi, A.; Chitour, Y.; Marigo, A. and Prattichizzo, D. (1996):** *Dexterity through rolling: Towards manipulation of unknown objects*. In Proceedings of the 3<sup>rd</sup> International Symposium on Methods and Models in Automation and Robotics, pp. 879-886.
- Bicchi, A.; Marigo, A. and Prattichizzo, D. (1998):** *Robotic dexterity via nonholonomy editors*. Control Problems in Robotic and Automation, pp. 35-49.
- Bicchi, A.; Marigo, A. and Prattichizzo, D. (1999):** *Dexterity through rolling: Manipulation of unknown object*. In Proceedings of the IEEE International Conference on Robotics & Automation, pp. 1583-1588.
- Bicchi, A. (2000):** *Hands for dexterous manipulation and robust grasping: A difficult road towards simplicity*. IEEE Transaction on Robotics and Automation, Vol. 16.

- Boie, R. A. (1984):** *Capacitance impedance readout tactile image sensor*. In Proceedings of the IEEE International Conference on Robotics and Automation, pp. 370-378.
- Borovac, B.; Nagy, L. and Sabli, M. (1996):** *Contact Tasks Realization by sensing Contact Forces*. Theory and Practice of Robots and Manipulators, Springer Wien New York, pp. 381-388.
- Borst, C.; Fischer, M.; Haidacher, S.; Liu, H. and Hirzinger, G. (2003):** DLR hand II *Experiments and experiences with an antropomorphic hand*. In IEEE International Conference on Robotics and Automation.
- Bowden, F. P. and Tabor, D. (1950):** *The friction and lubrication of solids*. Clarendon Press, Oxford.
- Bowden, F. P. and Tabor, D. (1964):** *The friction and lubrication of solids*. Oxford University Press, Part II, Chapter IV.
- Bowden, F. P. and Tabor, D. (1974):** *Friction: an introduction to tribology*. Heinemann, London.
- Box, G. E. P.; Hunter, W.G. and Hunter, J. S. (1978):** *An Introduction to Design, Data Analysis and Model Building*. Statistics for experimenters, John Wiley & Sons Inc., New York.
- Brooks, R. A. (1985):** *A Robust Layered Control System for a Mobile Robot*. MIT AI Lab Internal Memo 864.
- Brooks, R. A. (1987):** *Planning is just a way of avoiding figuring out what to do next*. Cambrian intelligence, Cambridge, Massachusetts: The MIT Press, pp. 103-110.
- Burdea, G. C. and Coiffet, P. (2003):** *Virtual Reality Technology*, Wiley-IEEE Press, pp. 100-101.
- Cadoret, G. and Smith, A. M. (1996):** Friction, not texture, dictates grip forces used during object manipulation. *Journal Neurophysiol*, Vol. 75, pp. 1963-1969.
- Canepa, G.; Petrigliano, R.; Campanella, M. and Rossi, D. D. (1998):** *Detection of incipient object slippage by skin-like sensing and neural network processing*. IEEE Transactions on Systems, Man, and Cybernetics – Part B: Cybernetics, Vol. 28, pp.348–356.
- Carlson, J. (2000):** *Mass fraction measurements in multiphase flows using a clamp-on PVDF array*, IEEE Ultrasonics Symposium, Vol. 1, pp. 471-474.

- Childress, D. S. (1985):** *Historical aspects of powered limb prosthesis*, Clinical Prosthetics and Orthotics, Vol. 9, pp. 2–13.
- Christopher, R.; Cutkosky, M. R. and MacLean, K. (1999):** *Friction identification for haptic display*. In Proceedings of the ASME Dynamic Systems and Control Division, pp. 327-334.
- Ciocarlie, Matei; Miller, Andrew and Allen, Peter (2005):** *Grasp Analysis Using Deformable Fingers*. In Proceedings of the IEEE IROS, pp.1327-1334.
- Coelho J.; Piater, J. and Grupen, R. (2001):** *Developing haptic and visual perceptual categories for reaching and grasping with a humanoid robot*. Robotics and Autonomous Systems, Vol. 37, p.195–218.
- Crowder, R. M. (1998):** *Whole Arm Manipulator: Upgrade Assessment*. Technical Report.
- Cotton, D. P. J.; Chappell, P. H.; Cranny, A.; White, N. M. and Beeby, S. P. (2007):** *A Novel Thick-Film Piezoelectric Slip Sensor for a Prosthetic Hand*, IEEE Sensors Journal, Vol. 7, No. 5, pp. 752-761.
- Cranny, A.; Cotton, D. P. J.; Chappell, P. H.; Beeby, S. P. and White, N. M. (2005a):** *Thick-film force, slip and temperature sensors for a prosthetic hand*, Measurement and Science Technology, Vol. 16, pp. 1–11.
- Cranny, A.; Cotton, D. P. J.; Chappell, P. H.; Beeby, S. P. and White, N. M. (2005b):** *Thick-film force and slip sensors for a prosthetic hand*, Sensors and Actuators A: Physical., Vol. 123–124, pp. 162–171.
- Cuttino, J. F.; Huey, C. O. and Taylor, T. D. (1988):** *Tactile Sensing of Incipient Slip*. Proceeding of the USA-Japan Symposium on Flexible Automation.
- Dai, Min and Newman, T. S. (1998):** *Hyperbolic and Parabolic Quadric Surface Fitting Algorithms - Comparison Between the Least Squares Approach and the Parameter Optimization Approach*, Technical Report TR-UAH-CS-1998-02, Computer Science, Dept., Univ. Alabama in Huntsville.
- Dario, P.; Rossi, D. D.; Domenci, C. and Francesconi, R. (1984):** *Ferroelectric Polymer Tactile Sensors with Anthropomorphic Features*. In Proceedings of the IEEE International Conference on Robotics and Automation, pp. 332-340.
- Dario, P. and Rossi, D. D. (1985):** *Tactile sensors and the gripping challenge*. IEEE Spectrum, Vol. 5, No 22, pp. 46-52.

- Chua, C. S. and Jarvis, R. (1996):** *3d free-form surface registration and object recognition*. International Journal of Computer Vision, Vol. 17, pp. 77-99.
- Dieter, G. E. (1981):** *Metalurgia Mecânica*. Mc Graw Hill Inc.
- Dong-Hwan, K. and Hahn, H. (1996):** *Recognition of contact surfaces using optical tactile and F/T sensors integrated by fuzzy fusion algorithm*. IEEE Transaction on Robot and Human Communication, pp. 352-357.
- Donald, F. G. and Salisbury, J. K. (1997):** *Texture sensing and simulation using the phantom: Towards remote sensing of soil properties*. In Proceedings of the 2<sup>nd</sup> PHANToM Users Group Workshop.
- Dorai, C. and Jain, A. K. (1997):** *Cosmos-a representation scheme for 3d free-form objects*. IEEE Transactions on Pattern Analysis and Machine Intelligence, Vol. 19, pp. 1115-1130.
- Dornfeld, D. and Handy, C. (1987):** *Slip detection using acoustic emission signal analysis*. In the Proceedings of the IEEE International Conference on Robotics and Automation, Vol. 3, pp. 1868-1875.
- Dubey, R. V.; Chan, T. F., and Everett, S. E. (1997):** *Variable Damping Impedance Control of a Bilateral Telerobotic System*. IEEE Control Systems, pp. 37-45.
- Dundurs, J. and Comninou, M. (1983):** *An Education Elasticity Problem With Friction, Part3: General Load Paths*. Journal of Applied Mechanics, Vol. 50, pp. 77-84.
- Eberman, B. and Salisbury, J. K. (1994):** *Application of change detection to dynamic contact sensing*. International Journal of Robotics Research, Vol.13, pp. 369-394.
- Edgar, Dehn (1930):** *Algebraic Equations: An Introduction to the Theories of Lagrange and Galois*. Columbia University Press.
- Ellis, R. E.; Ganeshan, S. R. and Lederman, S. J. (1993):** A tactile sensor based on thin-plate deformation, Robotica.
- ESD STM 11.11-2001 Standard,** Surface resistance measurement of static dissipative planar materials, 2001.
- Everson, R. and Roberts, S. (2000):** *Inferring the Eigenvalues of Covariance Matrices From Limited, Noisy Data*, (Original Research report TR-98-11, Sept 1998), IEEE transactions on signal processing, Vol. 48, Issue 7, pp. 2083-2091.
- Famularo, D. and Muraca, P. (1995):** *Tactile sensor pad: shape recognition*. Proceedings of the IEEE International Symposium on Intelligent Control, pp. 338–342.



- Fearing, R. S. and Hollerbach, J. M. (1985):** *Basic solid mechanics for tactile sensing*. International Journal Robotics Research, Vol.4, No.3, pp. 40-54.
- Fearing, R. S. (1986):** *Implementing a Force Strategy for Object Re-orientation*. IEEE International Conference on Robotics and Automation, San Francisco, CA.
- Fearing, R. S.; Rise, A. and Binford, T. O. (1986):** *A tactile sensing finger tip for a dextrous hand*. 5<sup>th</sup> SPIE Intelligent Robotics and Computer Vision, Cambridge, MA.
- Fearing, R. S. (1990):** *Tactile Sensing Mechanisms*. International Journal Robotics Research, Vol.9, No.3, pp. 3-23.
- Ferrari, C. and Canny, J. (1992):** *Planning optimal grasps*. In Proceedings of the IEEE International Conference on Robotics and Automation, pp. 2290-2295.
- Fischer, M. and Hirzinger, G. (1997):** *Fast planning of precision grasps for 3D objects*. In Proceedings of the IEEE/RSJ International Conference on Intelligent Robots & Systems, pp. 120-126.
- Frederick, D. and Chang, T. S. (1965):** *Continuum Mechanics*. Allyn and Bacon, Inc. Boston, pp. 172-221.
- Funkhouser, T.; Min, P.; Kazhdan, M.; Chen, J.; Halderman, A.; Dobkin, D. and Jacobs, D. (2003):** *A search engine for 3d models*. ACM Transactions on Graphics, Vol. 22, pp. 83–105.
- Godfrey, D. (1967):** *Vibration reduced metal-to-metal contact and causes an apparent reduction in friction*. ASLE Transactions, Vol.10, pp. 183-192.
- Goyal, S.; Ruina, A. and Papadopoulos, J. (1991):** *Planar sliding with dry friction*. part 1 Wear, Vol. 143, pp. 307–330.
- Guo, B. (1995):** *Quadric and Cubic Bitetrahedral Patches*. The Visual Computer, Vol. 7, pp. 253-262.
- Hackwood, S.; Beni, G.; Hornak, L. A. and Wolfe, R. (1983):** *Torque-Sensitive Tactile Array for Robotics*. International Journal Robotics Research, Vol. 2, pp. 46-50.
- Heaney, M. B. (1999):** *The Measurement, Instrumentation and Sensors Handbook*. chapter Electrical Conductivity and Resistivity, CRC Press.
- Hakozaki, M. and Shinoda, H. (2002):** *Digital Tactile Sensing Elements Communicating Through Conductive Skin Layers*. In Proceedings of the IEEE International Conference on Robotics and Automation, pp. 3813-3817.
- Harmon, L. D. (1982):** *Automated tactile sensing*. International Journal Robotics Research, Vol. 2, pp. 3–31.

- Hatamura, Y.; Matsumoto, K. and Morishita, H. (1989):** *A miniature six-axis force sensor of multi-layer parallel plate structure.* In Proceedings Conference IMEKO (Budapest: IMEKO) pp. 567-582.
- Hayes, W. C.; Keer, L. M.; Herrmann, G. and Hlockros, L. F. (1972):** *A mathematical analysis for indentation tests of articular cartilage.* Journal of Biomechanics, Pergamon Press, Vol. 5, pp. 541-551.
- Heckl M. A. and Abrahams I. D. (1996):** *Active control of friction-driven oscillations,* Journal of Sound and Vibration, Vol. 193, pp. 417-426.
- Hilaga, M.; Shinagawa, Y.; Kohmura, T. and Kunii, T. (2001):** *Topology matching for fully automatic similarity estimation of 3d shapes.* In Proceedings of SIGGRAPH, pp. 203–212.
- Hilbert, D. and Cohn-Vossen, S. (1999):** *The Second-Order Surfaces. Geometry and the Imagination.* New York: Chelsea, pp. 12-19.
- Hosada, K.; Tada, Y. and Asada, M. (2002):** *Internal representation of slip for a soft finger with vision and tactile sensors.* In IEEE/RSJ International Conference on Intelligent Robots and Systems.
- Howell, H. G. and Mazur, J. (1953):** *Amontons' Law and Fibre Friction.* Journal of the Textile Institute, pp. 59-69.
- Howe, R. D. and Cutkosky, M. R. (1989):** *Sensing Skin Acceleration of Slip and Texture Perception.* IEEE International Conference on Robotics and Automation, pp. 145-150.
- Howe, R. D. (1990):** *Dynamic tactile sensing.* PhD Thesis, Stanford University.
- Howe, R. D. (1992):** *A force reflecting teleoperated hand system for the study of tactile sensing in precision manipulation.* In the Proceedings of the IEEE International Conference on Robotics and Automation, pp. 1321-1326.
- Howe, R. D. and Cutkosky, M. R. (1993):** *Dynamic Tactile Sensing: Perception of Fine Surface Features with Stress Rate Sensing.* IEEE Transaction on Robotics and Automation, Vol. 9, No. 2, pp. 140-151.
- Howe, R. D. and Cutkosky, M. R. (1996):** *Practical force-motion models for sliding manipulation.* International Journal of Robotics Research, Vol. 15, no. 6, pp. 557–572.
- Hutchings, I. M. (1994):** *Tribological properties of metal matrix composites.* Materials Science and Technology, Vol. 10, pp. 513-517.

**IAN, M. A. and James, C. B. (1984):** *Curvature and Tangential Deflection of Distance Arcs: A Theory Based on the Commutator of Scatter Matrix Pairs and Its Application to Vertex Detection in Planar Shape Data.* IEEE Transaction on Pattern Analysis and Machine Intelligence, Vol. 6, No. 1, pp. 27-40.

**Ibrahim, R. A. (1994):** *Friction-induced vibration, chatter, squeal, and chaos: Part i-mechanics of contact and friction.* Applied Mechanics Reviews, Vol. 47, pp. 209-226.

**Ibrahim, M. Y., and Abdel-Malak, H. (2005):** *Study on Intelligent Grasping Techniques,* Paper presented at International Conference on Advances in the Internet, Processing, Systems and Interdisciplinary Research.

**Ibrayev, Rinat and Jia, Yan-Bin (2005):** *Semi-Differential Invariants for Tactile Recognition of Algebraic Curves.* International Journal of Robotics Research, Vol. 24, No. 11, pp. 951-969.

**IEC 60770, Transmitters for Use in Industrial-process Control Systems - Part 1:** Methods for Performance Evaluation, 1999-02, Part 2: Methods for Inspection and Routine Testing, 2003-01.

**IEC 61340-5-1 Standard,** Electrostatics – part 5-1: Protection of electronic devices from electrostatic phenomena - general requirements, 1998.

**Iwata, H. and Sugano, S. (2003):** *A system design for tactile recognition of human-robot contact state.* In Proceedings the IEEE/RSJ International Conference on Intelligent Robots and Systems, Vol. 1, pp. 7–12.

**Jenmalm, P. and Johansson, R. S. (1997):** *Visual and Somatosensory Information about Object Shape Control Manipulative Fingertip Forces.* Journal of Neuroscience, Vol. 17, pp. 4486–4499.

**Jibeteau, Dorina and Laurent, Monique (2005):** *Semidefinite approximations for global unconstrained polynomial optimization,* the SIAM Journal on Optimization.

**Jones, L. A., Hunter, I. W. (1992):** *Changes in pinch force with bidirectional load forces.* Journal of Motor Behavior, Vol.24, pp.157-164.

**Johansson, R. S., Westling, G (1984):** *Roles of glabrous skin receptors and sensorimotor memory in automatic control of precision grip when lifting rougher and more slippery objects.* Experimental Brain Research, Vol.56, pp. 550-564.

**Johansson, R. S. and Westling, G. (1987):** *Signals in tactile afferents from the fingers eliciting adaptive motor responses during precision grip.* Experimental Brain Research, Vol. 66, pp.141-154.

- Johansson, R. S. and Westling, G. (1990):** *Tactile afferent signals in the control of precision grip.* Attention and Performance, Vol. 8, pp. 677-713.
- Johnson, A. and Helbert, M. (1998):** *Efficient multiple model recognition in cluttered 3-d scenes.* In Proceedings of the IEEE Computer Vision and Pattern Recognition.
- Juhani, S. and Dinesh, K. P. (1996):** *Haptic texturing - a stochastic approach.* In Proceedings of the IEEE International Conference on Robotics and Automation, Vol. 1, pp.557-562.
- Kazhdan, M.; Chazelle, B.; Dobkin, D.; Funkhouser, T. and Rusinkiewicz, S. (2003):** *A reflective symmetry descriptor for 3d models.* Algorithmica.
- Kim, G.-S.; Rhee, S.; Um, K.-W. and Rhee, S.-H. (1999):** *Design and fabrication of a 6-component force/moment sensor.* Sensors Actuators 77, pp. 209-220.
- Kim, G.-S. (2000):** *The development of a six-axis force/moment sensor testing machine and evaluation of its uncertainty.* Measurement Science Technology, Vol. 11, pp.1377-1382.
- Kim, G.-S. (2001):** *The design of a six-axis force/moment sensor and evaluation of its uncertainty.* Measurement Science Technology, Vol. 12, pp.1445-1455.
- Kim, G.-S. (2003):** *Development of a six-axis force/moment sensor and its control system for an intelligent robot's gripper,* Measurement Science Technology, Vol. 14, pp. 1265-1274.
- Kim, Sung-Hoon; Engel, Jonathan; Liu, Chang and Jones, Douglas L (2005):** *Texture classification using a polymer-based MEMS tactile sensor.* Journal of Micromechanics and Microengineering, Vol.15, pp. 912–920.
- Kinoshita, G.; Kurimoto, Y.; Osumi, H. and Umeda, K. (2001):** *Dynamic contact sensing of soft planar fingers with tactile sensors.* In Proceedings of the IEEE ICRA International Conference on Robotics and Automation, Vol. 1, pp. 565–570.
- Kirkpatrick, D.; Mishra, B. and Yap, C. K. (1990):** *Quantitative Steinitz's theorems with applications to multifingered grasping.* In Proceedings of the 20<sup>th</sup> ACM Symposium on Theory of Computing, pp. 341-351.
- Laschi, C.; Gorce, P.; Coronado, J.; Leoni, F.; Teti, G.; Rezzoug, N.; Guerrero-González, A.; Pedreño Molina, J. L.; Zollo, L.; Guglielmelli, E.; Dario, P. and Burnod, Y. (2002):** *An antropomorphic robotic platform for experimental validation of biologicallyinspired sensory-motor co-ordination in grasping,* In IEEE/RSJ International Conference on Intelligent Robots and Systems.

- Lavallee, S. and Szeliski, R. (1995):** *Recovering the position and orientation of free-form objects from image contours using 3d distance maps.* IEEE Transactions on Pattern Analysis and Machine Intelligence, Vol. 17, pp. 378-390.
- Lederman, S. J.; Klatzky, R. L. and Pawluk, D. T. (1992):** *Lessons from the study of biological touch for robotic haptic sensing, in Advanced Tactile Sensing for Robotics,* H. R. Nicholls, Ed. Singapore: World Scientific.
- Lee, Yung-Chun and Chu, Chi-Chen (2005):** *A Double-Layered Line-Focusing PVDF Transducer and  $V(z)$  Measurement of Surface Acoustic Wave.* Japanese Journal of Applied Physics, Vol. 44, No. 3, pp. 1462-1467.
- Lincoln, B. Br. J. (1952):** *Frictional and elastic properties of high polymeric materials.* Apply Physics, Vol. 3, pp. 260-263.
- Li, Z. and Sastry, S. (1988):** *Task-oriented optimal grasping by multi-fingered robot hands.* IEEE Journal of Robotics and Automation, RA-4(1), pp. 32-44.
- Liu, Y. H. (1999):** *Qualitative test and force optimization of 3-D frictional form closure grasps using linear programming.* IEEE Trans. Robotics Automat, Vol. 15, pp. 163–173.
- Lynch, M. R. and Rayner, P. J. (1989):** *Optical Character Recognition Using a New Connectionist Model.* 3<sup>rd</sup> International Conference On Image Processing and Its Application, IEE.
- Maekawa, H.; Tanie, K.; Komoriya, K.; Kaneko, M.; Horiguchi, C. and Sugawara, T. (1992):** *Development of a Finger-Shaped Tactile Sensor and its Evaluation by Active Touch.* In Proceedings of the IEEE ICRA, pp.1327-1334.
- Maekawa, H.; Tanie, K. and Komoriya, K. (1993):** *A finger-shaped tactile sensor using an optical waveguide, 'Systems Engineering in the Service of Humans'.* Conference Proceedings International Conference on Systems, Man and Cybernetics, Vol. 5, pp. 403–408.
- Maekawa, H.; Tanie, K. and Komoriya, K. (1995):** *Tactile sensor based manipulation of an unknown object by a multi-fingered hand with rolling contact.* In Proceedings of IEEE International Conference on Robotics & Automation, pp. 743-750.
- Maekawa, H.; Tanie, K. and Komoriya, K. (1997):** *Tactile feedback for multi-fingered dynamic grasping.* IEEE Control Systems, Vol.17, pp. 63-71.

- Malchior, A; Ruoff, W. and Schmidberger, C. (1984):** *Sensors and Flexible Production*. Optical Engineering, Vol. 23, No. 5, pp. 507-511.
- Mark, H. L. (2000):** *Tactile Sensing: New Direction, New Challenges*. The International Journal of Robotics Research, Vol. 19, No. 7, pp. 636-643.
- Mason, M. T. (1981):** *Compliance and Force Control for Computer Controlled Manipulators*. IEEE Transactions on Systems, Man, and Cybernetics, Vol.11, pp. 418-432.
- Mason, M. T. and Salisbury, J. K. Jr. (1985):** *Robot Hands and the Mechanics of Manipulation*. MIT Press.
- McCarragher, B. J. and Asada, H. (1993):** *Qualitative template matching using process models for state transition recognition of robotic assembly*. ASME Journal of Dynamic Systems Measurement and Control, Vol.115, pp. 261-269.
- Mollin, R. A. (1995):** *Quadratics*. Boca Raton, CRC Press.
- Monkman, G. J. and Taylor, P. M. (1993):** *Thermal tactile sensing*. IEEE Transactions on Robotics and Automation, Vol. 9, Issue 3, pp. 313 – 318.
- Montana, D. J. (1992):** *Contact stability for two-fingered grasps*. IEEE Transaction on Robotics Automation, Vol. 8, pp. 421–430.
- Nagata, K.; Ooki, M. and Kakikur, M. (1999):** *Feature detection with an image based compliant tactile sensor*. In Proceedings of the IEEE/RSJ International Conference on Intelligent Robots and Systems, Vol. 2, pp. 838-843.
- Najarian, S.; Dargahi, J. and Zheng, X. Z. (2006):** *A novel method in measuring the stiffness of sensed objects with applications for biomedical robotic systems*, The International Journal Of Medical Robotics and Computer Assisted Surgery, Vol. 2, Issue 1, pp.84–90.
- Nakamura, Y.; Hanafusa, H. and Ueno, N. (1986):** *A piezoelectric film sensor for robotic and end-effectors*. Robot sensors, Vol. 2, pp. 247-257.
- Ng, E. (1989):** *Robot Arm World Visualisation By Tactile Exploration*. Project Report, E&E Engineering, Auckland University, New Zealand.
- Ng, E. W. K.; Coghill, G. G. and Tuck, D. L. (1991):** *Tactile robot shape recognition using geometrical angle/length sequences*. IEEE International Joint Conference on Neural Networks, Vol. 1, pp. 307–312.
- Nicholls, H. R. and Lee, M. H. (1989):** *A Survey of Robot Tactile Sensing Technology*. International Journal Robotics Res., Vol. 8, pp. 3-30.

**Nicholls, H. R. (1992):** *Advanced Tactile Sensing for Robotics*. Singapore World Scientific.

**Novak, J. L. (1989):** *Initial Design and Analysis of a Capacitive Sensor for Shear and Normal Force Measurement*. In Proceedings of the IEEE International Conference on Robotic and Automation, pp. 137-145.

**Novotni, M. and Klein, R. (2001):** *A geometric approach to 3D object comparison Shape Modeling and Applications*. SMI 2001 International Conference on, pp.167 – 175.

**Nowlin, W. C. (1991):** *Experimental results on bayesian algorithms for inpreting compliant tactile sensing data*. In IEEE International Conference on Robotics and Automation.

**Ohka, M.; Kobayashi, M.; Shinokura, T. and Sagisawa, S. (1994):** *Tactile Expert System Using a Parallel-fingered Hand Fitted with Three-axis Tactile Sensors*. JSME International Journal, Series C, Vol. 37, No. 1, pp. 138-146.

**Ohka M.; Mitsuya Y.; Takeuchi S.; Kamaekawa, O. and Ishihara, H. (1995):** *A 3-axis optical tactile sensor-FEM contact analysis and sensing experiments using a large-sized tactile sensor*. In IEEE International Conference on Robotics and Automation, pp. 706-713.

**Ohka, Masahiro; Takayanagi, Jyunichi; Kawamura, Takuya and Mitsuya, Yasunaga (2006):** *A surface-shape recognition system mimicking human mechanism for tactile sensation*, Robotica, Vol. 24 , Issue 5, pp. 595–602.

**Omata, S. and Terunuma, Y. (1992):** *new tactile sensor like human hand and its applications*, Sensors and actuators Apply Physics, Vol. 35, pp. 9-15.

**Ono, K. and Hatamura, Y. (1986):** *A new design for 6-component force/torque sensors*. Mechanical Problems in Measuring Force and Mass (Dordrecht: Kluwer), pp. 39-48.

**Osada, R.; Funkhouser, T.; Chazelle, B. and Dobkin, D. (2002):** *Shape distributions*. ACM Transactions on Graphics, Vol. 21, pp. 807–832.

**Pati, Y. C.; Friedman, D. ; Krishnaprasad, P. S. ; Yao, C. T.; Peckerar, M. C.; Yang, R. and Marrian, C. R. (1988):** *Neural networks for tactile perception*. In Proceedings of the IEEE International Conference Robotics Automat, pp. 134-139.

**Patterson, R. W. and Nevill, G. E. Jr. (1986):** *The induced vibration touch sensor- a new dynamic touch sensing concept*. Robotica, Vol. 4, pp. 27-31.

**Dario, P.; Domenici, C. and Bardelli, R. (1983):** *Piezoelectric Polymers: New Sensor Materials for Robotic Applications*. The 13th International Symposium on Industrial Robots and Robots 7, Vol.2, pp.1434–1449.

**Petchartee, S. (2007a):** *Strain Decomposition from Tactile Data for Six-Axis Force Sensing*. Technical Report, Fachbereich Elektrotechnik, Fachhochschule Regensburg.

**Petchartee, S. and Monkman, G. (2007a):** *Pre-slip detection based Tactile Sensing*. In Proceedings of the 3rd International Conference on Intelligent Sensors, Sensor Networks and Information Processing (ISSNIP 2007), Melbourne. (IEEE Xplore), pp. 233-238.

**Petchartee, S. and Monkman, G. (2007b):** *Contact Identification using Tactile Arrays*. In Proceedings of the 7th IEEE International Symposium on Signal Processing and Information Technology (ISSPIT 2007), Egypt, pp. 1105-1110.

**Petchartee, S. and Monkman, G. (2007c):** *Contact Classification using Tactile Arrays*. In Proceedings of the 3rd International Conference on Intelligent Sensors, Sensor Networks and Information Processing (ISSNIP 2007), Melbourne. (IEEE Xplore), pp. 227-232.

**Petchartee, S. and Monkman, G. (2008a):** *Optimisation of Prehension Force through Tactile Sensing*. Industrial Robot Journal, Emerald Group Publishing Limited, Vol.35 (4), pp. 361-368.

**Petchartee, S. and Monkman, G. (2008b):** *3D-Shape Recognition based Tactile Sensor*. In the Book Series “Lecture Notes in Electrical Engineering”, the issue titled “Smart Sensors and Sensing Technology”, Springer-Verlag Berlin Heidelberg, part 9 chapter 4, pp. 317-331.

**Piegl, L. A. and Tiller, W. (1996):** *The NURBS Book*, Springer Berlin, pp.117-138.

**Pollard, N. S. (1994):** *Parallel Methods for Synthesizing Whole-Hand Grasps from Generalized Prototypes*. Ph.D. thesis, Department of Electrical Engineering and Computer Science, MIT.

**Porto and Science (1998):** *Report of the 10th European Union Contest for Young Scientists*, Available from: <http://ec.europa.eu/research/youngscientists/15years/pdf/ys021998.pdf>

**Raibert, M. H. and Craig, J. J. (1981):** *Hybrid Position/Force Control of Manipulators*. ASME Journal Dynamic Systems, Measurement & Control, Vol. 103, No. 2, pp. 126-133.

**Raibert, H. M. and Tanner, J. E. (1982):** *Design and Implementation of a VSLI Tactile Sensing Computer*. International Journal Robotics Research, Vol. 1-3, pp. 3-18.



- Rayleigh, J. W .S. (1945):** *Theory of Sound*, Dover Publications, New York.
- Rebman, J. and Kallhammer, J. E. (1986):** *A search for precursors of slip in robotic grasp*. In *Intelligent robots and computer vision*, Vol. 726, pp. 329-337.
- Ricker, S. L. and Ellis, R. E. (1993):** *2-D Finite-Element Models of the Tactile Sensors*. In *Proceedings of the International Conference Robotics and Automation*, Atlanta, pp. 941-947.
- Russell, R. A. (1987):** *Compliant-skin tactile sensor*, In *Proceedings of IEEE International conference for Robotics and Automation*, pp. 2221-2233.
- Seguna, C. M. and Saliba, M. A. (2001):** *The Mechanical and Control System Design of a Dexterous Robot Gripper*. In *Proceedings of the 8<sup>th</sup> International IEEE Conference on Electronics, Circuits and Systems*, Vol. 3, pp. 1195-1202.
- Shinoda, H. and Ando, S. (1994):** *Ultrasonic emission tactile sensor for contact localization and characterization*. In *Proceedings of the IEEE International Conference on Robotics and Automation*, Vol. 3, pp. 2536-2543.
- Snyder, W. E. (1985):** *Industrial Robots: Computer Interfacing and Control*. Prentice-Hall, Inc. Englewood Cliffs, New Jersey, pp. 293 - 297.
- Son, J.; Monteverde, E. and Howe, R. (1994):** *A tactile sensor for localizing transient events in manipulation*. In *Proceedings of the IEEE International Conference on Robotics and Automation*, San Diego, CA, pp. 471–476.
- Son, J. S. (1996):** *Integration of tactile sensing and robot hand control (grasp refinement)*. Dissertation Harvard University.
- Soucy, M. and Laurendeau, D. (1998):** *A general surface approach to the integration of a set of range views*, *IEEE Transactions on Pattern Analysis and Machine Intelligence*, Vol. 17, pp. 344-358.
- Speeter, T. H. (1988):** *Flexible, Piezoresistive Touch Sensing Array*. *SPIE*, Vol. 1005, pp. 31-43.
- Speeter T. H. (1992):** *3-dimensional finite-element analysis of elastic continua for tactile sensing*. *International Journal of Robotics Research*, pp. 1-19.
- Srinivasan, M. A.; Whitehouse, J. M. and Lamott R. H. (1990):** *Tactile detection of slip: Surface micro geometry and peripheral neural codes*. *Journal of Neurophysiology*.

- Stavroulakis, G. E.; Goeleven, D. and Panagiotopoulos, P. D. (1996):** *New models for a class of adhesive grippers, the hemivariational inequality approach*, Archive of Applied Mechanics, Vol. 67, pp. 50–61.
- Takeuchi, S.; Ohka, M. and Mitsuya, Y. (1994):** *Tactile Recognition Using Fuzzy Production Rules and Fuzzy Relations for Processing Image Data from Three-dimensional Tactile Sensors Mounted on a Robot Hand*, In Proceedings of the Asian Control Conference, Vol. 3, pp. 631-634.
- Tangelder, J. and Veltkamp, R. (2002):** *Polyhedral model retrieval using weighted point sets*. In Proceedings of the 8<sup>th</sup> annual conference of the Advanced School for Computing and Imaging, pp. 223–230.
- Thirion, J. P. (1994):** *Extrema1 points: Definition and application to 3d image registration*. IEEE conf on Computer Vision and Pattern Recognition.
- Torah, R. N. (2004):** *Optimization of the Piezoelectric Properties of Thick-Film Piezoceramic Devices*, Ph.D. dissertation, University of Southampton, Southampton, U.K.
- Tremblay, M. R.; Packard, W. J. and Cutkosky, M. R. (1992):** *Utilizing sensed incipient slip signals for grasp force control*. In Proceedings of the Japan-USA Symposium on Flexible Automation, pp. 1237-1243.
- Turban, E. (1992):** *Expert Systems and Applied Artificial Intelligence*. Macmillan Publishing, New York, pp. 4-5.
- Turrell, Y. N.; Li F. X. and Wing, A. M. (2001):** *Estimating the minimum grip force required when grasping objects under impulsive loading conditions*. Behavior Research Methods, Instruments & Computers, Vol.33, pp. 38-45.
- Tzafestas, C. S. (2003):** *Whole-hand kinesthetic feedback and haptic perception in dextrous virtual manipulation*. IEEE Trans. System, Man, Cybernetics, Vol. 33, No. 1, pp. 100–113.
- Vellinga, W. P. and Hendriks, C. P. (2001):** *Sliding friction dynamics of hard single asperities on soft substrates*. Physic Review, Vol. 63, pp. 12-14.
- Weiß, Karsten and Wörn, Heinz (2004):** *Tactile Sensor System for an Anthropomorphic Robotic Hand*, In Proceedings of the IEEE International Conference on Manipulation and Grasping (IMG).

- Weiß, Karsten and Wörn, Heinz (2005):** *The Working Principle of Resistive Tactile Sensor Cells*. In Proceedings of the IEEE International Conference on Mechatronics & Automation.
- Westling, G. and Johansson, R. S. (1984a):** *Factors influencing the force control during precision grip*. Experimental Brain Research, Vol. 53, pp. 277-284.
- Worth, A. J. and Spencer, R. R. (1992):** *A neural network for tactile sensing: the Hertzian contact problem*. IEEE Transactions on Systems, Man and Cybernetics, Vol. 22, Issue 1, pp. 177-182.
- Yamada, Y. and Cutkosky, R. (1994):** *Tactile Sensor with 3-Axis Force and Vibration Sensing Function and Its Application to Detect Rotational Slip*. In Proceedings of the IEEE International Conference on Robotics and Automation, pp. 3550-3557.
- Yamada, Y.; Fujimoto, I.; Morizono, T.; Umetani, Y.; Maeno, T. and Yamada, D. (2001):** *Development of artificial skin surface ridges with vibrotactile sensing elements for incipient slip detection*, International Conference on Multisensor Fusion and Integration for Intelligent systems, pp. 251- 257.
- Yabuki, A. (1990):** *Six-axis force/torque sensor for assembly robot*. Fujitsu Science Technology, Vol. 26, pp. 41-47.
- Yan, H. (1990):** *Closed Boundary Recognition using a Multi-layer Neural Network*. In Proceedings of the 1<sup>st</sup> Australian Conference on Neural Networks, Sydney University Electrical Engineering, Australia.
- Yoshikawa, T.; Sugie, T. and Tanaka, M. (1988):** *Dynamic Hybrid Position Force Control of Robot Manipulators - Controller Design and Experiment*. IEEE Journal. Robotics and Automation, Vol. 4. No. 6, pp. 699-705.
- Yuji, J. and Shida, K. (2002):** *Thermal-type tactile sensor for material discrimination and contact pressure sensing*. In Proceedings of the 41<sup>st</sup> SICE Annual Conference, Vol. 1, pp. 588–589.
- Zhang, Z. (1994):** *Iterative point matching for registration of free-form curves and surfaces*. International Journal of Computer Vision, Vol. 13, pp. 119-152.
- Zhang, H. and Chen, N. N. (2000):** *Control of contact via tactile sensing*. IEEE Transactions on Robotics and Automation, Vol. 16, Issue 5, pp. 482-495.